Motorized Guitar Tuner

Bachelor Thesis
Telematics

Michael Weißensteiner
Robert Viehauser

Supervisor: Dipl. Ing. David Fischer

March 26, 2012

University of Technology, Graz, Austria
Telematics

Table of contents

1 Introduction

1.1 Abstract

For developing a motorized guitar tuner many topics had to be considered. An important point was a compatible selection of hardware components which would fulfil the requirements. Also the software implementation was challenging due to limited random-access-memory of our used micro-controller. Therefore efficient engineering was required.
Generally, the motorized guitar tuner represents a control system loop, which had to be developed by keeping its stability. Most important was the prevention of accuracy issues regarding frequency changing in tuning. By that reason, several software filters had been designed to provide valid frequency information at high enough resolution. Also an automatic string selection algorithm was developed which allows a fast guitar tuning, if the strings are relatively in-tune to each other. Furthermore, three different kinds of guitar-tunings are supplied (standard tunnig, drop-D tuning, one-step-down tuning). For actually interacting with the guitar machine-heads a servo motor was modified to allow angular-speed actuation by PWM. Hence, several PID-controllers were implemented due to different string characteristics. A connection with the guitar is provided by a 3,6mm phone jack.
The result is a complete designed hand-held device with display output and an internal servo motor. Software configurations and parameters can be modified by menu. The voltage supply is offered by a 5V voltage regulator which generally uses an internal 9V block accumulator.

1.2 Motivation

Basically, the idea of a motorized guitar tuner came up by playing an old de-tuned acoustic guitar. This idea seemed to be a challenging task for students of telematics in several aspects, including digital-signal-processing, electrical engineering, programming and designing/simulating by using official software. Even a complete product as hand-held-device was aspired. The main idea was to tune a guitar (principally electric guitars) by using a micro-controller which actuates a (servo) motor. Especially accuracy issues seemed to get problematic and also the mechanical slackness was discussed before starting this project. Because of the expected effort for this bachelor thesis it was required to separate the development into two parts which is basically represented by signal input and signal output related processes.
After all, this work was challenging all acquired knowledge of a telematic student and although of extensive time-costs, we are proud of the successful finalization.

1.3 Tasks

The main tasks of this project were on one hand processing the signal input precisely to provide high accuracy and on the other hand implementing an appropriate controlling algorithm for actuating the motor.

Figure 1 shows a graphical illustration of the system components. The red colored sections were assigned to the responsibilities of student Michael Weißensteiner, whereas the blue colored tasks were processed by student Robert Viehauser.

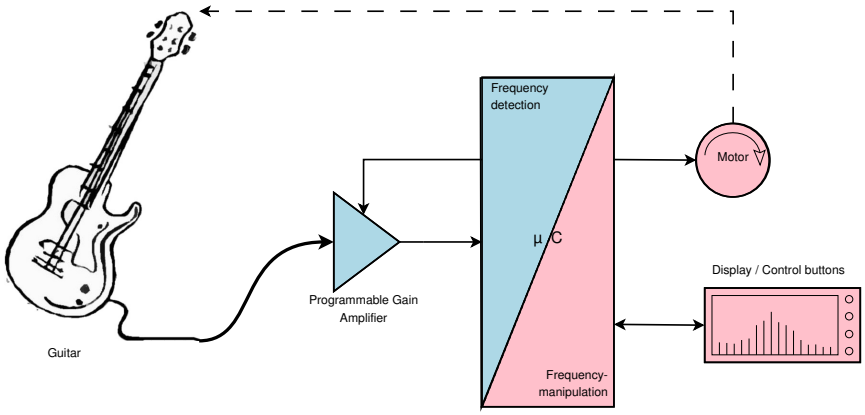

Figure 1: Task sharing

Part 1:

The pure electrical guitar signal had to be filtered with a pre-switched circuitry before sampled by an analog-digital-converter to get the desired frequency ranges. Furthermore a proper pre-amplification for processing was necessary. When the signal was digitized, software filters (especially bi-quad filters) were applied to eliminate existing noise or frequency overtones. Those were designed with the software MATLAB®. Additionally a stable algorithm for automatic string selection had to be developed. The goal was to deliver a (realtime) value of the actual string frequency.
In order to that, a layout design was required to actually allow a compact device by handicraft work.

This tasks were assigned to the student Robert Viehauser.

Part 2:

To actuate the motor a compatible PWM configuration had to be determined. Additionally, the motor had to be modified to allow a angular speed controlled operation.
To obtain an accurate tuning procedure, a control system was designed by using MATLAB®/Simulink. For this, researches about the guitar string behaviour were necessary. Mathematical descriptions and conclusions were made to create a control system model. Software supported simulating of different PID-controller parameters provided a comfortable method for controller design.
In addition to that, a menu structure was required for selecting different tuning modes and to access and edit tuning parameters.

This tasks were assigned to the student Michael Weißensteiner.

2 Frequency detection

2.1 Hardware

2.1.1 The μ-Controller[1]

The target of this project was to engineer a hand-held device and keeping everything as simple as possible to build this device with limited funds. To achieve this goal, a μ-Controller was chosen whose functionality is manageable and the appropriate circuit boards can be made by hand. This implies that a PDIP packaging type with a pin distance of 100 mil (2.54 mm) was preferred. Since we are in possession of a self made tiny USB programmer for ATMEL® products and had some experiences with these, the ATMEL® Mega32 μ-Controller was chosen. For this project important features of the μ-Controller are

- Up to 16MHz clock
- On-chip 2-cycle Multiplier
- Included 10-bit ADC[1]
- Build-in PWM[2]-Module
- SPI[3] module
- Programmable with our tiny USB programmer

2.1.2 Adaptive gain preamplifier

Before sampling the guitar signal with the implemented ADC of the μ-Controller is possible, some analog signal preprocessing stages are necessary. The signal which comes straight out of a normal electric guitar has typically $20mV$ to $80mV$ peak to peak voltage. This also depends strongly on the picked string. The thinner a guitar string is, the lower output voltage can be measured, as a fact of the lower swinging metal volume which inducts the tone as voltage signal in the pick-up of the guitar. Additionally the longer a string swings, the lower amplitude the signal gets. This is obviously a fact which has to be considered, since a sampling resolution as high as possible is desired. To deal with this issue, it was decided to implement a programmable gain stage.

[1] Analog Digital Converter
[2] Pulse Width Modulation
[3] Serial Peripheral Interface

The preamplifier should be programmed by the μ-Controller itself. For this purpose the MCP6S21 [2] from Microchip® is used, which also supports the SPI protocol. This chip consists of an integrated non-inverting amplifier, which can be programmed to one of 8 different gain levels.

The supported gain levels are
1x 2x 4x 5x 8x 10x 16x 32x

To achieve more and finer steps between two gain levels, two chips are driven in cascade. With this trick and ensuring that each chip can be programmed independently, the system is able to operate with the gain levels figured in table 1, which are numbered in ascending order by the resulting gain of both stages. This order defines the gain stage hierarchy used in the μ-Controller program.
The gain step factor describes the multiplication factor that an increase of one gain level (to the level in the corresponding row) implies. As this gain step factor is about 1.25 in a wide spread connected range of gain levels, a well controllable behavior of the whole preamplifier stage can be assumed, since mostly an increase of one gain level means that the signal amplitude increases up to 25%, which is quite good to handle.
This would be much more difficult with just one programmable amplifier chip of this type. Additionally to finer gain increases, using two chips enables the system to handle a bigger range of signal amplitudes too, which comes together with a better handling of different guitars and guitar types.

Additionally to these programmable gain amplifiers a fixed gain stage is introduced as well, to obtain a proper voltage level using the lower numbered but well controllable gain stages assuming a signal starting at a level of approximately $60mV$ peak to peak voltage. This achieves the possibility for flexible and fine gain adjustments, which leads to an optimal exploitation of the given ADC resolution during the whole tuning process.

These in sum three gain stages are also configured as active low- and high-passes. So an analog band-passing of the signal can be performed to avoid direct components and aliasing due to the sampling. The electrical circuit of the whole analog preprocessing is described in more detail in chapter 2.1.4

2.1.3 Single supply issues

Building a hand-held device often implies the usage of a battery which has one minus and one plus pole. For processing the negative and positive parts of the signal, the operational amplifiers need a positive supply voltage, a negative supply voltage and an additional ground potential as reference. So a virtual analog ground voltage whose electrical potential lies approximately

Level Nr	Gain of stage 1	Gain of stage 2	Gain of stage 1 × 2	Gain step factor	Resulting gain with 4.7x gain prestage
0	1	1	1	-	4.7
1	1	2	2	2	9.4
2	2	2	4	2	18.8
3	1	5	5	1.25	23.5
4	2	4	8	1.6	37.6
5	2	5	10	1.25	47
6	4	4	16	1.6	75.2
7	4	5	20	1.25	94
8	5	5	25	1.25	117.5
9	4	8	32	1.28	150.4
10	5	8	40	1.25	188
11	5	10	50	1.25	235
12	8	8	64	1.28	300.8
13	8	10	80	1.25	376
14	10	10	100	1.25	470
15	8	16	128	1.28	601.6
16	10	16	160	1.25	752
17	8	32	256	1.6	1203.2
18	10	32	320	1.25	1504
19	16	32	512	1.6	2406.4
20	32	32	1024	2	4812.8

Table 1: Gain table of cascaded stages

in the middle of the plus and minus supply voltage of the battery has to be generated. A simple method would be a 1-by-2 voltage divider, but its output would not be able to stabilize its voltage under load, so a unity gain buffer has to be added. Unfortunately our already ordered dual operational amplifier LM358 [4] doesn't support the usage as a unity gain buffer, so a 1-by-11 voltage divider followed by a 5.7x non inverting gain stage was used. This leads nearly to the same virtual ground voltage whose potential is capable to be constant even under alternating load conditions.

2.1.4 Connection scheme

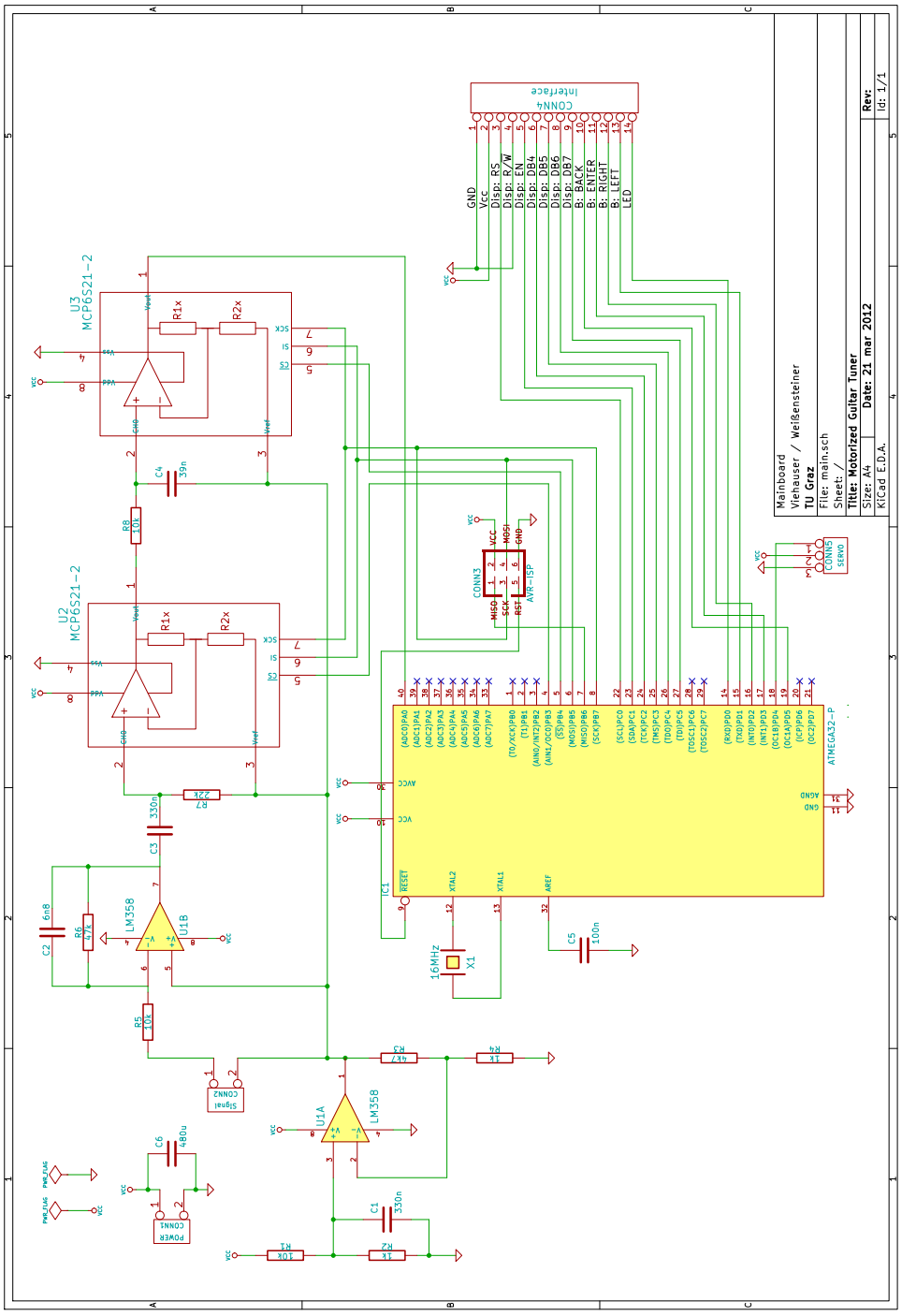

Figure 2: Connection scheme of the main electrical circuit

Figure 2 shows the electrical connection scheme of the main circuit. The virtual analog ground voltage which was mentioned above is generated in region `B1` of the scheme. This voltage is used as reference for the guitar signal and for the all following gain stages shown in region `A2` to `A4`. The absolute resistor values of the 1-by-11 voltage divider (`R1` and `R2`) are chosen as a tradeoff between noise immunity and low current flow. If the resistor values are chosen too high, the thermal resistor noise will influence the stability of the reference voltage. Choosing too low resistor values would cause a high current which effects the lifetime of the battery in a negative way. The capacitor `C1` is supposed to improve stability of the reference voltage in case of fluctuation of the supply voltage.
The non inverting gain stage will keep the output reference voltage constant, even under load. The gain can be calculated according to following equation 1.

$$G_{ref} = 1 + \frac{R3}{R4} = 1 + \frac{4,7k\Omega}{1k\Omega} = 5,7 \tag{1}$$

Assuming a supply voltage of $U_{sup} = 5V$ leads to a virtual ground voltage of

$$U_{sup} \cdot \frac{1}{11} \cdot G_{ref} = 5V \cdot \frac{1}{11} \cdot 5,7 = 2,59V \tag{2}$$

which is a satisfying reference voltage for this purpose.

The active low-pass with a fixed gain of $4.7x$ is represented in section `A2`. As input signal the guitar signal is directly connected by connector `CONN2`, which is also referenced by the virtual ground voltage. The cutoff frequency and the gain of the first stage can be calculated as shown in equation 3 and 4.

$$f_{c_{LP1}} = \frac{1}{2\pi \cdot C2 \cdot R6} = \frac{1}{2\pi \cdot 6,8nF \cdot 47k\Omega} = 497,98Hz \tag{3}$$

$$G_{fix} = -\frac{R6}{R5} = -\frac{47k\Omega}{10k\Omega} = -4,7 \tag{4}$$

As first gain stage an inverting amplifier circuit is used. This setup is much more resistant to noise than a non inverting amplifier, because the input resistance of a non inverting circuit is very high (theoretically infinite). The input resistance of a inverting amplifier circuit is approximately the value of the resistor between the input signal source and the inverting input of the operational amplifier (in figure 2 labeled as `R5`). The thermal noise of a resistor is directly related to its value, so a lower resistor inducts less noise. The value $10k\Omega$ for `R5` was chosen as a tradeoff of low thermal noise and keeping the load to the signal source small. If choosing the value for `R5` too low (high load), the voltage amplitude of the guitar signal will collapse.
Since just the frequency is interesting when tuning a string, the negative sign (and the whole phase response) is not relevant in this application.

The programmable gain stages shown in figure 2 (regions `A3-A4`) consist internally of non inverting gain stages. To drive them as active gain stages with low- and high-pass characteristics, the input signal of each stage is filtered through simple passive elements. The high-pass consists of `C3` and `R7`, the second low-pass consists of `C4` and `R8`.

$$f_{c_{HP}} = \frac{1}{2\pi \cdot C3 \cdot R7} = \frac{1}{2\pi \cdot 330nF \cdot 22k\Omega} = 21,92Hz \tag{5}$$

$$f_{c_{LP2}} = \frac{1}{2\pi \cdot C4 \cdot R8} = \frac{1}{2\pi \cdot 39nF \cdot 10k\Omega} = 408,09Hz \tag{6}$$

There are several reasons for this configuration of the gain stages. The high-pass stage is responsible for eliminating a possible direct component of the signal without influencing the interesting frequency components (the lowest target frequency of the system is the low D at $73,42Hz$, see table 2 in section 2.2.2). The two low-pass stages are responsible for avoiding aliasing caused by sampling the signal after the preamplifier stage. Also the amplitudes of harmonic frequencies get reduced while the interesting fundamental frequencies are not influenced (the highest target frequency the system is designed for is the high E at $329,63Hz$, also shown table 2 in section 2.2.2). Two cascaded low-pass stages cause a second order low-pass characteristic above the higher cut-off frequency ($497,98Hz$), so the harmonic components are much more suppressed as one low-pass stage would be able to.
The single frequency characteristics of the three stages don't interact with each other like pure passive networks would, because they are decoupled by the operational amplifiers.
The amplified and pre-filtered signal is directly connected to the input of the internal ADC of the μ-Controller (`ADC0` pin). Since the whole preprocessing components are referenced on the virtual ground voltage ($\approx 2,5V$) and the μ-Controller is able to sample values between $0V$ and $5V$, no additional decoupling is needed to measure the positive and negative alternations of the signal.
To enable data transfer, the programmable gain stages are connected to the `MOSI`[4] and the `SCK`[5] port of the μ-Controller. With additional independent chip select connections to each programmable amplifier ($\overline{\texttt{CS}} \rightarrow$ `PB3` and `PB4`), the μ-Controller is able to program the gain stages separately. For more information on this procedure see section 2.3.1.
Connector `CONN3` provides the ISP-Interface[6] for the μ-Controller and is used for updating and maintaining the software running on the chip without the need of disassembling. Due to the ISP-Interface uses the SPI protocol, some

[4] master-out-slave-in
[5] slave clock
[6] ISP = In-System-Programming

pins are connected to the same ports as the programmable gain amplifiers. Connector `CONN4` connects the hardware components of the interface with the main board and `CONN5` supplies the servo motor with power and command instructions (`OC1B`) from the μ-Controller.
Due to the high inrush current of the servo motor, the capacitor `C6` is needed to stabilize the supply voltage of the whole circuit. The $16MHz$ oscillating crystal is connected to its supposed ports `XTAL1` and `XTAL2` and `C5` is recommended to help the internal ADC to stabilize its reference voltage.

2.2 Pitch detection theory

There are many possible approaches to detect the pitch of the signal. In music theory the pitch is the subjective frequency like property of a tone, which is assigned by the human sense of hearing. Pitch and frequency are strongly related, but they are not equivalent. Whereas the pitch is a subjective opinion to categorize a tone, the frequency is a objective scientific property of a signal expressed by a value and its unit. In the following discussed approach(es) to detect the pitch, the pitch and the fundamental frequency of the sampled signal are assumed as equivalent. This assumption should lead to satisfying results even for trained musicians.

2.2.1 A resource saving frequency unit

Usually the unit of the frequency (in this application also the control parameter) is Hz. Its value is mostly determined by the inverse of the periodic time which is delivered by any chosen method. To calculate the periodic time within a discrete working system driven by a clock, also a division of a certain number of values between one period by the sample rate becomes necessary.

Additionally after determining the discrete values which represent the beginning and the end of a period, maybe some interpolation and averaging is needed to gain more accuracy.
All these calculations (interpolation, averaging, dividing by the sampling rate, calculating the inverse) costs additional time and are just transformations from a discrete number of samples to the well known unit Hz.

Since calculation resources are limited anyway, a new system-wide unit for the frequency, more precisely the periodic time was introduced: the number of samples within 4 periods. Hence, dividing by the sample rate and calculating the inverse become not needed anymore. This arrangement also makes interpolation unnecessary, since when speaking of one period the time between two samples divided by 4 can be distinguished. This trick has also the same effect like averaging 4 values (but without the dividing operation), so an accuracy which is high enough for the tuning process without the need to handle with decimal places is achieved.

2.2.2 Time and accuracy tradeoff

Before the different pitch detection methods are described, it has to be mentioned that special care has to be taken of running out of memory resources. A higher sampling rate means more accuracy, but also comes with more data to process. The chosen μ-Controller features an internal RAM of 2kB, whose usage has to be well-considered.
Because a control system has to be implemented, the time an update of the frequency information takes, is also an critical parameter. A tradeoff decision between accuracy, memory and speed has to be made.

The number of samples within 4 periods is an applicable control parameter for all further discussed methods to detect the pitch. Due to the minimal limit of the sampling rate (which is needed to provide accuracy without interpolating) and the necessary calculating time of a chosen method added to the time the controlling needs is too extensive to be finished in the time between two samples, it was decided to build a cycle of a measuring and a controlling task. The first task performs the recording of a part of the signal with simultaneously gaining the pitch information and the second one is doing the frequency tuning when the pitch is completely determined. After that, new samples are recorded and the cycle continues.

As a tradeoff of time, memory resources and accuracy a sampling rate of $8kHz$ was chosen. With this sampling rate a number of about 1000 samples can be recorded to gain the frequency information also comes with still having enough memory for other required tasks. For the three tuning modes which should be implemented (standard tuning, drop-d tuning, one-step-down tuning) 12 target notes are necessary. Table 2 shows these target notes together with their defined physical frequencies, the number of samples within 4 periods (@ a sampling rate of $8kHz$) and the error due to the representation in the introduced unit. The frequency values were taken from reference [5].
The gray marked rows are the notes which are used in one-step-down tuning, where notations on white background representing the standard tuning. Drop-D tuning consists of a low D tuned first string and standard tuning of the other five strings.
The representation error is shown in Hz and in *cent*. *Cent* is a unit which tries to model the human sense of hearing. The number of *cents* between two different tones which a human is able to distinguish, varies from human to human. According to the most people humans can distinguish $5-6$ *cents*, but for tuning a guitar an error of $5-6$ *cents* should be quite satisfying. As you can see in table 2 the representation of the frequency information in the

English notation	Frequency $[Hz]$	# samples within 4 periods @ $8kHz$	Representation error $[Hz$ / *cent*$]$
high E	329.628	97	0.269 / 1.412
high D	293.665	109	0.087 / 0.513
B (ger: H)	246.942	130	0.788 / 5.517
A	220	145	0.690 / 5.419
G	195.998	163	0.321 / 2.833
F	174.614	183	0.249 / 2.471
D	146.832	218	0.043 / 0.507
C	130.813	245	0.201 / 2.655
A	110	291	0.034 / 0.541
G	97.9989	327	0.140 / 2.464
low E	82.4069	388	0.067 / 1.414
low D	73.4162	436	0.022 / 0.512

Table 2: Table of all target notes

introduced unit should lead to very good results, because the error caused by this representation measured in *cents* is pretty low.

2.2.3 The signal

Since only the frequency information has to be extracted out of the signal and due to memory issues, it was decided to use just 8-bit values to represent the signal.

Figure 3 shows the recorded signal like it is sampled by the μ-Controller. To simulate different methods as realistic as possible, different guitars connected to the MIC input of the PC were recorded at a sampling rate of $8kHz$, followed by an amplitude quantization down to 8 bit using MATLAB®. About 12 different test signals of 4 different guitars were taken as a good base to develop a practicable pitch detection method. Figure 3 shows the oscillation of a correctly tuned low E string. It is clear to see, that the guitar signal doesn't consist of just a single sine wave.
Many methods to detect the pitch of the guitar signal try to gain the frequency information by determining an oscillation whose frequency is equal to the frequency of the fundamental oscillation and extracting the number of samples within one period by detecting zero crossings. Some methods to determine this oscillation are described in the following sections.

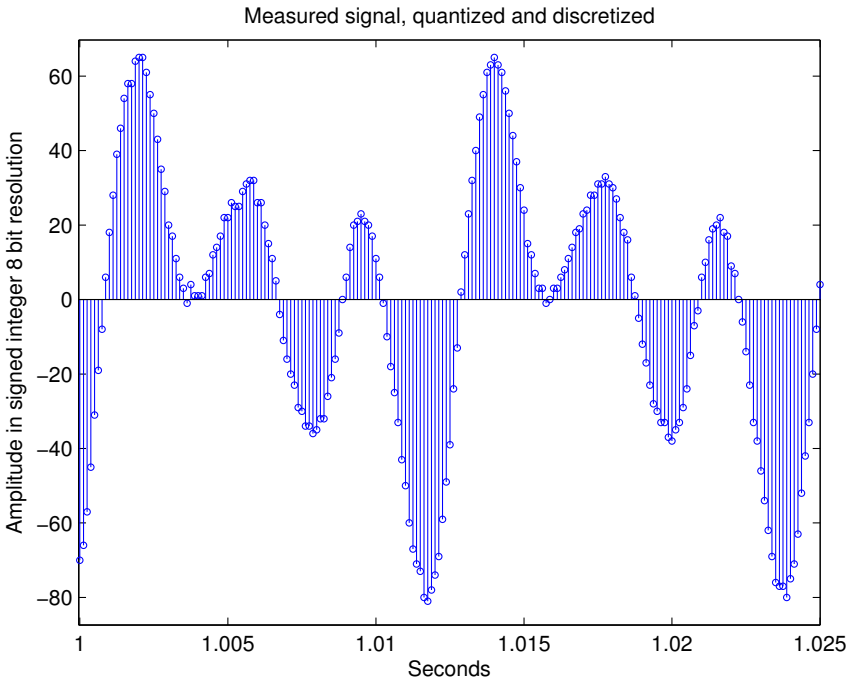

Figure 3: Signal sampled at $8kHz$

2.2.4 Pure Zero Crossings

This method tries to determine zero crossings without any previous calculations. As you can see in the plot of the test signal, the oscillation of a guitar string and the resulting voltage signal contains in addition to the fundamental frequency many harmonic oscillations, which makes the approach to count the zero crossings of the pure signal unusable. Also other threshold values than zero have been tried, but a working threshold was very difficult to determine and different for each test signal, even within areas of a single test signal. This method was rejected because of robustness reasons.
Detecting the zero or threshold crossings will constitute the final step of the following frequency detection methods. Therefore also the edge direction of the signal will be considered.

2.2.5 Autocorrelation

Another more promising method is the autocorrelation function. The strength of this function is to point out periodic components very well, even if the signal is noisy or the amplitudes of the harmonic oscillations are quite distinctive.

The formula to calculate the autocorrelation function is

$$R_{xx}(\tau) = \lim_{N\to\infty} \frac{1}{N} \sum_{n=0}^{N-1} x_n \cdot x_{n-\tau}$$

where x_n is the recorded signal and N is the length of the signal. Since the system operates with discrete finite signals, a condition for the signal boundaries has to be defined. In this application $x_n = 0 : n < 0,\ n > N-1$ was chosen, because enough samples are taken and this constraint prohibits from additional calculation effort, which would require more resources.

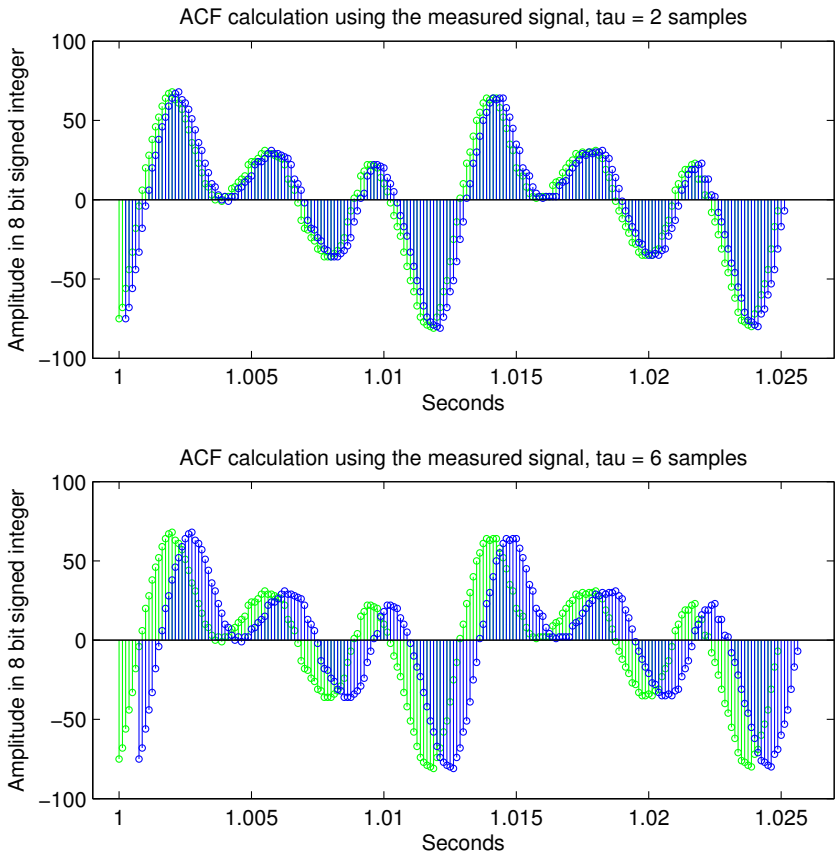

Figure 4: Illustration ACF-calculation

Figure 4 shows a graphical demonstration how to calculate the ACF (autocorrelation function) $R_{xx}(\tau)$ for 2 values ($\tau = 2; \tau = 6$). To generate this plot, the signal of figure 3 was used as input signal. To calculate one value of the ACF, all overlapping values of the green function and the blue function shifted by τ are point-wise multiplied and accumulated. The sum is then

divided by the number of samples to normalize the result. In this illustration the whole signal consists of about two periods, in practice the number of samples is much higher (like about one thousand samples as mentioned before).

Unfortunately the calculation task of the ACF is very tough for the calculation capability of the chosen μ-Controller and each value of the autocorrelation function depends on the whole signal, that means before the first data point of the ACF can be determined, the recording of the full signal must be finished. This circumstance would lead to a long frequency detection delay, which would be very difficult to handle for the controlling task.

Hence an approach which uses just a part of the signal for one value of the autocorrelation function was developed. Much less calculations are needed when only a small amount of samples is used to "slide" over the whole signal. This so called partial autocorrelation function should also fulfill the same characteristics of the full autocorrelation function. Of course this small amount of samples should be at least greater than the samples within one period. When a lowest frequency to detect of about $70Hz$ is assumed, the number of samples to represent one period at a sample rate of $8kHz$ is

$$\frac{\text{sample rate}}{\text{frequency}} = \frac{8000Hz}{70Hz} \approx 114 \; samples$$

So a sliding signal of 120 samples was chosen. This signal always covers areas where the full signal is defined. Hence, no boundary condition is necessary. Assuming the length of the sliding signal is L, when starting at $\tau = 0$ (where the first value of the sliding part of the signal overlaps with the first value of the full signal) and ending at $\tau = N - L$ (where the last value of the sliding signal values overlaps with the last value of the full signal), we get a partial autocorrelation function which consists of $N - L + 1$ values.
This method can also be interpreted as a cross correlation of a part of the signal with the signal itself. Using just a part of the signal for one multiplicand, changes the formula of the autocorrelation as follows

$$R_{x_p x}(\tau) = \frac{1}{L} \sum_{n=\tau}^{L-1+\tau} x_n \cdot x_{n-\tau} \qquad 0 \leq \tau \leq N - L$$

where x is the full recorded signal, $x_{n-\tau}$ indexes the sliding part of the signal, L indicates its length (120 samples) and N is the length of x.

Figure 5 shows a illustration how this approach works. In practical application the full signal (the green colored values) consists of much more values than the sliding part of the signal (about 9 times).

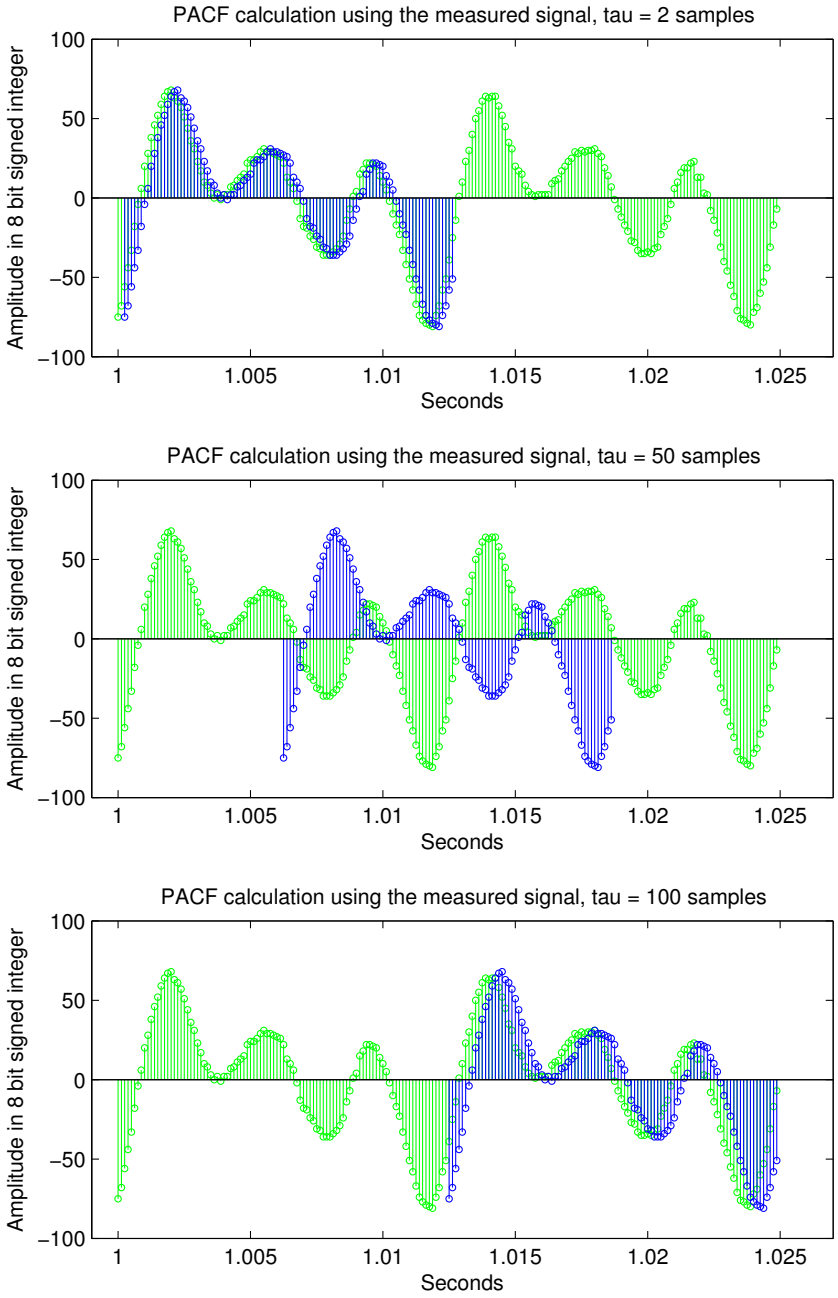

Figure 5: Partial ACF-calculation

The big advantages gained by using this method are a much less number of multiplications to compute and the ability to calculate values of the PACF function even if the signal isn't completely recorded. This leads to much more efficient usage of time, memory and processing resources.

Table 3 illustrates how values of the PACF function can be calculated, even if the recording process hasn't been finished.
Assuming a sliding signal size of $L = 5$ samples, the first value of the PACF ($R_{x_p x}(0)$) equals the sum of the products of $x_{0..4}$ and $x_{0..4}$, ($n = 0..4$). After the first L samples, the calculation of $R_{x_p x}(0)$ is done. The next value $R_{x_p x}(1)$ is calculated by summing up the products of $x_{0..4}$ and $x_{1..5}$ ($n = 1..5$), and so on.
To use the time resources as efficient as possible, the calculation of the required products can be performed during the waiting periods between two samples. When the first value is sampled, it can be multiplied by itself. Since each product is just needed once, it's unnecessary to save them. The first product is stored in an cleared accumulator variable of a size of 32-bit (to prevent overflow effects). When the second value is sampled, two products which are necessary for the PACF value can be calculated. x_1 times x_1 will be added to the first accumulator variable, and x_0 times x_1 will be the content of a second accumulator variable. When the third value is sampled, 3 products can be determined and so forth. Due to this procedure the time resources are used optimally. When L values are sampled, the first accumulator variable contains the result of $R_{x_p x}(0)$. After checking for zero crossings, this result becomes unimportant and the variable is free for reset and reuse. Hence just L accumulator variables are needed for the whole algorithm, so this method is quite memory resources saving.
The procedure of sampling the signal and calculating the PACF simultaneously leads to following pseudo code:

```
PACF[0..L-1] = 0 //accumulator variable array
for n = 0:N-1
   x[n] = getNextValue()
   for i = 0:min(n,L-1)
     idx = (n - i) mod L
     PACF[idx] += x[i]*x[n]
   end
   if n >= L-1
     checkForZeroCrossing(PACF[idx])
     PACF[idx] = 0
   end
end
```

	n									
x	0	1	2	3	4	5	6	7	8 ...	$N-1$
0	x	o	x	o	x	o	x	o	x	o
1		o	x	o	x	o	x	o	x	o
2			x	o	x	o	x	o	x	o
$n-\tau$ 3				o	x	o	x	o	x	o
4					x	o	x	o	x	o
:				$R_{x_p x}$	(0)	(1)	(2)	(3)	(4)	..$(N-L)$
$L-1$										

Table 3: Calculation table of the optimized PACF

To save additional processing resources, it was passed on normalizing the resulting PACF, because we are just interested on detecting zero crossings.

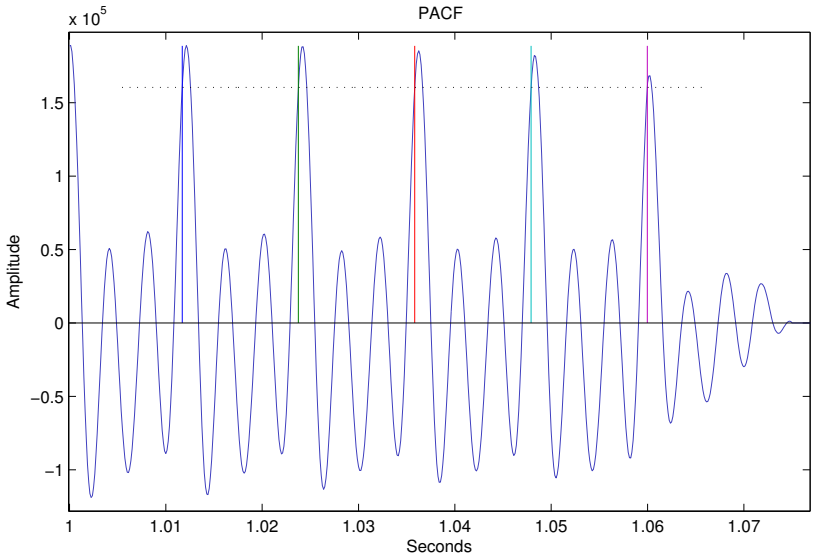

Figure 6: Resulting partial autocorrelation function

Performing the described calculations on a tuned low e string (see figure 3) leads to the function which is shown in figure 6. (This function representing the PACF is still a discrete function, it is just plotted as connected line diagram to illustrate the threshold crossings described underneath.) The test signal was contaminated by white Gaussian noise with a signal to noise ratio (SNR) of $40dB$.

It is clear to see, that there are still harmonic components indicated by a lower amplitude in the function. So detecting the zero crossings would lead to wrong frequency results. The pitch of the signal is represented by significant higher amplitudes. So a threshold whose value is proportional to the highest value of the PACF is used. The pitch is detected by the threshold crossings with respect to the edge of the PACF. Because the amplitude of the pure signal is not expected to change within 4 periods, the maximum of the PACF is assumed to equal the first value of $R_{x_p x}(\tau)$ at $\tau = 0$. At this point the signal is correlated by itself and is expected to cause the highest value for the correlation function.
Different trials showed, that a threshold whose value equals 85% of the first value gives the most robust results.
In figure 6 the threshold is represented by the dotted black line and its crossings are indicated by vertical colored lines. Since the calculation of the PACF is canceled when its value crosses the threshold the fifth time, the last ridge which crosses the threshold looks lower than the others. Continuing the calculation of the PACF would cause a similar ridge as those which occur after the first four threshold crossings. Canceling the calculation doesn't effect the result, because the checking for threshold crossings is executed for finished values only. That means, that in figure 6 the first value after the fifth threshold crossing is the last finished one, the subsequent values equal the unfinished accumulator states.

Although this method looks quite robust and the calculation effort is reduced to a minimum, there is a more efficient and accurate method to calculate the pitch of the signal. Due to the harmonic components which are still included in the PACF, the resulting frequency information can be influenced by these components and can cause critical inaccuracy.

2.2.6 Digital Filters

The autocorrelation points out periodic components of the input signal by analyzing the unchanged measured values. The approach to use digital filters tries to manipulate the signal in a way, that there is just the fundamental frequency left. After that filtering, a zero crossing detection should lead to the pitch information.
There exist many types of digital filters. The two major groups are finite impulse response filters (FIR-filters) and infinite impulse response filters (IIR). The result of a FIR filter is calculated by a linear combination of a finite number N of past input values, whereas IIR filters also take past output values into account. FIR filters require usually much more multiplication and storage elements to determine the filtered signal. N is also called the order these filters. The filter operation of a FIR filter can be mathemati-

cally described using equations 7 and 8, where x is the input signal, y is the output signal and b_k are the filter coefficients.

$$y[n] = b_0x[n] + b_1x[n-1] + b_2x[n-2] + ... + b_Nx[n-N] \quad (7)$$

$$= \sum_{k=0}^{N} b_kx[n-k] \quad (8)$$

Represented as block diagram, a FIR filter looks like shown in figure 7. The memory elements are shown as z^{-1}, due to the representation of delay elements after the z-transformation.

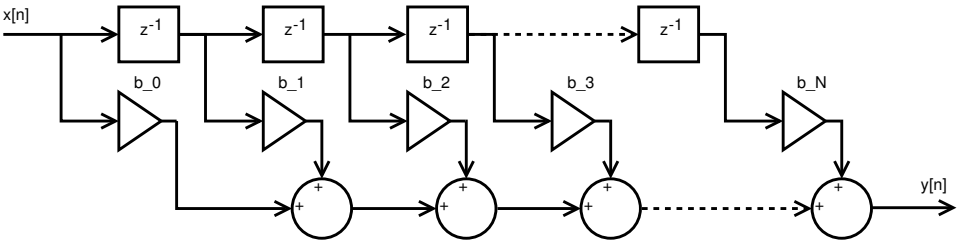

Figure 7: Block diagram of a FIR-filter

To design useful filters for this application, a FIR filter would need too much multiplication and storage resources. The advantage of FIR filters is that the calculation task can be massively parallelized if there are enough calculation units available like in a digital signal processor (DSP).
In case of a single core processing unit like the ATMEGA 32, it is much more efficient to use an IIR filter. The output function of this type of filter can be mathematically described as follows (9). In addition to the FIR filter the output filter coefficients a_k are introduced.

$$\begin{aligned} y[n] = &- a_1y[n-1] - a_2y[n-2] - ... - a_Ny[n-N] \\ &+ b_0x[n] + b_1x[n-1] + b_2x[n-2] + ... + b_Nx[n-N] \end{aligned} \quad (9)$$

Again, N defines the order of the IIR filter. To design similar filter characteristics as known FIR filters, the order of the IIR filters can be much lower. This is the advantage of IIR filters for systems with limited resources. An IIR filter with order $N = 2$ is called "biquad filter", which is already a very powerful construct. Equation 10 describes the calculation for a biquad filter, which is quite simple.

$$y[n] = -a_1y[n-1] - a_2y[n-2] + b_0x[n] + b_1x[n-1] + b_2x[n-2] \quad (10)$$

This formula can be illustrated as a block diagram in the z-domain too, shown in figure 8. This form is called the direct form 1.

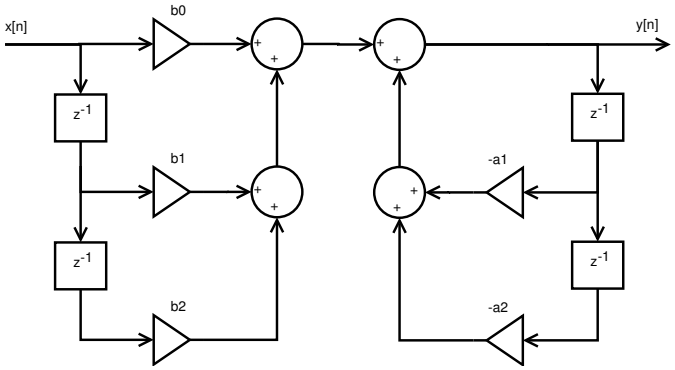

Figure 8: Block diagram of a biquad filter: direct form 1

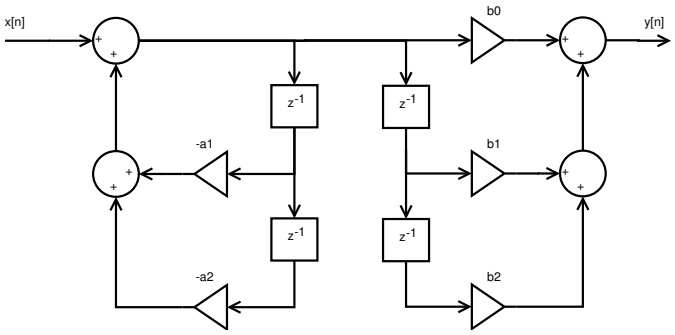

Figure 9: Block diagram of a biquad filter: switched stages

The block diagram can be seen as a transfer function in the z-domain which consist of two parts. The part which determines the linear combination of the input values and the b_k coefficients, is called $H_B(z)$. The other part is called $H_A(z)$, respectively. According to the commutative law for Z-transfer functions ($H(z) = H_B(z) \cdot H_A(z) = H_A(z) \cdot H_B(z)$), the parts of the block diagrams can be switched which leads to the illustration showed in figure 9.

Now it is clear to see, that the horizontal neighbored memory blocks contain always the same value. So these blocks can be replaced by one, shown in figure 10. This constellation of the elements in the block diagram is called direct form 2.

To save additional memory resources, biquad filters of the direct form 2 are used in this application.

As powerful and flexible the biquad filters are, their magnitude response is too flat to extract the fundamental frequency of a guitar string oscillation and simultaneously suppress the harmonic components completely. In

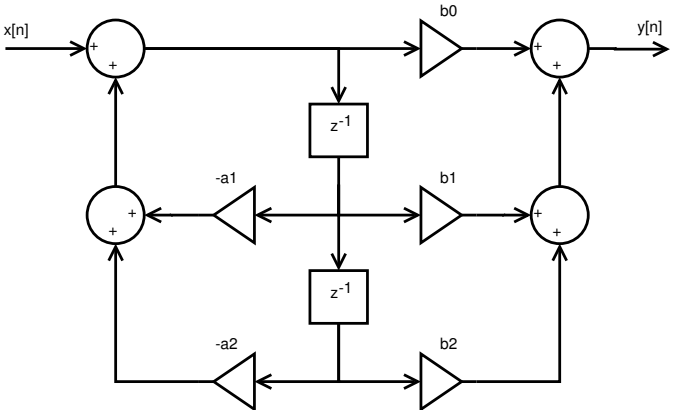

Figure 10: Block diagram of a biquad filter: direct form 2

respect to the 8 bit signed integer representation of the measured values (-128 to 127), a harmonic component suppression of about $-40dB$ is desired. To achieve this constraint, higher ordered digital filters or a cascade of biquad filters can be used. Since the filters have to be implemented on a 8-bit architecture, it was decided to use cascaded biquad filters, because these constructs are much more immune to stability issues than higher ordered filters. Figure 11 shows the so called second-order-sections filter (SOS filter), which consists of a cascade of two biquad filters.

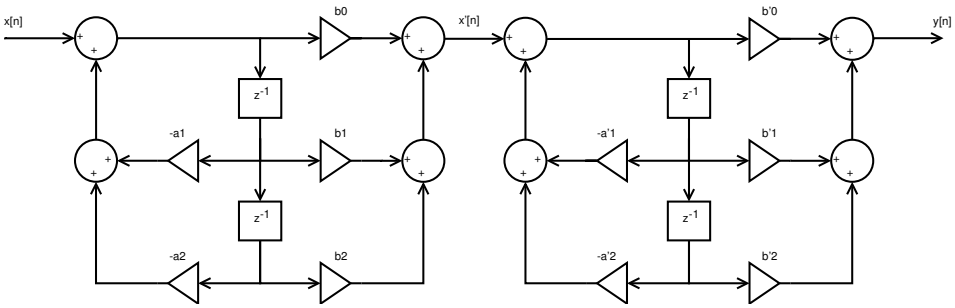

Figure 11: Block diagram of a second-order-section filter

After deciding which filter architecture is applied, the different filters can be designed. To extract the fundamental frequency for the different target frequencies as accurate as possible, for each target frequency one specialized filter is needed. These filters are supposed to suppress the harmonic components about $40dB$ at least and have their maximum magnitude responses at the corresponding target frequencies. The major problem of such specialized filters is the difficulty to detect frequencies which are not in the small frequency band around the target frequencies. To ensure this functionality, also some generalized filters are necessary. The decision was made, that one

generalized filter should cover the expected frequency range of one string. To choose the best filter for the actual fundamental frequency, filter boundaries are defined. If the current detected frequency crosses such a boundary, the recorded values of the next cycle are processed with the filter corresponding to that next frequency band.
Figure 12 shows a screenshot of the filter design and analysis tool ("fdatool") of MATLAB®. Aided by this tool, 12 specialized and 6 generalized second-order-section filters have been designed.

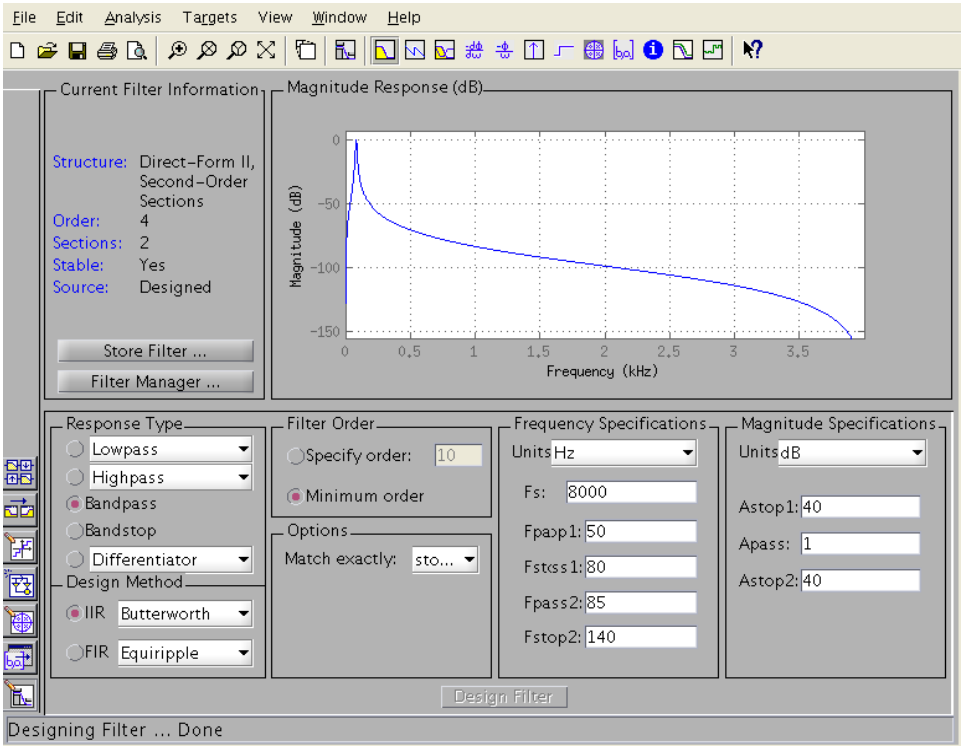

Figure 12: Designing the SOS-filters using "fdatool" in MATLAB®

The magnitude responses of the designed filters are illustrated in figure 13. The black dashed lines represent the generalized filters, the blue lines indicate the specialized filters for the standard tuning and the magenta lines extended with the yellow line show the magnitude response for the specialized filters for the one-step-down tuning. For drop-D tuning the yellow drawn filter and the five most right aligned blue lined filters are used. The threshold boundaries between the generalized filters were defined at their crossing points and the boundaries of the specialized filters were defined at their undercut of the $-3dB$ threshold.

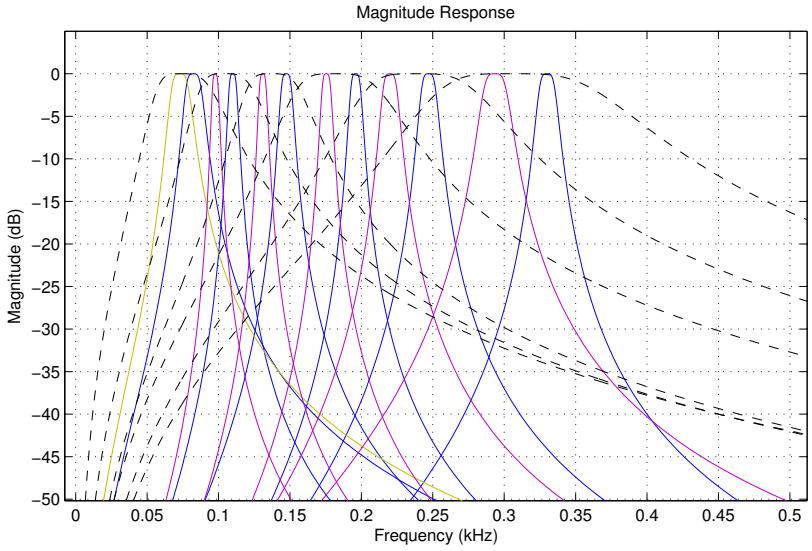

Figure 13: Magnitude response of used filter bank

2.2.6.1 Representation of numbers A critical issue of working with IIR filters is always the stability. Their filter coefficients consist usually of numbers with many decimal places. The designed filters can become unstable easily, if too much rounding errors are made. Due to the missing floating point functionality of the μ-Controller, special care has to be taken to the representation of numbers. To be able to represent numbers between 0 and 1, a fixed decimal point is introduced. This is a common method to represent decimal numbers, when digits are limited.
For example in a binary numbering system of 8 bit, the usual number representation looks like shown in table 4. The highest (unsigned) number which can be represented is 255 (sum of the worth row).
If a 2 bit fix point representation is defined per convention, the worth of each bit equals the values shown table 5. The highest number which can be represented now decreases to 63.75, but a decimal resolution of 0.25 is achieved.

bit number	7	6	5	4	3	2	1	0
worth	2^7	2^6	2^5	2^4	2^3	2^2	2^1	2^0
	128	64	32	16	8	4	2	1

Table 4: Standard 8 bit number representation

The chosen μ-Controller can handle a maximum of 32 bit per variable. First of all a decimal point after the 16^{th} digit was introduced. This enables to

bit number	7	6	5	4	3	2	1	0
worth	2^5	2^4	2^3	2^2	2^1	2^0	2^{-1}	2^{-2}
	32	16	8	4	2	1	0.5	0.25

Table 5: 8 bit number representation using 2 bits as decimal digits

distinguish values with a resolution of

$$2^{-16} = \frac{1}{2^{16}} \approx 0.00001526,$$

which is small enough to ensure stability of the filters. Unfortunately choosing the 16$^{\text{th}}$ digit to represent "1" implies, that there are just 16 bits left to represent higher numbers. So choosing the 16$^{\text{th}}$ digit reduces the range of 32 bit signed integer numbers from

$$-2^{31} \ldots 2^{31} - 1 = -2.147.483.648 \ldots 2.147.483.647$$

to

$$-2^{16} \ldots 2^{16} - 1 = -65.536 \ldots 65.535.$$

This smaller range seems to be sufficient for the coefficients and the filtered signal values, but not for the multiplication operation. Assuming a convention of 2 binary decimal places like in table 5, an integer number can be transformed from the standard convention as shown in table 4 to this new numbering format by shifting its binary value 2 digits to the left. In a binary system this equals a multiplication operation with 4 (2^2). To perform a multiplication of two values in this fixed decimal point representation, the result was implicitly multiplied by $2^2 \cdot 2^2 = 16$. Hence the result has to be shifted back to the right by the defined number of decimal digits. So even if the result of the multiplication fits in this range, the intermediate result before the right shift operation may not. Indeed, some intermediate calculation results exceed this range when placing the virtual decimal point after the 16$^{\text{th}}$ digit, which causes again instability as a result of bit overflow. Simulations showed, that these intermediate calculations require often 20 bits to represent the result in binary representation. So the decimal point was placed after the 20$^{\text{th}}$ bit. The number of remaining bits ($32 - 20 = 12$) leads to a resolution of

$$2^{-12} = \frac{1}{2^{12}} \approx 0.0002441$$

which is still small enough to save stability, if the filter coefficients of the cascaded filters vary at least a certain value. This is the reason for some specialized filters represented in figure 13 covering a wider frequency band than others. Defining the decimal point after the 20$^{\text{th}}$ bit leads to a range for signed integer values of

$$-2^{20} \ldots 2^{20} - 1 = -1.048.576 \ldots 1.048.575.$$

2.2.6.2 Evaluation of the filtered signal After providing the 12 bit fixed-point convention to be able to calculate the filtered output signal, the result has to be evaluated. Figure 14 shows the filtered signal of the MATLAB® simulation calculated according to figure 11, using the filter coefficients of the specialized filter for the low E string. To generate this plot, the same input signal (tuned low E) of the demonstration of the PACF (figure 6) was used. As done in figure 6, the signal is plotted as connected line diagram to point out the shape of the output signal, but it still consists of discrete values. To model the the limited capacities of the μ-Controller, also the 12 bit fixed-point representation was implemented in the simulation. In figure 14 the whole plot was clipped to the range of about one recording cycle consisting of 1000 values.
As the filters are designed to suppress all harmonic components, detecting the zero crossings will offer the frequency information of the fundamental oscillation. Due to the introduced system-wide periodic time unit, just the number of samples between 5 zero crossings has to be determined.

Before every recording cycle, the storage elements of the SOS filter have to be reset to zero. Hence the filter needs some samples to establish the full amplitude in each cycle. Due to this and possible additional information delay, only the samples between the last 5 determined zero crossings are taken into account. In this implementation the falling edge is considered, but there is no special reason for that. The rising edge could be used as well.
In the example shown in figure 14 the detected samples within 4 periods would be $97 + 97 + 97 + 98 = 389$, so the string is tuned slightly too low (should be 388, according to table 2).

Figure 15 shows the same signal as plotted in figure 14 filtered by the generalized filter for the first string. The rough and non sinusoidal establishment of the full amplitude and the variance of the number of samples between two zero crossings of the falling edge indicate, that there are still harmonic components in the signal. This is quite plausible when looking at the magnitude response of the filter (see figure 13). Determining the frequency information would retrieve $97 + 97 + 97 + 96 = 387$, a slightly hearable varying result as above. Hence, the introduction of specialized filters is quite advantageous and reasonable.

Figure 16 shows the filtered signal of a D string filtered by the specialized filter for standard D. The number of samples within two zero crossings is varying between 54 and 55, but is mostly 55. This depends on the discretization. When a value was sampled right after the afterwards detected zero crossing, there is more change that the 55^{th} sample also falls into this period. Statistically the number of samples in one period of 54 and 55 have

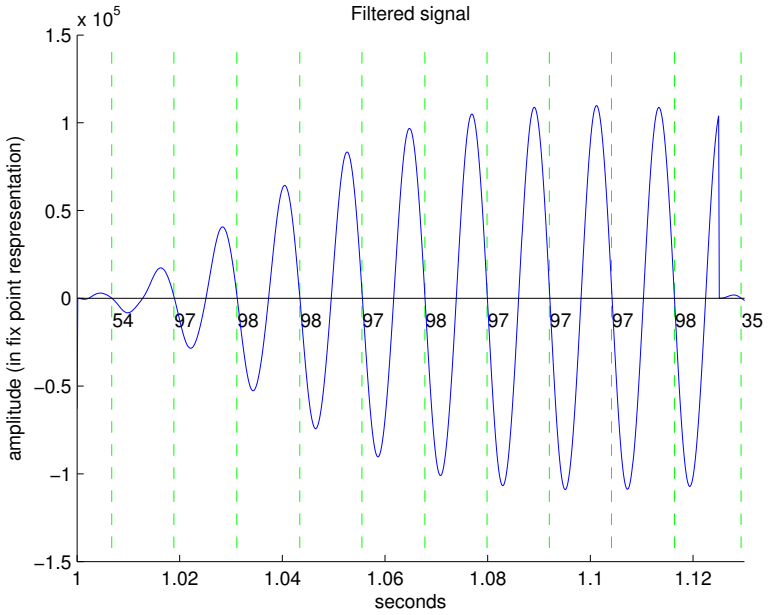

Figure 14: Evaluation of the filtered signal

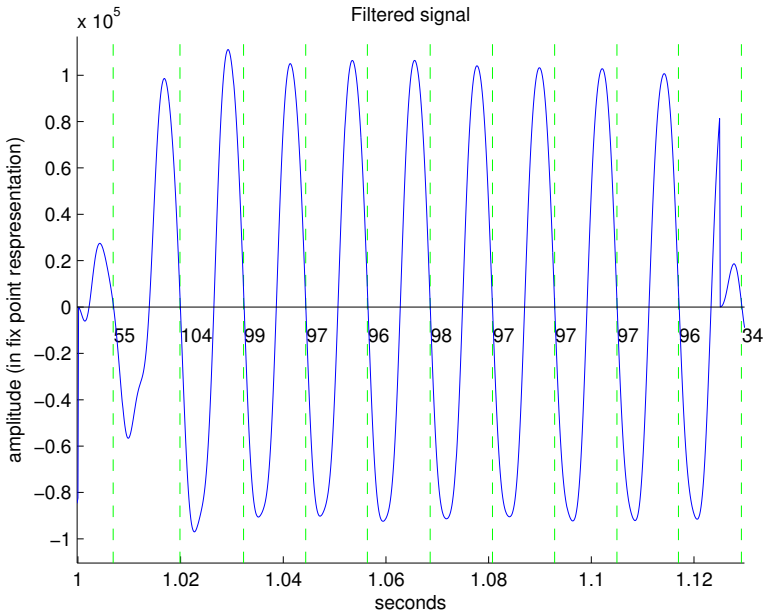

Figure 15: Evaluation of the filtered signal

to be equal when sampling a correctly tuned D string. (As you can see in table 2, the number of samples within 4 periods should be 218 on a tuned string. To get this value when evaluating the samples between 5 zero crossings, there has to be $55 + 54 + 55 + 54 = 218$ or a similar constellation.) In figure 16 there would be determined $55 + 55 + 55 + 54 = 219$ samples as frequency information, which indicated that the string is tuned also slightly too low. This minimal divergence is pointed out by the introduced unit, because counting the number of samples within 4 periods implies an average determination. This example shows how sensible the introduced unit is, even without decimal places.

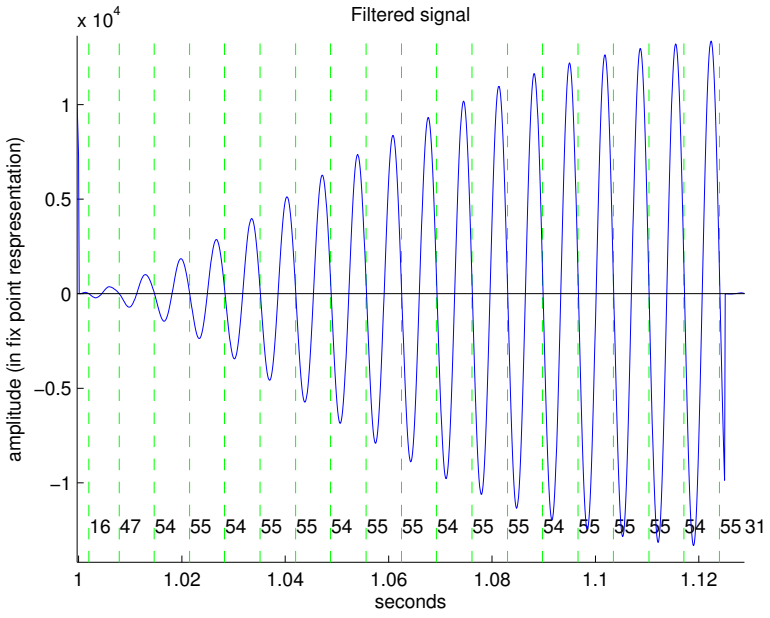

Figure 16: Evaluation of the filtered signal

2.2.6.3 String detection method for digital filters The major disadvantage of digital filters compared to the (partial) autocorrelation function is that there has to be some information about the frequency before starting the calculation. Without this additional information, the wrong filter could be chosen which leads to extracting a harmonic component of the signal instead of the fundamental frequency.
An approach which would work pretty sure, is to detect the first frequency information using the autocorrelation function the first time. But it was decided, that this approach would lead to unnecessary high effort for distinguishing between only six frequency intervals. Hence a method to select the first generalized filter was developed which takes advantage of the high

quantity of taken samples. As the analysis process of the partial autocorrelation, the number samples between threshold crossings are evaluated. But unlike the approach using the autocorrelation function, the unprocessed input signal is evaluated.
To manage the quantity of the expected threshold crossings, a voting scheme was introduced. Each voting bin corresponds to one string. To evaluate a vote, the number of samples between each fifth threshold crossing is counted. Therefore the borders of the generalized filters can be used as voting bin borders. For instance if the counted number of samples lies between the two borders of the generalized filter of the fourth string, the voting bin of the fourth string is incremented by 1.
85% of the biggest value of the input signal is used as threshold. After evaluating all numbers of samples between every firth threshold crossing, the temporary detected frequency is set to the mean of the standard and the one-step-down target frequency of the string which got the most votes. So the filter choosing algorithm will use the generalized filter for the string which got the most votes.

Figure 17 shows the voting result of 4 different strings tuned correctly in standard tuning. For this simulation a Gaussian white noise with a signal to noise ratio (SNR) of $40dB$ was added.

Figure 18 shows the voting result of the same 4 input signals of figure 17 without the white Gaussian noise. All strings, noisy or not, were determined correctly, so this simulation indicates that the introduced voting scheme is a well working and resource saving method to choose the first generalized filter.

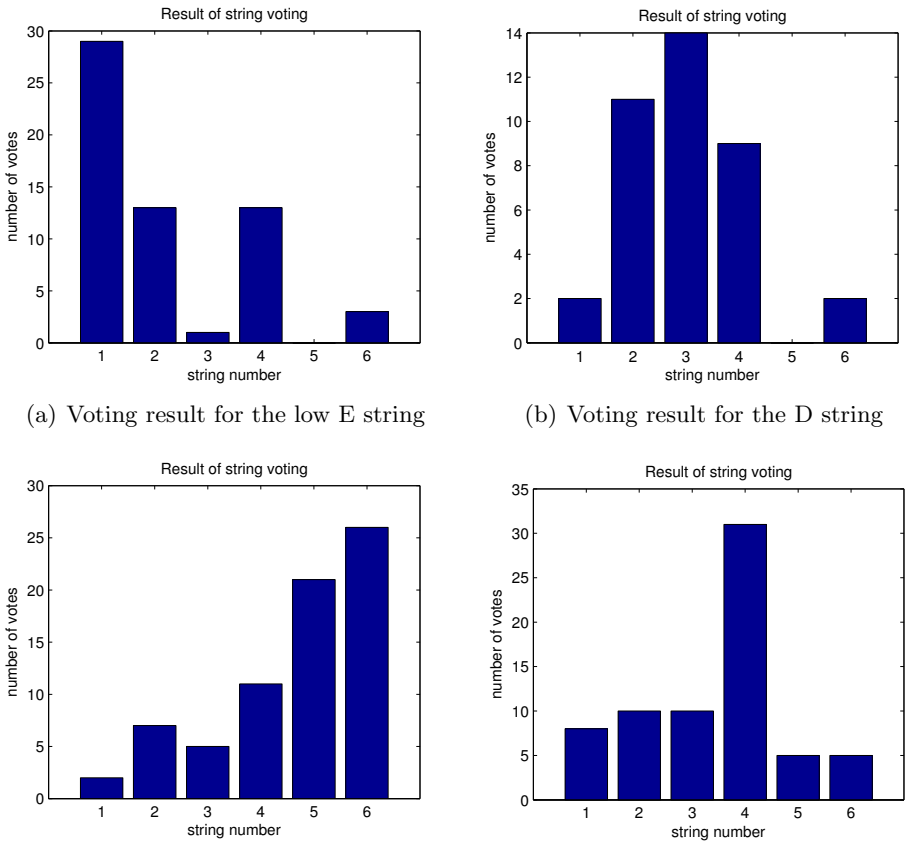

(a) Voting result for the low E string

(b) Voting result for the D string

(c) Voting result for the high E string

(d) Voting result for the G string

Figure 17: Voting results of different strings with white Gaussian noise of 40dB SNR

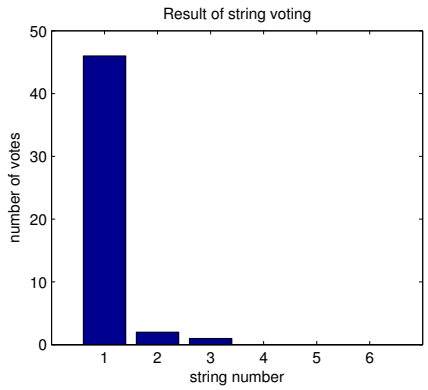

(a) Voting result for the low E string

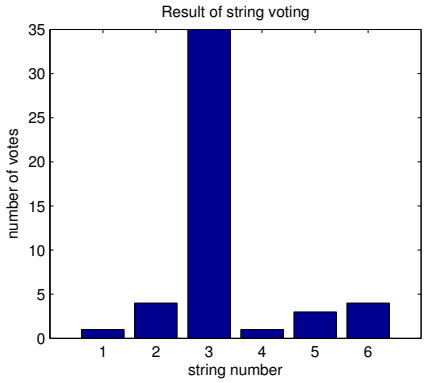

(b) Voting result for the D string

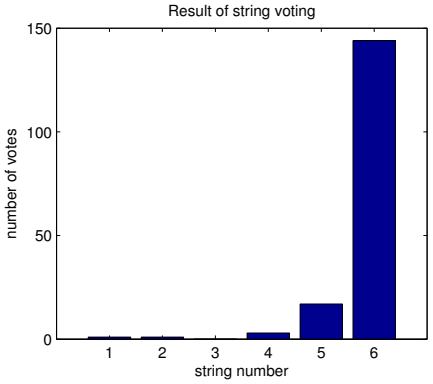

(c) Voting result for the high E string

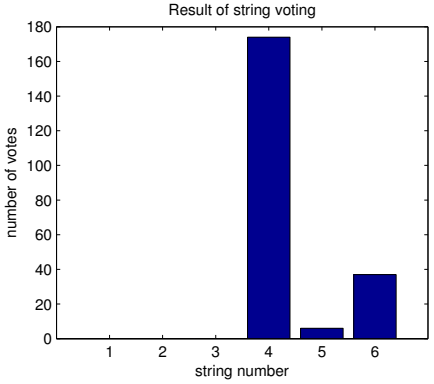

(d) Voting result for the G string

Figure 18: Voting results of different strings of the unaffected recorded signals

2.3 Implementation

This chapter describes how the required tasks of frequency detection are realized using different physical components in a more practical view.

2.3.1 Programming the gain stages[2]

The programmable amplifiers MCP6S21 from Mircochip® are programmed via the SPI-module. This protocol uses the master-slave concept and separate sending and receiving ports for data transfer. Thus full duplex connections are possible, that means that data can be sent and received at the same time. If a component has to be configured as master or as slave, depends on its functionality and on the application. Even the μ-Controller itself could be configured as slave to receive instructions and the (SPI-)clock for example from another μ-Controller.
The SPI bus consists of following wires

- `MOSI` ... Master Out - Slave In, for serial data transfer from the master to the slave
- `MISO` ... Master In - Slave Out, for serial data transfer from the slave to the master
- `SCK` ... slave clock (controlled by the master), for synchronizing the data transfer

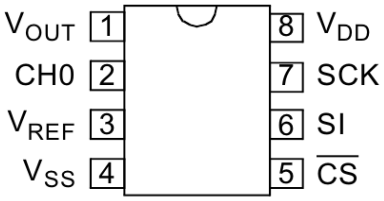

Figure 19: MCP6S21 pin configuration[2]

Figure 19 shows the pin configuration of the MCP6S21 programmable gain amplifier. The positive supply voltage is connected to V_{DD} and the negative to V_{SS}. V_{REF} defines the reference voltage of the internal non inverting amplifier. This pin is connected to the generated virtual analog ground. `CH0` is supposed to carry the input signal of the amplifier and V_{OUT} the amplified output signal. For more details how to connect the pins of each chip for this application, see chapter 2.1.4.
The remaining pins `SCK`, `SI` and $\overline{CS}$ are necessary for programming the gain factor of the amplifier. The MCP6S21 can only operate in slave mode. So

the SCK pins of the μ-Controller and the chip were connected, and the SI[7] pin has to be connected to the MOSI port of the μ-Controller. To initiate communication to the chip, the $\overline{\text{CS}}$[8] pin has to be set to digital ground and is directly connected to an output port of the μ-Controller. Each chip gets its own output port for the $\overline{\text{CS}}$ pin. Hence the two chips can be programmed independently.
After setting the $\overline{\text{CS}}$ pin to LO, the MCP6S21 expects a 16-bit instruction word, consisting of two 8 bit values. The first 8 bit value define the content of the instruction register.

REGISTER 5-1: INSTRUCTION REGISTER

W-0	W-0	W-0	U-x	U-x	U-x	U-x	W-0
M2	M1	M0	—	—	—	—	A0
bit 7							bit 0

bit 7-5 **M2-M0: Command Bits**
000 = NOP (Default) **(Note 1)**
001 = PGA enters Shutdown Mode as soon as a full 16-bit word is sent and $\overline{\text{CS}}$ is raised. **(Notes 1 and 2)**
010 = Write to register.
011 = NOP (reserved for future use) **(Note 1)**
1XX = NOP (reserved for future use) **(Note 1)**

bit 4-1 **Unimplemented:** Read as '0' (reserved for future use)

bit 0 **A0: Indirect Address Bit**
1 = Addresses the Channel Register
0 = Addresses the Gain Register (Default)

Note 1: All other bits in the 16-bit word (including A0) are "don't cares".
2: The device exits Shutdown mode when a valid command (other than NOP or Shutdown) is sent and $\overline{\text{CS}}$ is raised; that valid command will be executed. Shutdown does not toggle.

Legend:			
R = Readable bit	W = Writable bit	U = Unimplemented bit, read as '0'	
-n = Value at POR	'1' = Bit is set	'0' = Bit is cleared	x = Bit is unknown

Figure 20: Screenshot of the MCP6S21 datasheet[2]: Instruction register

Figure 20 shows a screenshot of the datasheet of the MCP6S21 which describes the possible instructions recognized by the chip.
In our application only the "write to the gain register" command configuration is used. Because the MCP6S21 has only one input channel, setting the channel is not necessary. Also the shutdown functionality is not used. So according to figure 20, the instruction register has to be set to 0x40 for reconfiguring the gain.

The second 8 bit value of the 16 bit instruction word defines the new value of the gain register. Figure 21 shows all possible gain configurations and

[7] Slave In
[8] (inverted) chip select

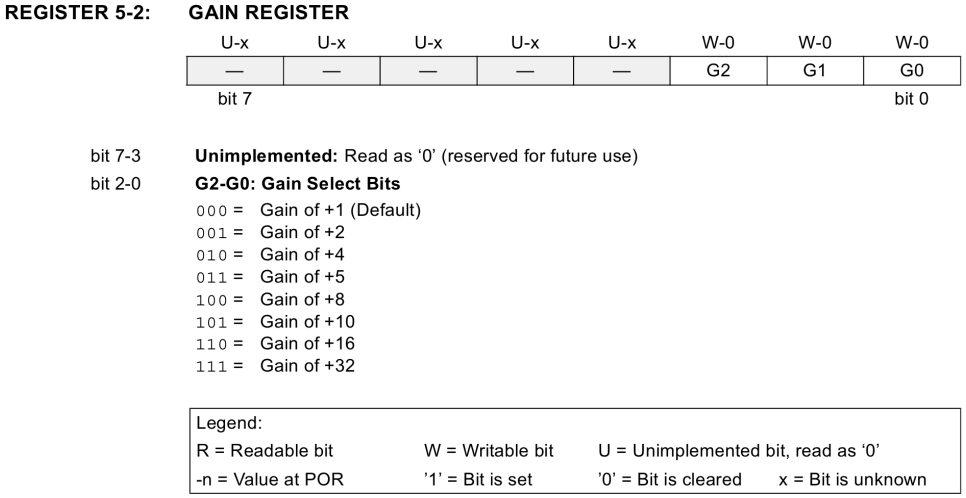

REGISTER 5-2: GAIN REGISTER

U-x	U-x	U-x	U-x	U-x	W-0	W-0	W-0
—	—	—	—	—	G2	G1	G0
bit 7							bit 0

bit 7-3 **Unimplemented:** Read as '0' (reserved for future use)

bit 2-0 **G2-G0: Gain Select Bits**

000 = Gain of +1 (Default)
001 = Gain of +2
010 = Gain of +4
011 = Gain of +5
100 = Gain of +8
101 = Gain of +10
110 = Gain of +16
111 = Gain of +32

Legend:			
R = Readable bit	W = Writable bit	U = Unimplemented bit, read as '0'	
-n = Value at POR	'1' = Bit is set	'0' = Bit is cleared	x = Bit is unknown

Figure 21: Screenshot of the MCP6S21 datasheet[2]: Gain register

how they are decoded.

To send the two bytes which are necessary to program one amplifier, the build in SPI module of the μ-Controller can be used. Before using, it has to be enabled in the course of an initialize sequence. Listing 1 shows the initializing of the SPI module. This code sequence sets the data direction registers (`DDR`) of the pins which are used for the communication to output mode, sets the $\overline{\texttt{CS}}$ pins to HI and configures the SPI module of the μ-Controller by setting 3 flags of the SPI control register (`SPCR`):

- `SPE` ... serial peripheral enable: to enable the SPI module
- `MSTR` ... Master/Slave select: defines the role of the μ-Controller as master
- `SPR0` ... SPI clock rate select: together with the `SPR1` flag set to zero, a clockrate of $1MHz$ ($f_{OSC}/16$) is defined for the SPI bus

```
1 //set mosi and sck, cs0, cs1 as output
DDR_SPI = (1<<DD_MOSI) | (1<<DD_SCK) | (1<<SPI_CS0) | (1<<
    SPI_CS1);
3 //set chips inactive
SPI_PORT |= (1<<SPI_CS0) | (1<<SPI_CS1);
5 //enable SPI, master, set clock rate fck/16
SPCR = (1<<SPE) | (1<<MSTR) | (1<<SPR0);
```

Listing 1: Initializing the SPI module of the μ-Controller

To send the first byte of the 16 bit instruction word after pulling the $\overline{\texttt{CS}}$ pin to LO, the byte to send has to be written in the SPDR[9] of the μ-Controller. When updating this register, the data transfer is performed automatically. After the transfer is finished, the SPIF[10] flag is set.

Listing 2 shows the program code of the function which performs the programming of both amplifiers. As argument it expects the gain code of both amplifiers combined in one byte. This gain code consists of two 4 bit codes according to figure 21. The combination of the codes for both amplifiers in one 8 bit value is possible, because only 3 bits are used to decode the desired gain. An internal array of 8 bits per entry was introduced, which maps exactly the gain table (table 1). An index variable called `cur_gain_number` stores the actual gain level. An increase of the gain can easily performed by executing `spi_set_gain(gain_table[++cur_gain_number])`.

```
#define SPI_GAIN_INSTRUCTION 0x40

void spi_set_gain(uint8_t gain)
{
  //send instruction to SPI0
  SPI_PORT &= ~(1<<SPI_CS0);
  SPDR = SPI_GAIN_INSTRUCTION;
  while(!(SPSR & (1<<SPIF)));
  SPDR = (gain & 0x0F);
  while(!(SPSR & (1<<SPIF)));
  SPI_PORT |= (1<<SPI_CS0);

  //send instruction to SPI1
  SPI_PORT &= ~(1<<SPI_CS1);
  SPDR = SPI_GAIN_INSTRUCTION;
  while(!(SPSR & (1<<SPIF)));
  SPDR = (gain >> 4);
  while(!(SPSR & (1<<SPIF)));
  SPI_PORT |= (1<<SPI_CS1);
}
```

Listing 2: programming the gain stages

The gain is controlled by the actual maximal sampled value of the signal. By introducing two thresholds, the gain level is increased when the maximal sampled value of the last value series underruns the lower threshold. A decrease of the gain level is performed when the maximal sampled value overruns the upper threshold, respectively.

[9] serial peripheral data register
[10] serial peripheral interrupt flag

2.3.2 Recording the signal

2.3.2.1 Ensuring a frequent analog-digital conversion[1] To achieve a constant sample rate of $8kHz$, an internal timer/counter module is used to trigger the conversion procedure of the analog digital converter. For this task, the timer 0 is used and can be configured by three registers:

- `TCCR0` ... Timer/Counter Control Register 0: defines the operation mode of the timer/counter 0
- `OCR0` ... Output Compare Register 0: stores the value the counter gets compared with in compare mode
- `TIMSK` ... Timer/Counter Interrupt Mask Register: defines which interrupts are executed on different events

For this application the clear timer on compare match (CTC) mode is used. In this mode the counter value of the timer is compared with the `OCR0` register and is reset to zero after the contents of the registers match. The time one increment of the counter value needs is defined by a own prescaler, which generates a clock (f_{timer0}) depending on the operation clock of the μ-Controller. To achieve that a compare match occurs exactly 8000 times a second, a prescaler of $f_{OSC}/8$ and a compare value of 250 was chosen. With a system clock of $16MHz$ this configuration results a interrupt frequency (f_{int}) of

$$f_{timer0} = \frac{f_{OSC}}{scaler} = \frac{16MHz}{8} = 2MHz \quad (11)$$

$$f_{int} = \frac{f_{timer0}}{\texttt{OCR0}} = \frac{2MHz}{250} = 8kHz \quad (12)$$

To trigger an interrupt on compare match, the `OCIE0`[11] flag of the `TIMSK` register must be set to 1.

After the timer is configured to trigger an interrupt 8000 times per second, the ADC has to be forced to trigger a conversion when this interrupt occurs. This can be done by setting the `ADTS2` to `ADTS0`[12] bits in the `SFIOR`[13] register correctly. To start a conversion on a compare match of timer/counter 0, the `ADTS2` bit must be set to zero and the `ADTS1:0` bits must be set to 1.

Also the ADC has some more options which have to be set. The ATmega32 provides an analog digital converter of 8 channels and two different input

[11] Timer/Counter 0 Output Compare Match Interrupt Enable
[12] ADC Auto Trigger Source
[13] Special FunctionIO Register

modes. The two modes are called the single ended input mode and the differential input mode. In single ended input mode, the absolute analog voltage is converted to a discrete value, whereas the differential input mode converts the differential voltage between two channels into its digital representation. In this application the single ended input mode for channel 0 (port `ADC0`) is used.
Also different reference sources for the ADC conversion circuit can be selected. For this purpose, as reference voltage which represents the highest possible value in single ended mode, the external `AVCC` pin is used. This pin is connected to the positive supply voltage. (When choosing this option, it is recommended to connect an external capacitor to the `AREF` pin.)
Since the internal ADC supports a native resolution of 10 bit, the conversion result needs two 8 bit registers to save its value. These two registers can be configured as left or right adjusted. A left adjusted setup leads to storing the most significant bit of the conversion result to the most significant bit of the higher ordered result register. Because is was decided to use 8 bit resolution anyway, this option was chosen. So the conversion result equals the content of the higher ordered conversion result register and value of the lower ordered conversion result register can be rejected.
To configure the ADC according to these decisions, some bits in the `ADMUX`[14] register must be set. For selecting the `AVCC` pin as reference voltage source, the bits `REFS1:0`[15] must be set to 0 and 1.
To set the conversion result left adjusted, the bit `ADLAR`[16] must be set to 1. To define the `ADC0` pin as single ended input channel, the `MUX4..0` bits must be all set to 0.
As last step, the ADC control logic has to be told a few settings using the `ADCSRA`[17] register. For the internal successive approximation converter, also a clock has to be provided by a configurable prescaler. This can be done by setting the `ADPS2:0`[18] bits.
Also the ADC conversion complete interrupt must be enabled, in whose interrupt service routine (ISR) the result register is read. This functionality is provided by the `ADIE`[19] flag. Because the ADC should start a conversion automatically when the timer compare event occurs, the control logic must enable auto triggering by setting the `ADATE`[20] flag.
Setting the `ADEN`[21] bit is needed to activate the ADC module and make it ready for conversions.

[14] ADC Multiplexer Selection Register
[15] Reference Selection Bits
[16] ADC Left Adjust Result
[17] ADC Control and Status Register A
[18] ADC Prescaler Select Bits
[19] ADC Interrupt Enable
[20] ADC Auto Trigger Enable
[21] ADC enable

Listing 3 contains the code which is necessary to configure the timer and the ADC functionalities as described above.

```
void ADC_Timer0_init( void )
{
        // Configure Timer 0
        // Prescaler 8, CTC mode, no output on pins
        //TCCR0:
        // FOC0 WGM00 COM01 COM00 WGM01 CS02 CS01 CS00
        //  0     0     0     0     1    0    1    0
        TCCR0 = 0x0A; //0b00001010;

        //compare-register: 250 -> 8kHz @ 16MHz clk
        OCR0 = 0xFA;

        //output compare interrupt enable for timer 0
        TIMSK |= (1<<OCIE0);

        // trigger source: timer0 compare match
        //SFIOR:
        // ADTS2 ADTS1 ADTS0   x   ACME PUD  PSR2 PSR10
        //   0     1     1     0    0    0    0     0
        SFIOR = 0x60;

        // AVCC ref with external capacitor, left adjusted
           result
        // MUX4..0: 00000 = single ended ADC0
        //ADMUX:
        // REFS1 REFS0 ADLAR MUX4 MUX3 MUX2 MUX1 MUX0
        //   0     1     1    0    0    0    0    0
        ADMUX = 0x60;

        // auto-triggered mode, interrupt enable, prescaler:
           f_osc/128
        //ADCSRA:
        // ADEN ADSC ADATE ADIF ADIE ADPS2 ADPS1 ADPS0
        //  1    0     1    X    1     1     1     1
        ADCSRA = 0xAF;
}
```

Listing 3: initialization of the ADC and Timer 0 functionality

2.3.2.2 Starting and stopping a conversion cycle

To store the sampled signal temporarily for further processing steps on the μ-Controller, a global buffer array of 1000 8-bit values is used.
To start a sampling sequence, the `ADSC`[22] flag of the `ADCSRA` register must be set to 1. This triggers a frequently conversion cycle with a sampling rate

[22] ADC Start Conversion

of $8kHz$ on channel 0, when the initializing was executed correctly. Listing 4 shows the start routine for sampling the signal.

```
void ADC_start(void)
{
  //initialize the ADC and Timer0
  ADC_Timer0_init();
  //start conversion sequence
  ADCSRA |= (1<<ADSC);
}
```

Listing 4: ADC start routine

When the ADC module finished a single conversion, the ADC conversion complete ISR is executed (see listing 5).
This routine saves the new value in its supposed slot in the array. To determine this slot, a global value counter variable was introduced. This counter variable is also used to determine when the whole array is filled. When the counter value exceeds the length of the buffer array, the recording stops.
During the recording process of the values stored in the buffer, also the maximum value is logged. The information of the highest value is used to adjust the gain of the programmable amplifiers for the next recording cycle.

```
ISR(ADC_vect)
{
  //subtract the direct component
  int8_t val8 = (ADCH-128);
  //log the maximum value
  if(val8 > max_value)
    max_value = val8;
  //store the sample into the sample buffer
  values_buffer[values_cnt++] = val8;
  //abortion condition
  if(values_cnt == VALUES_NR)
  {
    STATUS &= ~(1<<STAT_RECORDING);
    ADC_stop(); //stop sampling
  }
}
```

Listing 5: Interrupt service routine for finished ADC conversions

```
void ADC_stop(void)
{
  //stop timer0 interrupts
  TIMSK &= ~(1<<OCIE0);
  //disable ADC
  ADCSRA &= ~(1<<ADEN) & ~(1<<ADSC);
}
```

Listing 6: ADC stop routine

Listing 6 shows the stop routine of the recording process. This function stops the ADC sampling cycle by disabling the triggering timer interrupt and the ADC itself.

2.3.3 Filtering the signal

To calculate the filtered signal according to figure 11 on the 8 bit architecture of the μ-Controller, the filter coefficients have to be transformed into the 12 bit fix-point representation. This was done after the filter design in MATLAB® by multiplying the coefficients by 2^{12} followed by a rounding operation.

Table 6 shows the transform of the filter coefficients of the specialized filter for the standard D string from floating point to 12 bit fix point representation for both biquad sections.

Coefficient	Floating point representation	12 bit fix-point representation
a_1	-1.9813639...	-8116
a_2	0.9952795...	4077
b_0	1.0000	4096
b_1	0.0000	0
b_2	-1.0000	-4096
a'_1	1.9826170...	-8121
a'_2	0.9954637...	4077
b'_0	1.0000	4096
b'_1	0.0000	0
b'_2	-1.0000	-4096

Table 6: Representation of filter coefficients (specialized standard D)

Due to the high number of filters (and their coefficients), the coefficients were stored in the flash memory of the μ-Controller using the `pgmspace.h` library for AVR. This library allows to save constant variables into the flash memory by adding the `PROGMEM=` keyword after the declaration of the name of the variable. In the developed program, the filter coefficients of all filters were stored into an array of structs called `filters`.
To read the stored variables, the `pgm_read_word(&void)` function returns a reference to the desired object. For instance, to get the a_1 coefficient of the current filter indexed by the variable `filter_nr`, `int16 coeff = (int16_t)pgm_read_word(&filters[filter_nr].stg1_a1);` has to be executed. `stg1_a1` is the struct element in `filters`, representing the a_1 coeffi-

cient of the first biquad stage.

So the filtered value can be calculated by following the graphical instruction of figure 11. As described in chapter 2.2.6.1, after multiplying two values in 12 bit fix-point representation, the result has to be shifted to the right by 12 binary places. In two's complement, the sign of signed values is stored in the most significant bit (MSB). Hence, shifting negative numbers (MSB is 1) without care leads to wrong results. The solution for this problem, which takes the least processing time for the μ-Controller, is also the most intuitive: an if statement.
Listing 7 shows a part of the calculation of the filtered signal. The result of the multiplication (`result`) should be subtracted from the variable called `temp`. To perform the right shift of the multiplication result, an if statement checks if the result is negative. If so, the result is transformed to its positive value, shifted and added to the `temp` value. Otherwise it is shifted and subtracted directly.

```
#define FIX_BITS 12

result = z1[0]* (int16_t)pgm_read_word(&filters[filter_nr].
    stg1_a1);
if(temp < 0)
{
  result = -result;
  result = result >> FIX_BITS;
  temp1 = temp1 + result;
}
else
{
  temp1 = temp1 - (result >> FIX_BITS);
}
```

Listing 7: Multiplication in 12 bit fix-point representation

After finishing the calculation of one filtered value, it is checked for zero crossing by comparing the sign of the past value with the sign of the new calculated value. An array stores the previous 4 numbers of samples between the last zero crossings and a counter variable counts the samples after the last zero crossing. If a zero crossing occurs, the most previous value of the array is overwritten by the counter value and the counter gets cleared. After determining the filtered values of the whole signal, the number of samples within 4 periods is calculated by summing up the values of the array. The current frequency information, represented in number of samples within 4 periods, is updated each new recording cycle and can be accessed by the controlling functions by a global variable.

3 Frequency manipulation

The frequency manipulation basically consists out of a PID-Controller and a servo motor what is accessed by Pulse-Width-Modulation. For dimensioning the PID-Controller the software MATLAB®/SIMULINK®was used. Two Guitar models "Framus" and "Jackson" have been considered for modeling, which have both a different kind of torque increase when tuned up.

The following sections will go into detail, describing the specific issues and resulting solutions.

3.1 Hardware

To provide an automated tuning procedure, a motor is attached on the tuning pegs (for further details see figure 45). To make this possible certain requirements have to be fulfilled:

- sufficient motoring torque, about 20 - 35 Ncm
- angular velocity as controlled parameter
- controlling by Pulse-Width-Modulation
- affordability
- advantageous design for application

Two types of motors have been considered based on the requirements above, a step motor and a servo motor. The disadvantages of a step motor are uncomfortable design and a need of an extra control unit what would have to be developed to actuate the motor by PWM.

The servo motor on the contrary has a control unit included and is more affordable than the step motor. Also the design saves more space for developing a hand-held device. The only disadvantage that occurs is the parameter controlled by PWM, which is the angle itself. To achieve an angular-speed control the motor has to have the ability to rotate continuously or if its not able to do so, at least a simple modification should be possible.

Researches have shown that the servo motor "Futaba S3003" is very suitable for the discussed requirements and so the decision was made for this one.

Figure 22: Servo Motor "Futaba S3003"

Futaba S3003 Specification	
Torque	**32 Ncm**
Speed for 45°	**0,17 sec**
Size	**40,1 x 19,8 x 36 mm**
Weight	**37,2 g**
Operation Voltage	**4,8 - 6 V**
Neutral Impulse	**1,52 ms**

The servo motor has an included electronic control unit that normally rotates the drive shaft in its appropriate position according to the PWM signal. The potentiometer of the main shaft inside the servo is measuring the position at any given time and so the controller is able to drive the motor properly.

So if the position of the drive shaft is not correct, the motor is moving it into place by reducing its angular-speed depending on the proximity of the actual angle to the target angle.
This non-linear characteristic will be exploited to control the angular velocity by the PWM signal.

To achieve this kind of parameter control the servo motor shown in figure 22 has to be modified from position-controlled to rotation-speed-controlled. The following instructions show how the "hacking" of the servo motor was performed.

3.1.1 Continuous Rotation Modification [3]

1. First of all any wheels or arms that may be attached to the main shaft were pulled off.
   Then the 4 screws on the back of the servo were removed, see figure 23. (Note that it's not necessary to remove the back of the servo.)

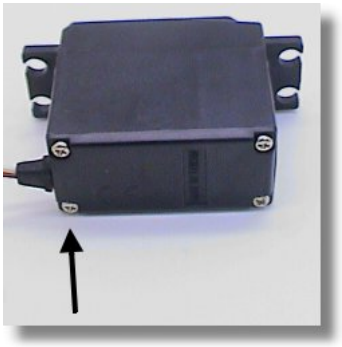

Figure 23: Removing screws

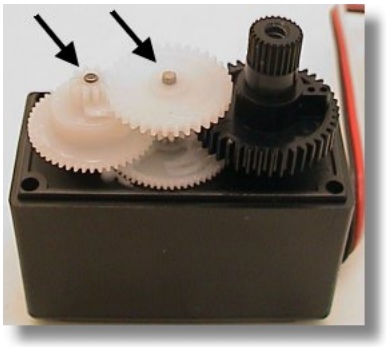

Figure 24: Opening the gear case

2. Now the gear case (top of the servo) was lifted carefully where it has to be made sure that the two gear wheels shown in figure 24 may stay attached to the casing. If they do, they were removed and inserted into position as shown.

3. The intermediate gear wheel and the main shaft were taken off by just lifting them, see figure 25.

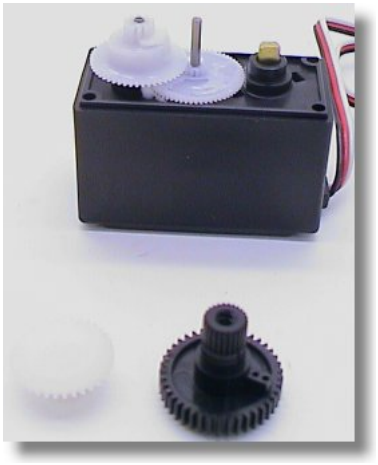

Figure 25: Lifting Gear Wheels

4. With fingers or some small pliers the potentiometer shaft was placed into center position.

Figure 26: Potentiometer shaft

5. Using a thin blade of a razor saw or a cutting disk on a rotary tool, a small slot was cut in the potentiometer shaft of the servo as shown in figure 27. This will allow calibrating the servo motor later.

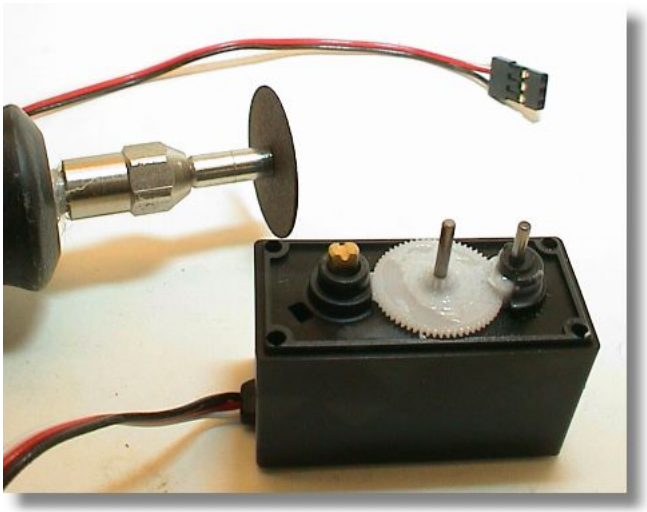

Figure 27: Potentiometer shaft

6. A small stop had to be removed from the main shaft wheel by using a small wire cutter.

Figure 28: Main shaft wheel

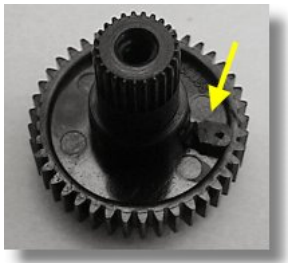

Figure 29: Main shaft wheel modified

7. Inside the main shaft wheel were two slots which are used to access the potentiometer. These slots were removed using a drill bit by reaming them out carefully.

Figure 30: Main shaft wheel

Figure 31: Main shaft wheel modified

8. Drilling through the top of the main gear wheel as shown in figure 32 made it possible to adjust the potentiometer by a micro screw driver.

Figure 32: Potentiometer shaft

9. Then the main shaft wheel was inserted again into the top of the servo chassis as shown in figure 33.
   Further it was assembled with the potentiometer where it should rotate freely without catching.

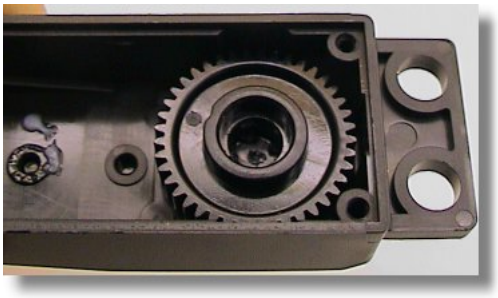

Figure 33: Testing the main shaft wheel

10. At last the two gear wheels were reassembled and some oil was added. The casing was reattach again with the 4 rear screws.

Figure 34: Reassembling the servo motor

11. To calibrate the servo a control signal with 1500μs PWM (neutral position) was generated and the potentiometer was adjusted with a micro screw driver through the main shaft hole until the drive shaft stopped rotating.

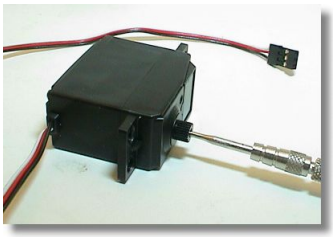

Figure 35: Calibrating the servo motor in neutral position

After these steps the servo motor has the ability to control the angular velocity and to rotate continuously as needed to tune a guitar.

3.1.2 Servo control by ATmega32

To control the servo motor Pulse-Width-Modulation is used. The μC ATmega32 provides two 8-bit Timer/Counter and one 16-bit Timer/Counter, each with separate prescalers and three different kinds of PWM operation modes.
Before the timer resolution and prescaler value is considered, the appropriate PWM operation mode has to be chosen. For this the micro-controller provides "Fast PWM Mode", "Phase Correct PWM Mode" and "Phase and Frequency Correct Mode".

3.1.2.1 Fast PWM Mode

This mode is able to generate a high frequency PWM waveform by its single-slope operation. The counter counts from bottom to top, then restarts from bottom. Due to the single-slope operation, the operating frequency of the fast PWM mode can be twice as high as the other two PWM modes which use dual-slope operation.
The PWM resolution for fast PWM can be fixed to 8-bit, 9-bit or 10-bit. For the two last ones the 16-bit timer 1 has to be used. The counter is incremented until its value matches either one of the fixed values (example: 0x00FF for 8-bit), then it is cleared and restarts again.
Figure 36 shows the timing diagram which illustrates the single-slope operation. The small horizontal line marks on the TCNT1 slopes represent compare matches between OCR1x and TCNT1. In non-inverting mode the output compare OCnx pin is then set to LOW and this causes the "end" of the pulse. The counter continues counting up until the sequence is restarting again. [1]

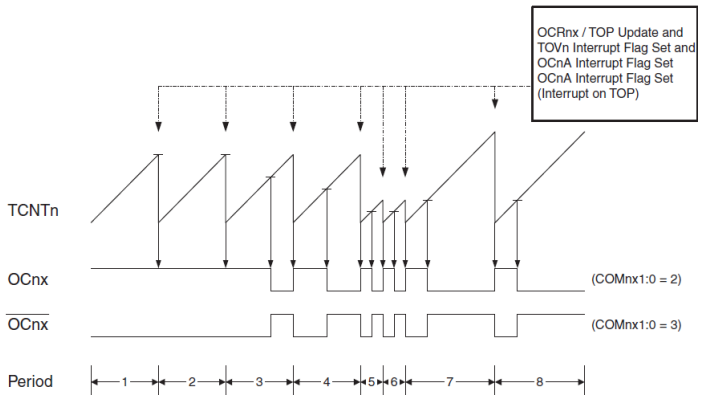

Figure 36: Fast PWM timing diagram [1]

3.1.2.2 Phase Correct PWM Mode

Based on a dual-slope operation, this mode provides a high resolution phase correct PWM waveform generation option. The counter counts repeatedly from bottom to top and then from top to bottom. In non-inverting compare output mode, the output compare (OC1x) is cleared on the compare match between TCNT1 and OCR1x while upcounting, and set on the compare match while downcounting.
The dual-slope operation has lower maximum operation frequency than single slope operation. See the timing diagram in figure 37 for illustration. [1]

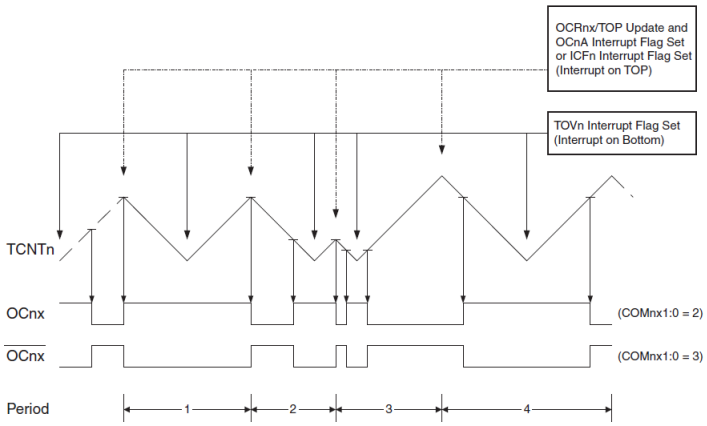

Figure 37: Phase Correct PWM timing diagram [1]

3.1.2.3 Phase and Frequency Correct Mode

This mode provides a high resolution phase and frequency correct PWM waveform generation option. Like the phase correct PWM mode mentioned before, a dual-slope operation is used. The counter counts repeatedly from bottom to top and then from top to bottom. The output is generated like in the phase correct PWM mode.
The main difference between the phase correct and the phase and frequency correct PWM mode is the time the OCR1x Register is updated by the OCR1x Buffer Register, see figure 37 and figure 38. [1]

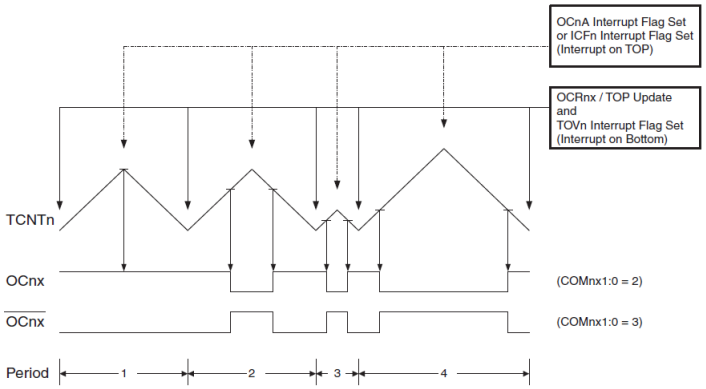

Figure 38: Phase Correct PWM timing diagram [1]

For further details concerning the different PWM modes it is referred to the datasheet [1].

To achieve a simple and prompt PWM waveform control that suits best for the servo motor and offers a plain software implementation, the fast PWM mode is applied. Therefore only the two OCR1x registers have to be set to define the proper pulse-width with constant period time (see figure 36).

In addition to the selected operation mode the appropriate parameters have to be resolved.

To check which combination out of bit-resolution and prescaler value at the given clock rate of 16MHz allows a smooth motor control, several pulse periods have been considered, shown in table 7.

***FRAMUS* - up tune with full speed**

Pulse-Periods	**Fast-PWM-Resolution**			
Prescaler	8 bit	9 bit	10 bit	16 bit
1	0.016 ms	0.032 ms	0.064 ms	4.096 ms
8	0.128 ms	0.256 ms	0.512 ms	32.768 ms
64	1.024 ms	2.048 ms	4.096 ms	262.144 ms
256	4.096 ms	8.192 ms	16.384 ms	1048.576 ms
1024	16.384 ms	32.768 ms	65.536 ms	4194.304 ms

Table 7: Pulse time periods at different timer configurations

The 16MHz external clock rate (quarz) is divided by the prescaler and defines the frequency of the timer. For a 16-bit resolution timer 1 has to be used. The neutral-pulse of 1500μs duration has to occur at least every 16.384ms, marked green. If this time period is reduced below this value,

the servo motor starts to vibrate due to the fact that one period is actually reinterpreted as one pulse.

The second aspect is the resolution of the count value related to the timer. This value has to be incremented and decremented to set the certain pulse-width and if the minimal possible step is too inaccurate, also the servo access would be so. It turned out that a period length of 16.384ms, independent of the resolution, only allows a minimal pulse-width grading of 16μs, which has shown to be not very precise for varying the angular velocity.
Hence, the 16-bit timer with the prescaler value of eight was chosen, marked yellow in table 7. This period length seems nearly too long, but the grading of the pulse is fine enough with 0.5μs.

With this configuration it is now possible to actuate the servo motor in both rotation directions. The neutral position is defined with 1500μs PWM, at where the motor is not rotating and trying to hold its position with a certain torque. This neutral control pulse is later on software-defined "zero". This zero-point allows a setup with either negative or positive values, accordingly to the rotation direction. Experiments have shown that the *Futaba S3003* has its full strength at a value about ± 300, which means a pulse-length of $\pm 300 * 0.5\mu s = \pm 150\mu s$.
In chapter 3.3 the setup with value 300 will also be called as *full speed tuning*.

3.1.3 Servo voltage supply

The current required by the servo motor while rotating causes disruptions on the voltage supply. Even worse is the start-up process of the servo, which temporarily can take about $600mA$. This short-term consumption cannot be supported by the voltage regulator and may lead to voltage drop out causing micro-controller malfunction.
To avoid this, a capacitor with $470\mu F$(6V) was applied to the voltage supply which provides more stability.

3.2 Control theory

Basically, control theory deals with the analysis and design of closed loop control systems. So the main structure in control systems is based on negative feedback. The goal in control of physical systems is to track the output signal (e.g. frequency, room temperature, speed of a motor, level of a tank, etc.) according to a reference signal and to reject the effect of the disturbances.
Furthermore it has to be distinguished between a system that has to be controlled and the whole control system itself. The requirements of a control system are dependent of its type, distinguishing between discrete digital implementation and analog continuous operation. First of all it has to be stable, so that no oscillating occurs. Then, it has to meet the quality specifications for steady-state accuracy, dynamic properties such as overshoot, setting time, latency, etc. Also the control signal which actuates a system input has to be inside its technical limits (anti-windup). In addition to that a control system has not to be very sensitive to measurement noise and to plant/model mismatch.

The following block diagram (figure 39) illustrates the schema of the feedback loop control system or closed-loop control system.

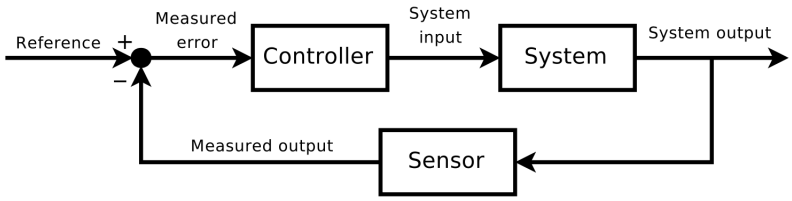

Figure 39: Closed-loop control system [6]

The so called **system** is also known as plant or process. A real physical system is represented by a mathematical model which is used for analysis and designing a appropriate control system. The math behind a plant is also represented as a transfer-function which delivers a certain output regarding of a temporary input.
The output value of a plant is then being measured by a **sensor** and compared to a reference value by subtracting. The resulting difference called error is then amplified or modified by the **controller** to create the control signal. This signal affects the input of the process in order to reach the desired behaviour.
In this structure the output signal is fed back to the input of the plant, thus the controlling is realized by negative feedback.

Before going further into control theory, it has to be mentioned that it con-

sists of way too many topics of detail to discuss all of them, so only the basics are treated.

In feedback systems the execution of the control command is always delayed to a certain degree, because of inherent delays and dead time in the individual (electronic) components. This disturbing effect is a general part of digital discrete control systems. Therefore unstable behavior may be evoked when steady or increasing oscillations do appear in the process output. This has to be avoided.[7] Hence disturbances will always occur in real-life.

The sensor shown in figure 39 is, as already mentioned, measuring the actual output value of the plant. Control system components sometimes act as controller and sensor simultaneously (like our μ-Controller).

Basically, the control operation can be described with several mathematical terms individually or in combination. Therefore the most common type of controller is used, the so called *PID controller* which is named after its three correcting therms, the proportional term, the integral term and the derivative term. The PID controller can be used to control any measurable variable, as long as this variable can be affected by manipulating some other process variables [8].

Before the PID Controller is considered in 3.2.4, the respective terms will be discussed individually.

3.2.1 Proportional term

The proportional term is providing an overall control action proportional to the error. This is done by multiplying the factor K_p, called the proportional gain, with the error signal.

The proportional term is given by:

$$P(t) = K_p * e(t) \tag{13}$$

Increasing the proportional gain K_p causes in general a small increase of the setting time and a light decrease of the steady-state error, but may degrade the stability of the control system. In this case, the term value may increase too quickly and will "overshoot" the desired value. In worst case the control loop will begin to oscillate around the target value which is also called "hunting". If the gain is determined too low, the controller is less sensitive

and may compensate disturbances too slow.

Figure 40 shows a response to the proportional gain without overshoot.

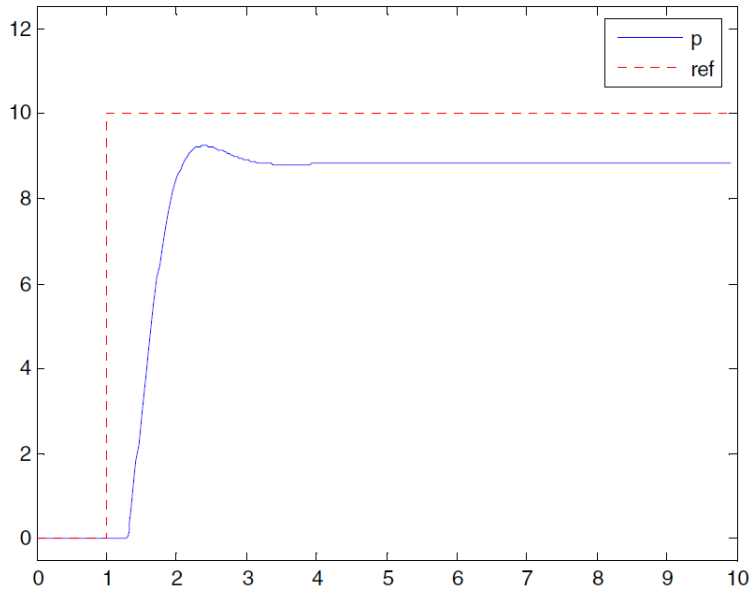

Figure 40: Response to $P(t)$ at set-point = 10 over time [9]

In fact, the proportional term alone will rarely reach the desired target value which results in a steady state error, because of drift by analog components or quantization error in digital controllers.[9]

As a matter of this, discrete control systems will never be able to eliminate a steady-state error completely, so further accuracy requirements have to be fulfilled.

3.2.2 Integral term

The integral term corresponds to the error magnitude and the error duration. The error is summed up over time and gives an accumulated value which is multiplied with the integral gain K_i. Typically this is used to get rid of offset error. As long as the target value is missed, the integral term will change accordingly (permanent).

The integral term is given by:

$$I(t) = K_i * \int_0^t e(\tau)\,\mathrm{d}\tau \tag{14}$$

This term acts like a kind of weight traced by the controller which is also called "memory", because difference values of the past are considered. If the integral gain K_i is set too high, the control system easily tends to overshoot and begins to oscillate. On the other side, with a too low gain the individual term looses its control-effect and causes a very slow control behaviour. However, the integral term is widely used together with at least the proportional term.

In the diagram of figure 41 you can see the proportional response and the integral response. Also a combinational response of these is shown.

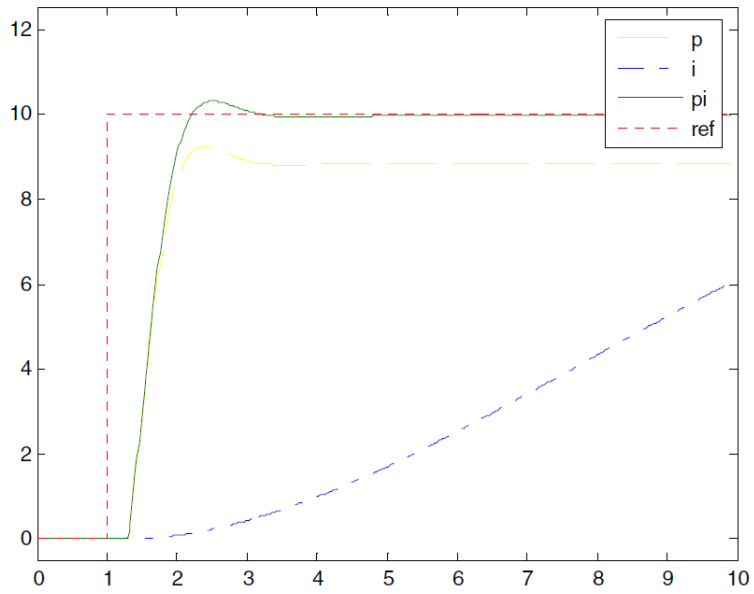

Figure 41: Responses to $I(t)$ and $P(t)$ at set-point = 10 over time, p...proportional term, i...integral term, pi...combination of the two terms [9]

The main advantages of the integral term are an improvement of the setting time and an elimination of the steady-state error. So an aberration to the target value caused by the proportional term may be wiped out.

Regarding a digital discrete control system also the integral term can't prevent a persistent real error which is discussed later in chapter 3.2.4.

3.2.3 Derivative term

This term is typically used in combination with a proportional term and/or an integral term, because here not the magnitude of the error is regarded but its changing speed. This improves the response to a sudden change in the system state or reference value. So the error value is derived by time as the following equation shows.

$$D(t) = K_d * \frac{de(t)}{dt} \tag{15}$$

So if the error has a constant change in its value the derivative term delivers an constant output dependent on the factor K_d. Because of this the derivative term will never be able to control by its own.

In figure 42 the responses between proportional term and derivative gain are shown.

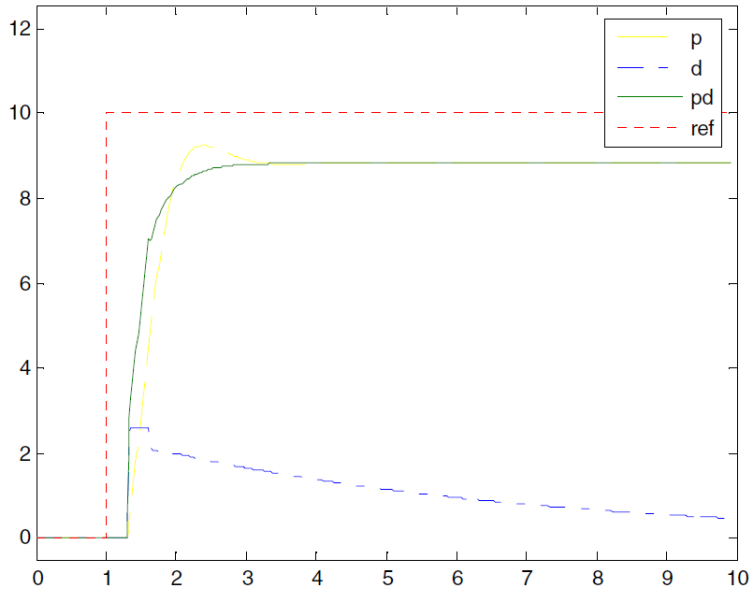

Figure 42: Responses of $D(t)$ and $P(t)$ at set-point = 10, p...proportional term, d...derivative term, pd...combination of the two terms [9]

Generally it is very difficult do determine the derivative gain K_d properly because, on the one hand this term reduces the overshoot caused by an integral component, but on the other hand noise is amplified as well as the signal change and so if the gain is set too high the whole control system could become unstable quickly. So the derivative term can also be seen as a kind of high-pass filter.

Basically the response of a PD controller leads to a faster rising time than a single P controller but it is also impossible to prevent steady-state errors without an additional integral term. [8]

3.2.4 PID controller

In general the PID controller is designed with three terms (these are discussed in chapters before), which manipulate the controller input known as error in three ways: to handle the present, through the proportional term; recover from the past, using integral term; and to anticipate the future, through the derivative term [8].

Figure 43 shows a schematic block diagram of a control system with PID controller.

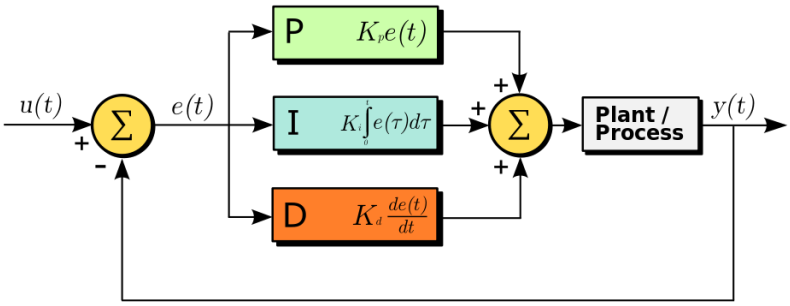

Figure 43: PID controlled loop [10]

A PID controller uses all three terms by adding the outputs together, which then actuates as control signal for the plant. The ideal parallel form for calculating the control output $C(t)$ is done in equation 17.

$$C(t) = P(t) + I(t) + D(t) \tag{16}$$

$$C(t) = K_p * e(t) + K_i * \int_0^t e(\tau)\,\mathrm{d}\tau + K_d * \frac{de(t)}{dt} \tag{17}$$

For an illustration of the resulting behaviour the following diagram is shown with different kinds of controllers.

All in all, using all terms together usually gives the best performance. In figure 44 the PI controller improves the result by removing the stationary error leafed by the proportional term and the PID controller again improves

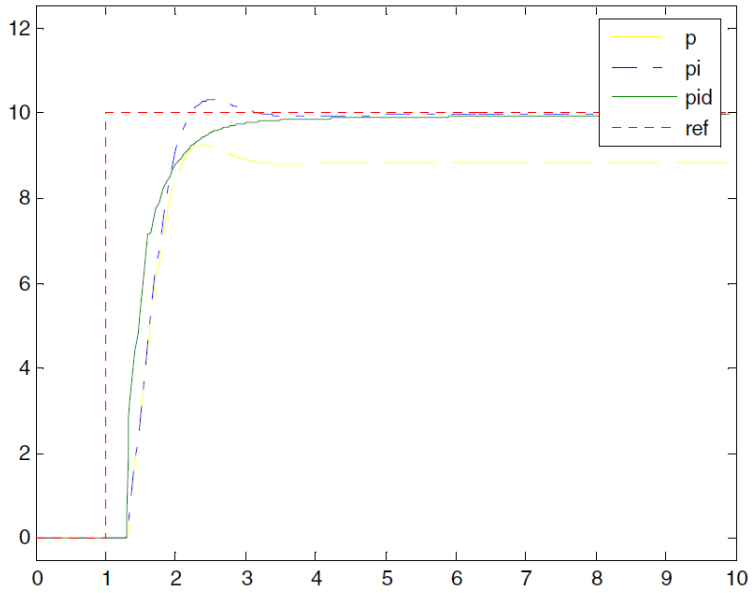

Figure 44: Varying controller types compared [9]

the result of the PI by faster response and no overshoot.
To determine the proper gain values for the certain terms several tuning methods exist. Often a detailed mathematical description of the system is unavailable due to missing measurable values and/or formulas representing the process. For this **experimental tuning** of the PID parameters has to be performed. Finding the terms is often a challenging task and so good knowledge about the systems properties and the way the different terms work is essential.
The optimum behavior on a process change or set-point change depends on the application at hand. For some control systems an overshoot has to be prevented, others demand less energy consumption in reaching the target value. Typically, stability is the strongest requirement by designing a controller. [8]
The other methods for dimensioning, of course, do rely on some mathematical approximations. The choice of method will depend largely on whether the process can be taken off-line for tuning or not. The **Ziegler-Nichols method** is a well known online tuning strategy. The first step in this method is setting the integral term and the derivative term to zero, increasing the proportional gain until a sustained and stable oscillation (as close as possible) occurs on the output. Then the actual gain called critical gain K_c and the correspondent oscillation period P_c is recorded and the P, I and D parameters are adjusted accordingly using table 8. [8]

The time constants T_i and T_d are then used to calculate the K_i and K_d

Controller	K_p	T_i	T_d
P	$0.5 * K_c$		
PD	$0.65 * K_c$		$0.12 * P_c$
PI	$0.45 * K_c$	$0.85 * P_c$	
PID	$0.65 * K_c$	$0.5 * P_c$	$0.12 * P_c$

Table 8: Ziegler-Nichols method paramters

factors as follows:

$$K_i = \frac{K_p}{T_i} \tag{18}$$

$$K_d = K_p * T_d \tag{19}$$

Further tuning of the parameters is often necessary to optimize the performance of the PID controller.

Another tuning method that is considering the step response of the plant is done by opening the control loop. The step response is then recorded and analysed. For this, the steepest tangent of the rising curve at the beginning is determined and intersected with the maximum and minimum level of the response. The so triggered time periods are then measured and used for tuning the PID parameters with the rules of **Chien-Hrones-Reswick**, which will not be discussed further. Here, also the Ziegler-Nichols method can be applied.

Parameters also can be found by simulating the control system with common computer software. Hence, a system model has to be created preferably as an exact representation of the real world system. This requires in most cases the knowledge of the mathematical background that describes the real world model best.
(The decision has fallen to this kind of parameter tuning although we did not have a mathematical model of our plant. Therefore it is referred to chapter 3.3.)

There exist several other dimensioning methods like using the *Bode-diagram* (frequency based method) which will not be considered in this context.

3.2.4.1 Discrete PID controller

"A discrete PID controller will read the error, calculate and output the control input at a given time interval, at the sample period T. This sample time should be less than the shortest time constant in the system."[8] Because of this, the calculation of the control signal could not be done like in equation 17 anymore. Due to the fact that time is not continuous in this case, constant sample time and system defined latency are important aspects respectively to the integral term and the derivative term, which are calculated time dependent.

To process an discrete/digital output, the individual control terms have to be transformed into a discrete form. The integral can be regarded as a sum of values over the number of samples.

$$\int_0^t e(\tau)\,\mathrm{d}\tau \approx T * \sum_{k=0}^{n} e(k) \tag{20}$$

The derivative term can be represented as difference between the actual error and the error before.

$$\frac{de(t)}{dt} \approx \frac{e(n) - e(n-1)}{T} \tag{21}$$

Where n is the discrete step at time t and T is the sample time period. So the time $t = n * T$. [8]
This gives a controller output:

$$C(n) = K_p * e(n) + K_i * \sum_{k=0}^{n} e(k) + K_d * (e(n) - e(n-1)) \tag{22}$$

Where, for *Ziegler-Nichols* tuning, the gains are:

$$K_i = \frac{K_p * T}{T_i} \tag{23}$$

$$K_d = \frac{K_p * T_d}{T} \tag{24}$$

3.2.4.2 Integral windup

By the reason that every controller, especially a digital one, has its output signal limitation, it has to be made sure that a growth of the integral term does not produce a control output signal that is beyond its limitations. If so, the controller is calculating internally a value that can't be used for actuating, that's why the PID controller will then overcompensate the process input until the integral sum is back to normal.

This problem can be avoided in several ways, for example limiting the sum by not allowing it to become larger or lower than a certain value. This limitation value always depends on the system and the sample time used.

3.3 System modelling with MATLAB®/Simulink ®

For modelling our control system loop the software MATLAB®/Simulink®was used which provides tools for designing and developing control systems and models. Furthermore, the Simulink Control Design GUI provides a graphical environment for control system linearization and design. Additionally, settings can be restored and saved as well as results can be exported to the MATLAB®workspace. [11]

Before our Simulink control system model will be shown and discussed in 3.3.3, the following section will explain the behavior and characteristics of the individual real-world components.

3.3.1 Guitar

When someone buys a guitar there is never some kind of datasheet thereby which describes the the product behavior mathematically. Anyway, to create a virtual model of our guitar, researches have shown that some basic formulas about string oscillation and frequency-torque relation are very convenient for modeling.
A quick overview about the parts of an electric guitar shows figure 45.

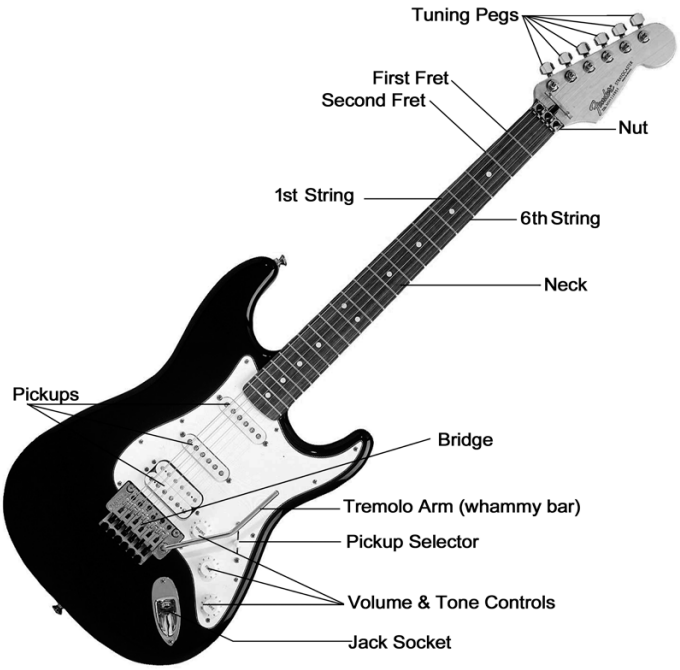

Figure 45: Electric guitar parts [12]

The six strings of a guitar can freely oscillate between the nut and the bridge. When a chord is played the fingers shorten the oscillating string so that the tone is heightened. At tuning the guitar the strings are not touched to allow the appearance of each lowest possible frequency. To record a frequency signal the pickups of an electric guitar seems very comfortable but also acoustic guitars strings could be measured by microphone.
We just decided to use only electric guitars for tuning because most acoustic guitars also have a too high string torque that cannot be handled by our chosen servo motor "Futaba S3003".

Generally, to determine certain characteristics two guitar models were available. A vintage model *FRAMUS - Billy Lorento 10* which was manufactured in 1969 and a *JACKSON® Soloist SL2H (Limited Sam Ash Edition)*.

(a) Framus BL10 [13]

(b) Jackson® Soloist SL2H [14]

Figure 46: guitar models used for modeling

The vintage model, of course, was more difficult to handle with regarding the servo motor torque limit but this will be explained in detail in the following sections.

3.3.1.1 Guitar string analysis

First it has to be mentioned that there exist various kinds of strings with different thickness, material and manufacturing technique which all influences the oscillating characteristics. In this case a matter of particular interest would be the relation between the string frequency change and the string tension change (which also results in torque change on the machine heads or tuning pegs).

Basically, if a string is oscillating a musician talks about a tone where a technician talks about frequency. It is also known that if a string is shortened the frequency would raise. As a matter of fact, if the oscillating string length is halved, the frequency is doubled. Regarding the tuning process here, the length of the string would always stay the same (from bridge till nut), so a relation between the tension-force and the frequency has to be found.
In oscillation physics the frequency always mentioned in this context would be the fundamental frequency f_0 which is defined as the lowest frequency of a periodic waveform's spectrum.

The fundamental frequency of a guitar string is given by

$$f_0 = n \cdot \frac{\sqrt{\Psi/\pi\rho}}{D \cdot L} = \frac{\sqrt{\Psi[N]}}{D[mm] \cdot L[m]} \cdot 6,3Hz \tag{25}$$

[15]

Using $n = 1$ (fundamental frequency) Ψ is the tension-force, ρ the material density, D the string diameter and L the length of the string. To calculate the necessary tension-force Ψ, the fundamental frequency and the string length will be multiplied together, and so if the tension-force is constant the string length and the frequency are acting reciprocal to each other (which has already been discussed before).

$$\Psi = (f_0 \cdot L)^2 \cdot \pi\rho D^2 \tag{26}$$

[15]

So if we want to double the frequency, the tension-force has to be increased four times.

Regarding equation 25 by contracting constant variables to ξ, the relation becomes more obvious.

$$f_0 = \sqrt{\Psi} \cdot \xi \tag{27}$$

The next step is to find out how the servo motor affects the tension-force or the according torque. If the servo motor is driving a tuning peg at a certain angular speed, the tension-force increase is proportional to an integral over time. So the following equation seems valid due to guitar experiments.

$$\Psi(t, \omega) = \int_0^t \omega \cdot (\eta(\Psi) + 1)\, \mathrm{d}\tau \tag{28}$$

This equation is recursive because of η, which represents a tension dependent resistance that will counteract the angular velocity ω. This resistance grows with the string tension and the servo motor can't actuate constantly anymore although there is a constant control signal. In order to that, the control signal has to adapt to this inconvenient behavior, which is discussed in 3.3.1.2.

If we now substitute the tension-force in equation 27 we get

$$f_0 = \xi \cdot \sqrt{\int_0^t \omega \cdot (\eta(\Psi) + 1)\, \mathrm{d}\tau} \tag{29}$$

which is again a recursive equation. We do not actually have to calculate with this recursive formula because we just use the individual terms of it for developing a model in Simulink.

All in all, the frequency depends on a constant factor ξ defined by the string physics, the integral of the actual angular velocity ω and a torque dependent resistance η. With these basic mathematical considerations we are now able to form a software supported model approximation.

3.3.1.2 Guitar string modeling

Simulink provides a huge repertory of graphical elements that can be combined together to form a representation of a "real world" system. In this case it's needed to model a guitar string which then could be used for simulating a control system loop.
In equation 29 the various terms of the string behavior are shown. Before the complete string model is specified, it has to be mentioned that a continuous integral form in Simulink is always described as a Laplace transformed term.

$$\int_0^t f(u)\,\mathrm{d}u \quad \circ\!\!-\!\!\bullet \quad \frac{1}{s}F(s) \tag{30}$$

By this reason we use the integrator block for integrating the certain value and then extract the root of it with the square-root block. These two blocks are responsible for the main characteristics of a guitar string. But we will also need a few more components to fulfill equation 29.

Before going into detail let's first consider the developed model that represents an approximation of the D-string of the guitar model Jackson®Soloist SL2H in figure 47.

As input the angular velocity acting at the tuning pegs was defined. Furthermore, a separation of the signal in two different "modes" was made because experiments have shown that one strings behaviour also differs in *tuning up* (frequency increase) or *tuning down* (frequency decrease) in unexpected big relations. This becomes obvious considering the actual string tension that on the one hand supports the down tuning procedure at decreasing the torque and on the other hand counteracts the up tuning process at increasing the torque. So the higher the absolute string frequency the more torque has to be applied if tuning up further. And even this effect is varying between all six guitar strings due to differences in string material and dimensions.
Additionally, there are two slackness blocks" (see figure 47) that characterize the effect of a certain dead-time interval of the angular speed. This is, because when the servo motor creates a too low mechanical torque for rotating the tuning pegs it would not be able to do so. Experiments revealed that up-tuning causes a wider dead-time interval. Also this effect is varying from string to string. For easier approximation a constant torque slickness over all six strings was assumed.

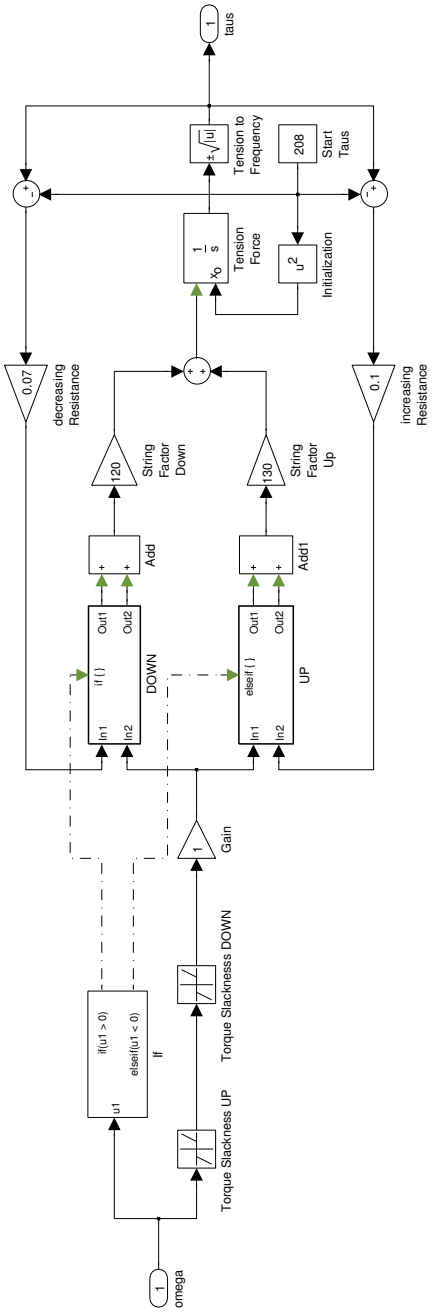

Figure 47: Guitar string model, string D

After the torque slackness has affected the model input value ω, the "data lane" now splits up into two boxes - *DOWN* and *UP*. These two boxes are linked with an if-conditioned box, which actuates with a logical signal each of them. So if the input ω (defined as $u1$ in the if-box) is positive, the *DOWN*-box is active and the modeled motor is tuning the string down. Otherwise the motor would tune the string up.
Figure 48 shows the content of the boxes "DOWN" and "UP".

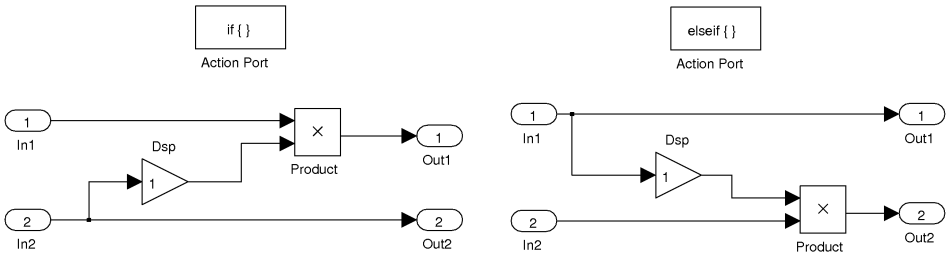

(a) DOWN Block of figure 47 (b) UP Block of figure 47

Figure 48: Content of conditioned blocks

The two blocks are actually calculating the term $\omega * \eta$, and on the outside the two outputs *Out1* and *Out2* are then added together to form the term $\omega * (\eta + 1)$. Now, an integrator component has to follow from which a square root has to be taken afterwards, so equation 29 will be designed completely. As plant output the previously defined *number of samples within 4 periods* unit is used (for further explanation read chapter 2.2.1). In the following sections this frequency dependent unit will also be called "*taus*-value".

The last step was to find out those gain values of the guitar string model that provide an approximation of the string physics factor ξ (string factor) and the matching torque dependent resistance η. Concerning the up/down tuning process, four different gain values have to be determined. To do this, some empirical measurements on both guitars were made.

At first the *FRAMUS* guitar model was inspected. Therefore, all six strings have been up-tuned and down-tuned for various periods of time with full servo motor torque. Then the resulting *taus*-values were noted and plotted to see the different string relevant performances.

***FRAMUS* - down tune with full speed**

Strings	Before	After 0.5sec	After 1sec	After 1.5sec
E	388	427	499	600
A	291	307	351	390
D	218	230	261	293
G	163	174	195	234
H	130	135	149	161
e	97	100	105	110

Table 9: Measured *taus*-values after various time periods with full-speed down tuning

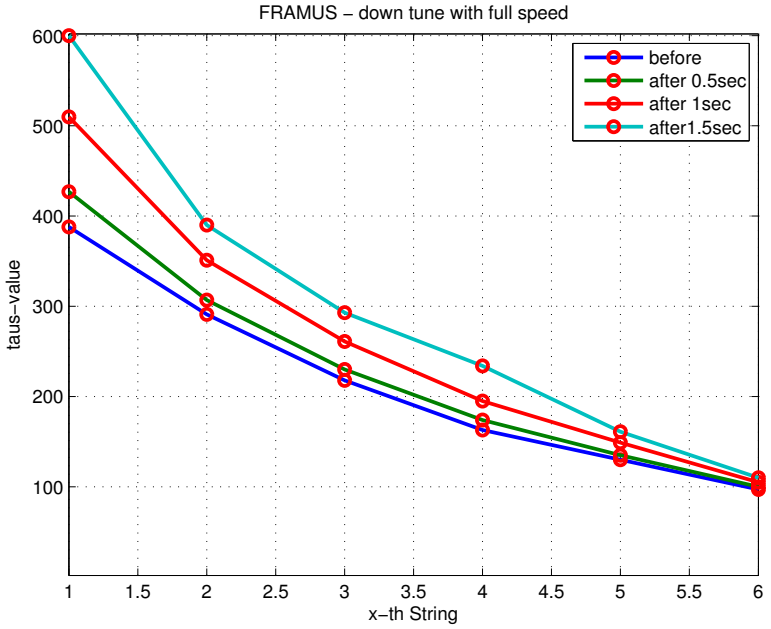

Figure 49: Plot of measured values of table 9 over strings (guitar *FRAMUS*)

As illustrated in figure 49 and figure 50, all six strings have different frequency decrease (or taus increase) by tuning with same motor strength. Especially the first string, the lower E (1th string), has an immense frequency decrease against the sixth string, the higher e (6th string).
This is due to the fact that in music theory the frequency always raises by the factor of two every octave step. In our case the measured periods (*taus*) will increase reciprocal to it. So, the lower the frequency the higher the measured *taus* will be.

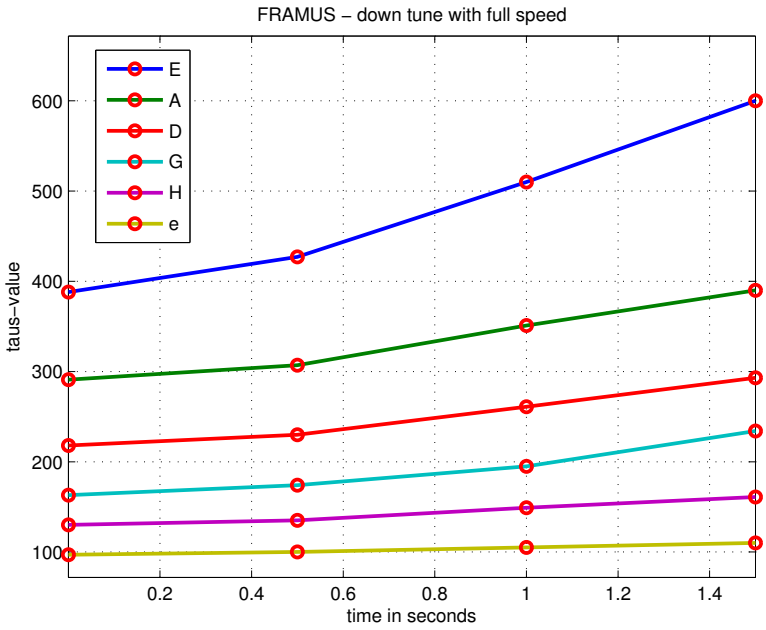

Figure 50: Plot of measured values of table 9 over time (guitar *FRAMUS*)

The increasing relations are plotted in figure 51, which show an average increase of about 1.75 times every half second with full servo strength. Only the fourth string D shows inconsistency which can be explained by a replaced new machine head (which was done by the other owner before).

Keeping these facts in mind for later conclusions the up-tuning behavior of all strings is tested, again with full servo motor strength.

***FRAMUS* - up tune with full speed**

Strings	Before	After 1sec	Before	After 1sec
E	388	371	438	395
A	291	287	331	313
D	218	204	258	228
G	163	154	193	175
H	130	161	150	139
e	97	96	107	103

Table 10: Measured *taus*-values by tuning up with full speed at different start values

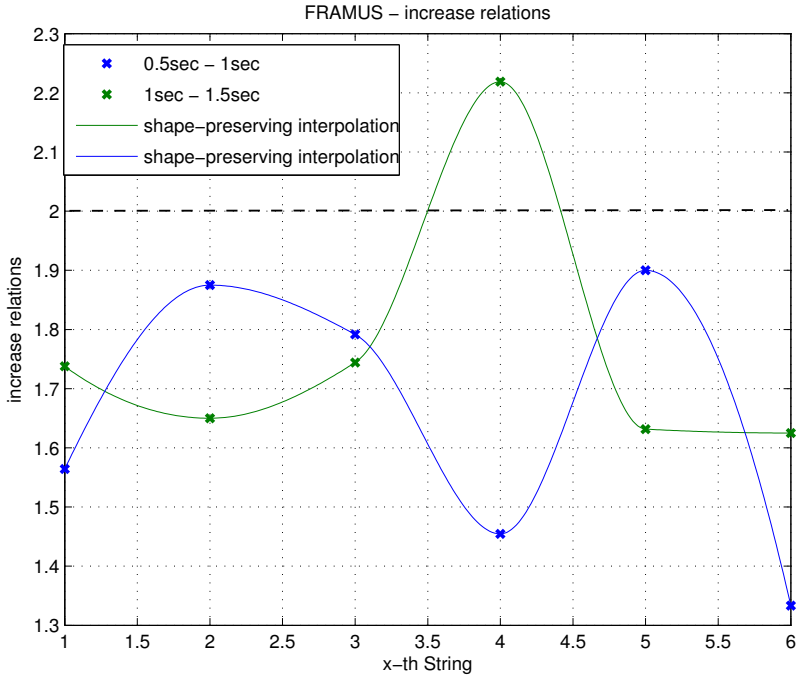

Figure 51: Plot of increase relations every half second when tuning down w.r.t. the start values (guitar *FRAMUS*)

For table 10 two different start values were adjusted and both times one second was tuned up. This was done because tuning-up experiments have shown that also the start value has an big impact on tuning behaviour due to current string tension forces.

High start frequencies means that the *taus*-values are at the beginning set like when the guitar is in right tune. Then the start values were set a little bit below the desired ones to see the detuned behavior.
Like in the plot of the down-tune experiment in figure 49, the up-tuning procedure acts in a similar relation between the six strings. Only the increasing tension resistance η causes a more difficult up-tuning of the servo motor, so the value-changes measured here are smaller.

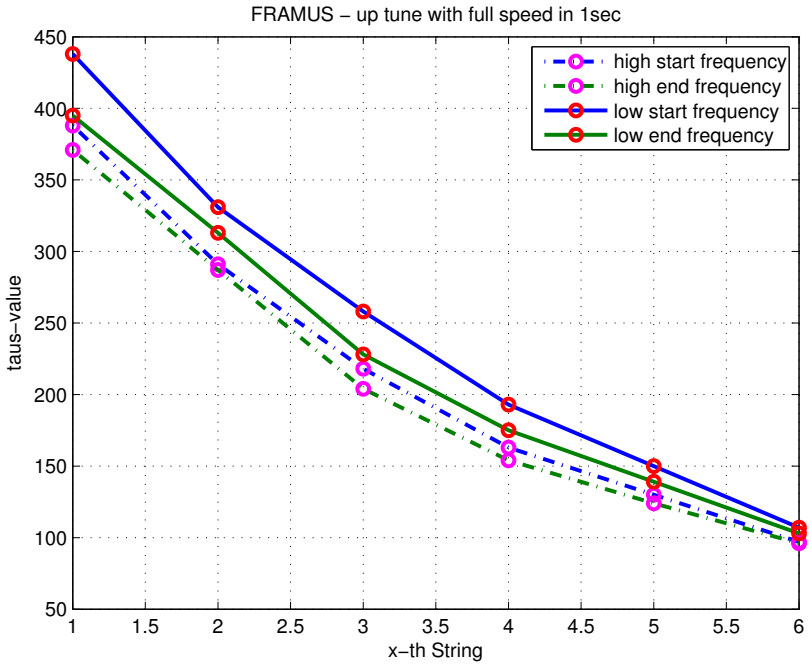

Figure 52: Plot of measured values when tuning 1sec up with full speed (guitar *FRAMUS*)

Up to here, the characteristic curves of the vintage guitar model *FRAMUS* had been gained. The second considered guitar model *JACKSON® Soloist* was expected to be more comfortable for the tuning process because of novel tuning pegs which need less motor torque for rotating compared to the guitar discussed before. By that reason the time periods the servo motor was rotating in were graded finer for getting a more accurate end-result. Furthermore, it has to be said that at testing this guitar the second string A was not available (unfortunately caused by damage).

First, again the down tuning process with full motor strength was recorded.

***JACKSON* - down tune with full speed**

Strings	Start	125ms	250ms	375ms	500ms	1sec	1.5sec
E	388	395	402	414	432	520	598
A	291	-	-	-	-	-	-
D	218	220	221	223	226	241	260
G	163	164	166	168	174	189	213
H	130	131	132	133	136	143	152
e	97	97	97	98	99	101	104

Table 11: Measured *taus*-values after various time periods with full-speed down tuning

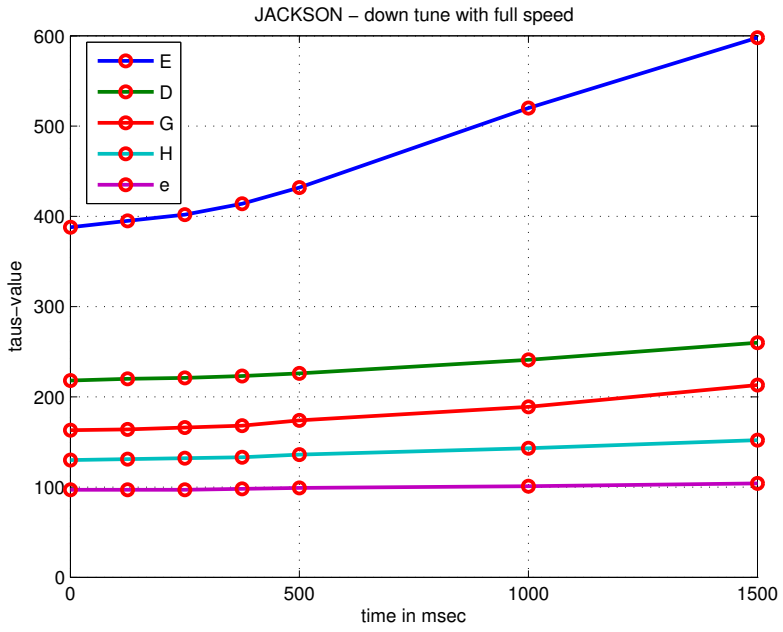

Figure 53: Plot of measured values of table 11 over time (guitar *JACKSON*)

Considering the two plots in figure 53 the same effect like mentioned at down-tuning of the previous guitar occurs. The lower the frequency the easier the tuning for the servo motor, of course due to additional torque decrease. Looking at figure 54 the increase relations show some inconsistency over all strings which can be interpreted that a high non-linear behavior is present.

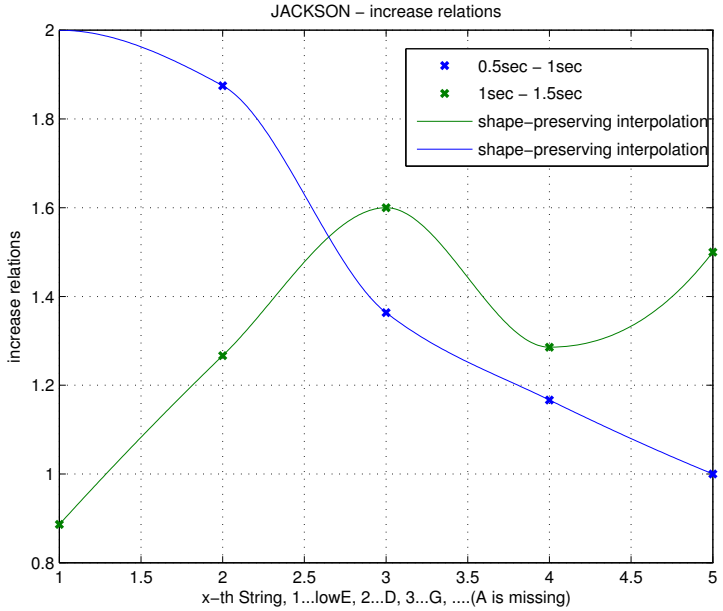

Figure 54: Plot of increase relations every half second when tuning down w.r.t. the start values (guitar *JACKSON*)

Continuing with the research about tuning up, the further values had been captured in table 12.

***JACKSON* - up tune with full speed**

Strings	Start	125ms	250ms	375ms	500ms	1sec
E	398	396	392	384	378	357
A	291	-	-	-	-	-
D	228	227	225	223	222	217
G	168	166	165	164	162	156
H	135	135	134	133	131	126
e	100	100	100	100	99	98

Table 12: Measured *taus*-values after various time periods with full-speed up tuning

Compared to the up-tuning table 10 of the *FRAMUS* model, table 12 involves time periods below a second. Like the detailed time resolution of the down-tuning records, this allows an explanation of the short-period behaviour of the motor/string dependencies.

At tuning up, the counteracting string-tension-dependent resistance η seems

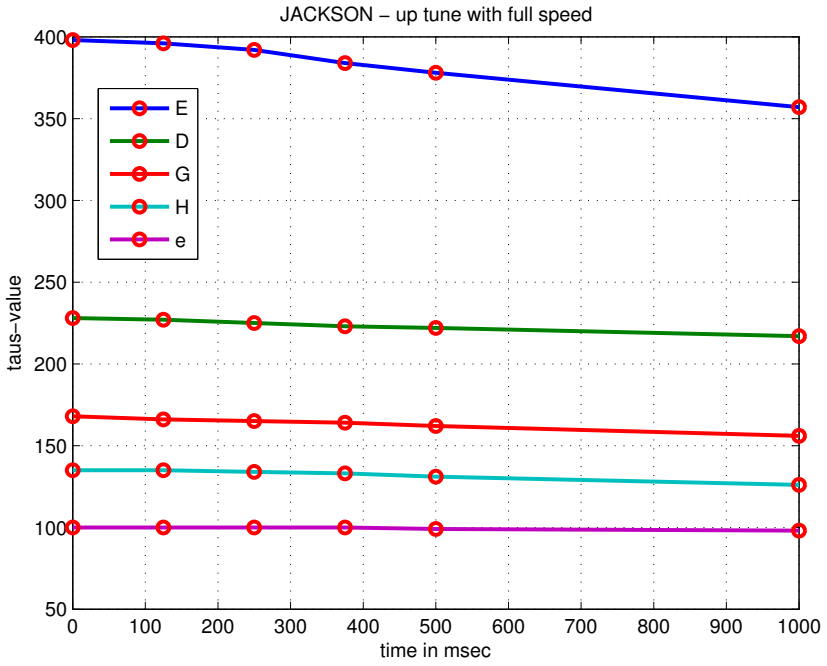

Figure 55: Plot of measured values when tuning up with full speed (guitar *JACKSON*)

to become a problem. The higher frequency strings *H* and *high e* have a too small changing in their *taus*-values which leads to inaccuracy regarding the maximum resolution of the internal ADC. This unfortunately causes less accuracy in tuning.

To sum up, the investigation of the two guitars has shown a slightly different behavior. Nevertheless, the decision was made for the model *Jackson® Soloist* due to easier handling by the chosen servo motor.

With the previously achieved data and characteristic curves it is now possible to complete our string model by designing the four gain factors, 2 x *String factor* (ξ) and 2 x *increasing/decreasing resistance* (η) (see figure 47). To show how this was done, the designing method for the D-string will be explained.

Generally, a system model can be configured regarding the response curves. It is referred to figure 47 for the following descriptions. At first we want to achieve the gain factors for the **down-tuning part of the model**, so the start value of the integral component has to be set accordingly to the *taus*-value of the D-string in table 11 (which actually is 218). The model input *omega* is set to its maximal possible magnitude to simulate the virtual full strength of the motor. Then the output *taus* is scoped to get the response curve visualized. Figure 56 shows the response output of the already adjusted model. The red boxes represent the certain time points at where the resulting virtual *taus*-values have to be adapted to the determined ones out of table 11. This was done by varying the gain factors till such time as the required characteristic curve arises.

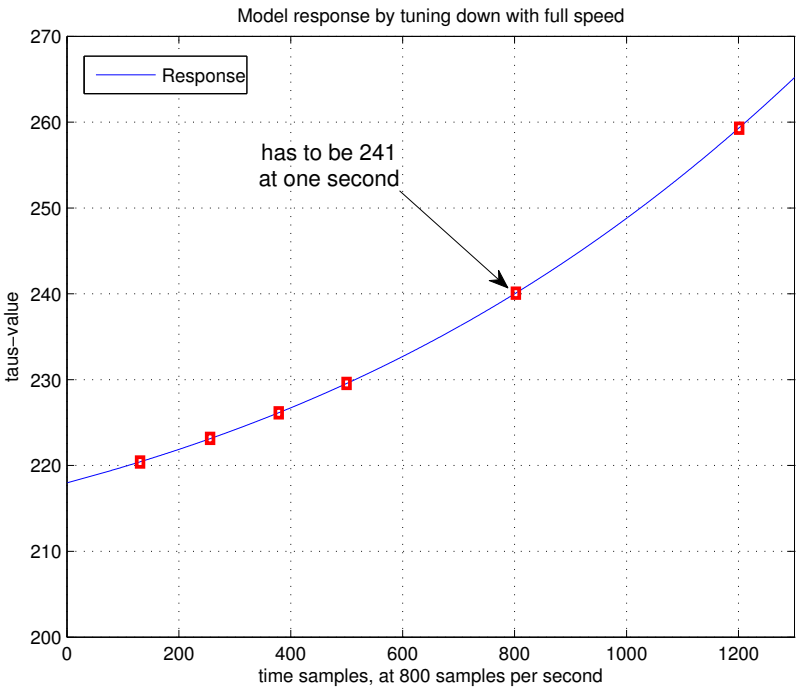

Figure 56: Plot of model response at 800 samples per second

In order to this, the same designing procedure was done with the up-tuning part of the model.
The delivered signals given by the up/down tracks in the model are then integrated and square-rooted to fulfil the last parts of our frequency equation 29.

All in all, only three strings were designed for simulation because of similar characteristics of two strings next to each other. So, a model was created for the lower E, the (middle) D, and the higher e. Each model represents a certain frequency range. The lower E-string model e.g. is also used for the A-string.

3.3.2 Servo motor

Unfortunately, tests have shown that also the intern control system unit of the servo motor actuates in a non-linear way. Because of this, also a servo motor model was developed.

PWM values	300	150	75	37
Rotations	2.125	1.75	1	0.375

Table 13: Determined rotations in three seconds at several PWM signals

By several given input PWM signals the absolute rotation of the drive shaft in three seconds was measured. This was done without load.

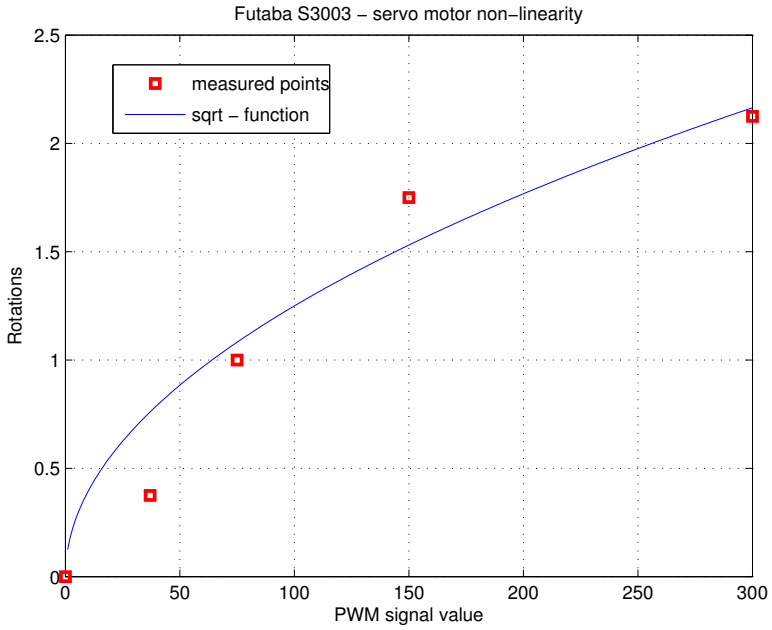

Figure 57: Measured data with spline interpolation (Values of table 13)

The plot in figure 57 illustrates the non-linear increase relation between the

PWM signal and the output rotation. A square root function seemed to be a sufficient approximation, which is also comfortable to design in Simulink.

$$\omega(t) = \alpha * \sqrt{s(t)} \tag{31}$$

Equation 31 represents the approximated transformation of the PWM signal $s(t)$ to the angular velocity ω. The factor α again was determined with adapting the response curve accordingly by a ramp formed PWM signal input. Figure 58 shows the simplified servo motor model in Simulink.

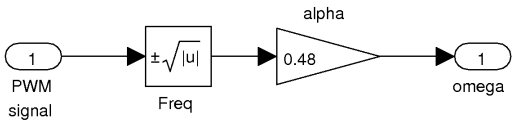

Figure 58: The Simulink model of the servo motor

3.3.3 Control system model

The complete control system was modelled in closed loop form like shown in figure 39.
To describe the plant, the servo motor model block was switched before the guitar model block. Of course, also a PID-controller block is necessary to generate the control PWM signal in the range of ±300. Simulink already provides a designed PID-block with many features, such as an integral windup prevention. This allows a relatively simple configuration with respect to the individual PID gain factors. The inside of the provided PID-controller block is shown in figure 59.

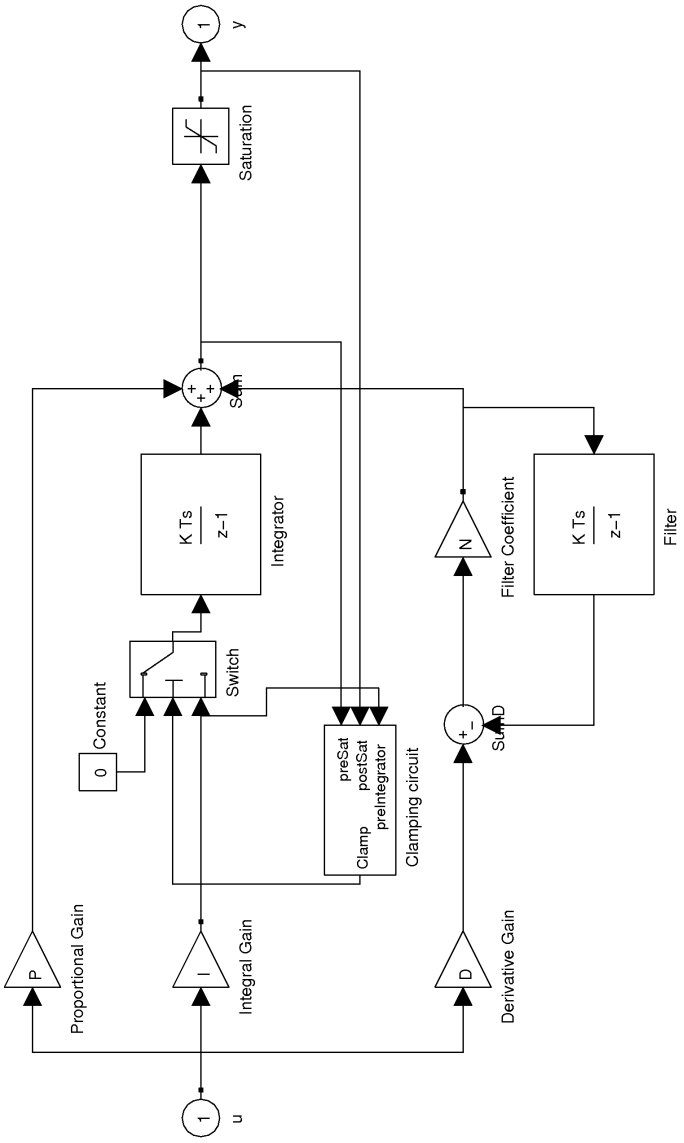

Figure 59: The Simulink model of the provided PID controller

All the variables in this block can be adjusted via user-interface. The saturation item at the end describes our signal limitation of ±300 and the filter coefficient N of the derivative part is set to 1 in our case. The clamping circuit of the integral part represents the anti wind-up mechanism. Basically this block describes the parallel PID control behaviour by summing all three terms up (see figure 43).

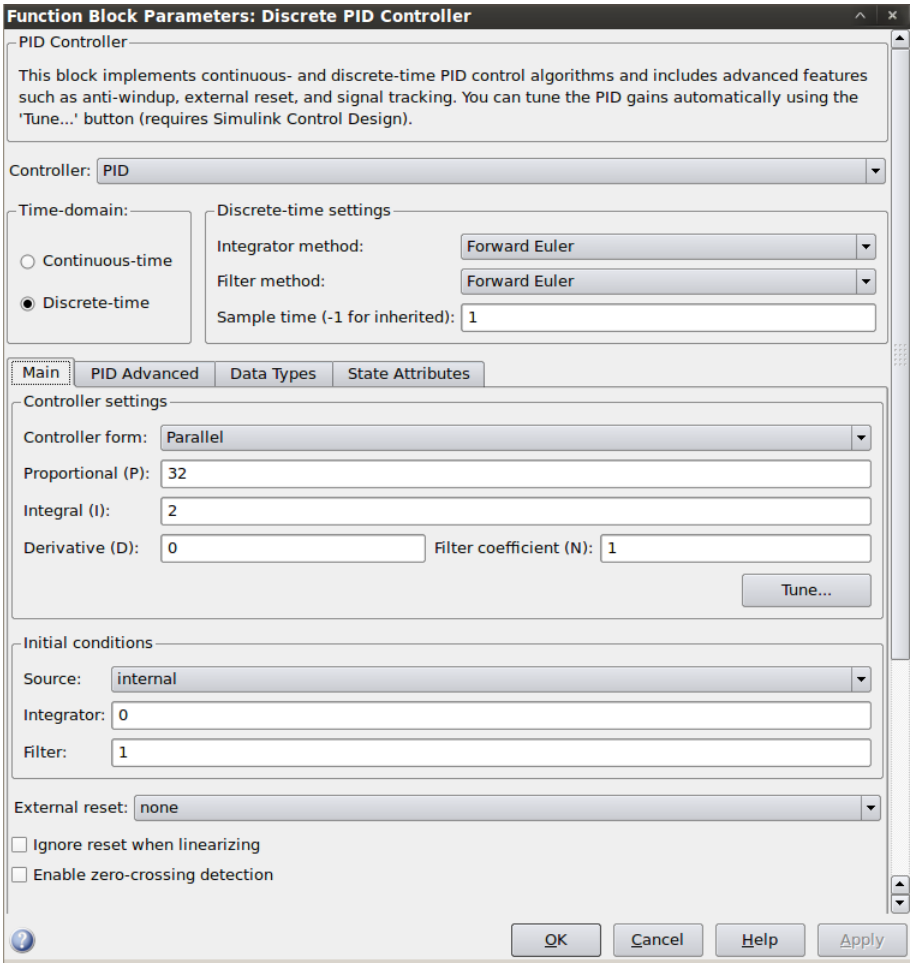

Figure 60: Screenshot of the provided PID controller user-interface

To sum up, all blocks created and discussed were now applied together to form a closed loop control system, for this see figure 61.

The blue highlighted part can be interpreted as the discrete part of our control system which represents our micro-controller. The motor model component (green) is then actuated by a given PWM signal of the PID-controller output, which further "generates" the angular velocity. Then the model block of the guitar string (red) is transforming the value into the corresponding frequency expression. This plant output is then compared to a reference value (our desired in-tune-value). The difference is then quantized by the micro-controller and leads to a further actualization of the control PWM signal.
The rate-transition items are virtually transforming the sample time from continuous (fixed sample step size of simulation = 0.01) to discrete (sample

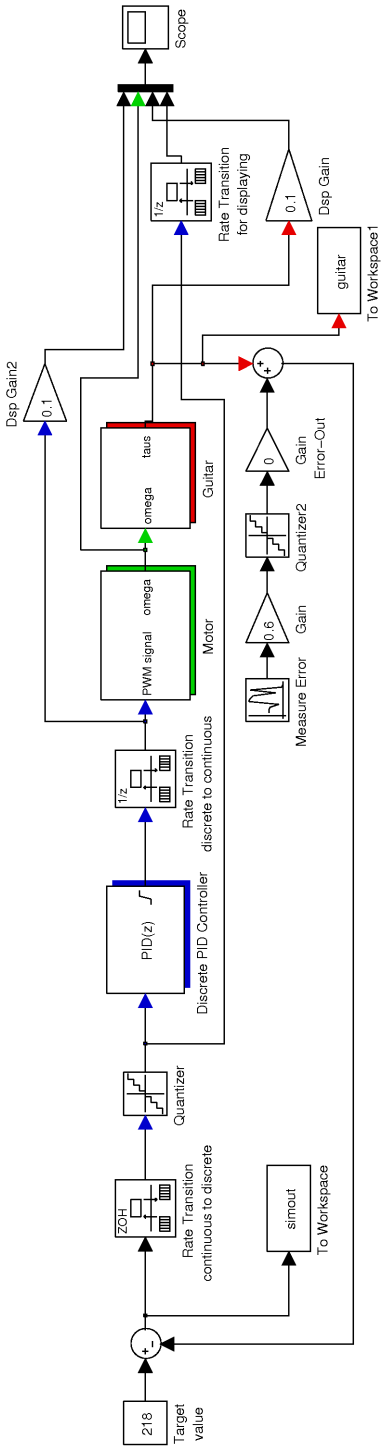

Figure 61: The Simulink model of the designed control system loop

step size = 1). This setup is related to the constantly given update rate of the frequency detection algorithm. Generally, the implementation of the PID controller terms was simplified by considering the time coefficients of the integral term and the derivative term as 1. Further it was assumed that the time coefficients will always stay constant which also concludes a constant calculation update rate of the control value. Time measurements of the frequency detection refresh rate resulted in eight updates per second. That means regarding our control system model simulation time, that each eighth sample step passing by (sample $n*8.00$) represents an elapsed second. Furthermore a Gaussian noise generator was added to disturb the error input of the PID controller. This also allows simulating the given quantization noise fluctuation (would be ± 1 digit) which may occur at the A/D-converter output.

3.3.4 Simulation / Dimensioning

For simulating the designed control system loop, the error value, the PID-controller output value and the plant output value were considered by plotting them with the *Scope* element provided in Simulink. This visualizes the interaction of all three values. Due to the fact that all six strings have different frequency levels and hence a different kind of frequency-changing-speed, more than one PID configuration seemed necessary. Therefore it was assumed that three types of controllers over six strings will be sufficient, thus, the first concept was one PID for the lower e-string and the H-string (high frequencies), another one for the two strings D and G in the middle of the guitar frequency range, and finally one PID for the low frequency strings A and lower E.
As a fact that the tension-force of a guitar string is affecting the tuning procedure a single PID would not be able to tune up *and* down. So this will require two PIDs for either down-tuning or up-tuning. Furthermore, when a musician is tuning his guitar and he has to tune a string down, he is turning the certain tuning peg a little bit below the target frequency and then back up again. The guitar player is doing this to make sure the guitar string is on full tension, because if it' not, a mechanic slackness could cause a short string slippage which will then de-tune the string again. Because of this, the down-tuning PID-controller terms have to be set in a way to produce only one intentional overshoot, so a light up-tuning follows.
Enhancing our controller concept this results in six different configuration-sets.

The following explanation shows the designing procedure for our PID controller parameters. Generally, the dimensioning was done empirical based on the *Ziegler-Nichols* method, but without really keeping its policy. Additionally it was attended to use only gain values referred to the **base-2 number system**, which allows a calculation by *shift-operations* only. As an example, the calibration of the down tuning controller for the lower E-string is explained.
At first the target *taus*-value had to be set, in this case the lower E is represented by 388. Then the de-tuned value (start-value, initialization of the integrator in the string model) of the virtual string was set, for instance, to 366. That will lead to an error of $388 - 366 = 22$ at the beginning of the simulation.
At second, *only* the proportional gain was heightened as long as oscillation comes up. As discussed before, the resulting overshoot is desired and had to be reduced to provide more stability. The two figures 62 and 63 contain the simulation plots of our P-controlled system with different set proportional gains, $P = 32$ and $P = 16$. As seen, the gain factor 16 seemed more applicable to continue with.

Because the P-term alone resulted in too less accuracy, the next step was to add an integral term. This was not always easy to do, because the right balance between integral gain and the derivative gain had to be determined, sometimes in a just experimental way. Generally, the integral gain was heightened until an oscillation appeared. In this case, the frequency information of the lower E string is given by an quite high value so that a integral gain of 2 is already causing oscillation (see figure 64 for the related simulation plots of the PI-controlled system).

The last step was finally to add the derivative term, which is responsible for a more rapid adaptation to the target value. On the other hand, this term can quickly affect the control system stability when set wrong. By raising the derivative gain until the remaining oscillation disappears and the target value is reached, we will get our desired PID-controller. Here, this final gain value was 8. Figure 65 shows the achieved control system simulation, which finally was implemented for the down-tuning process of our motorized guitar tuner regarding to the lower E-string.

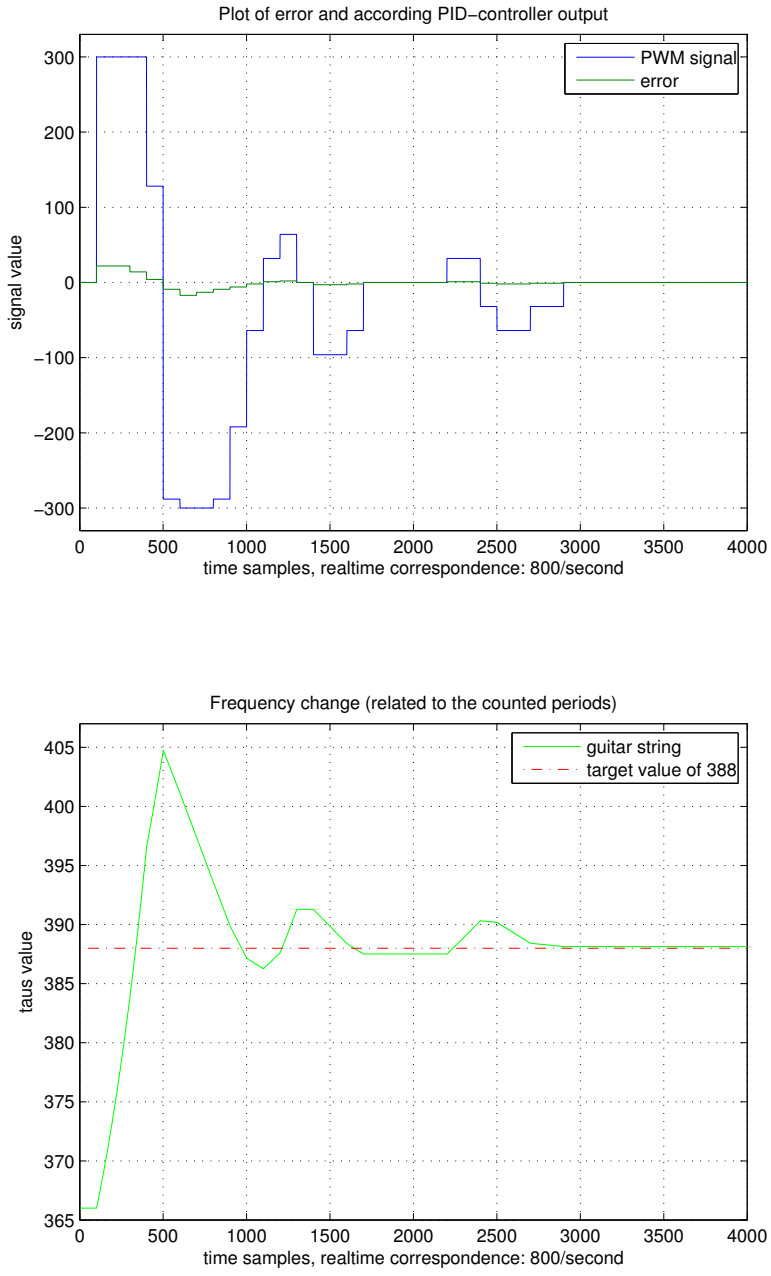

Figure 62: Simulation plots with proportional gain of 32 only

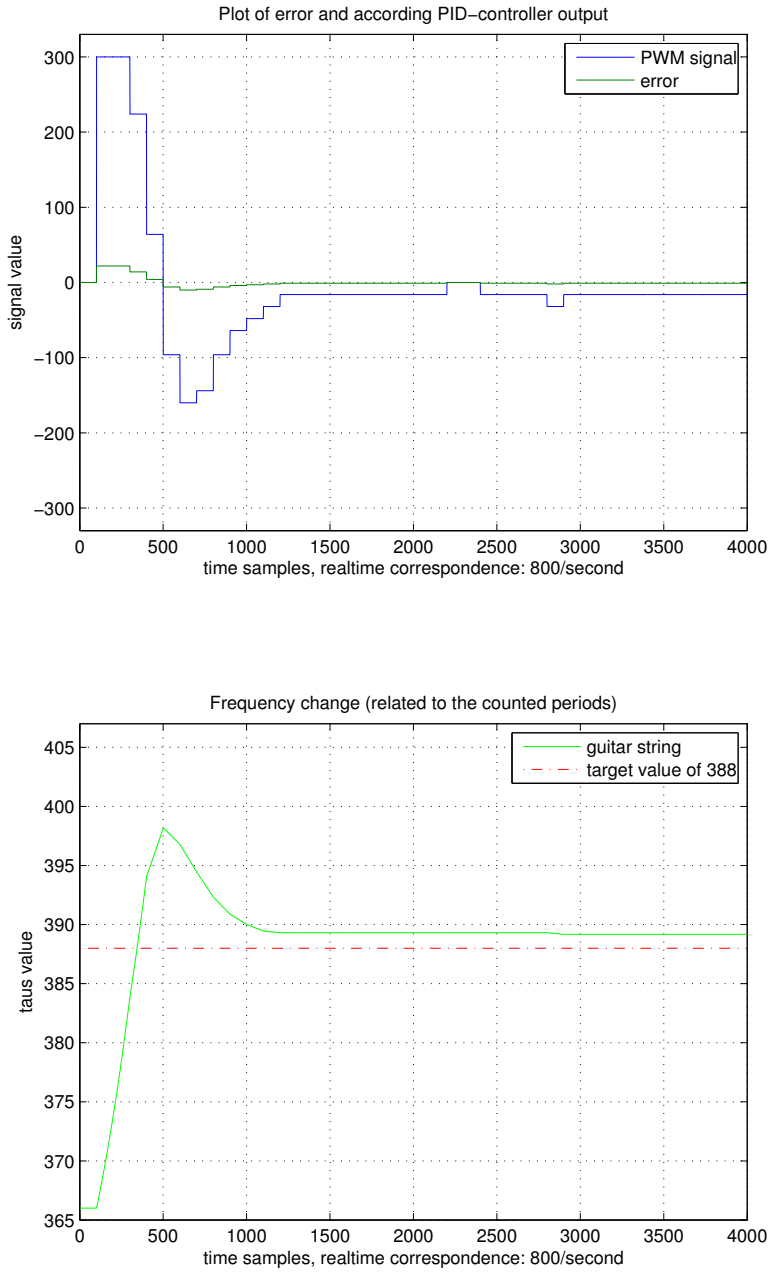

Figure 63: Simulation plots with proportional gain of 16 only

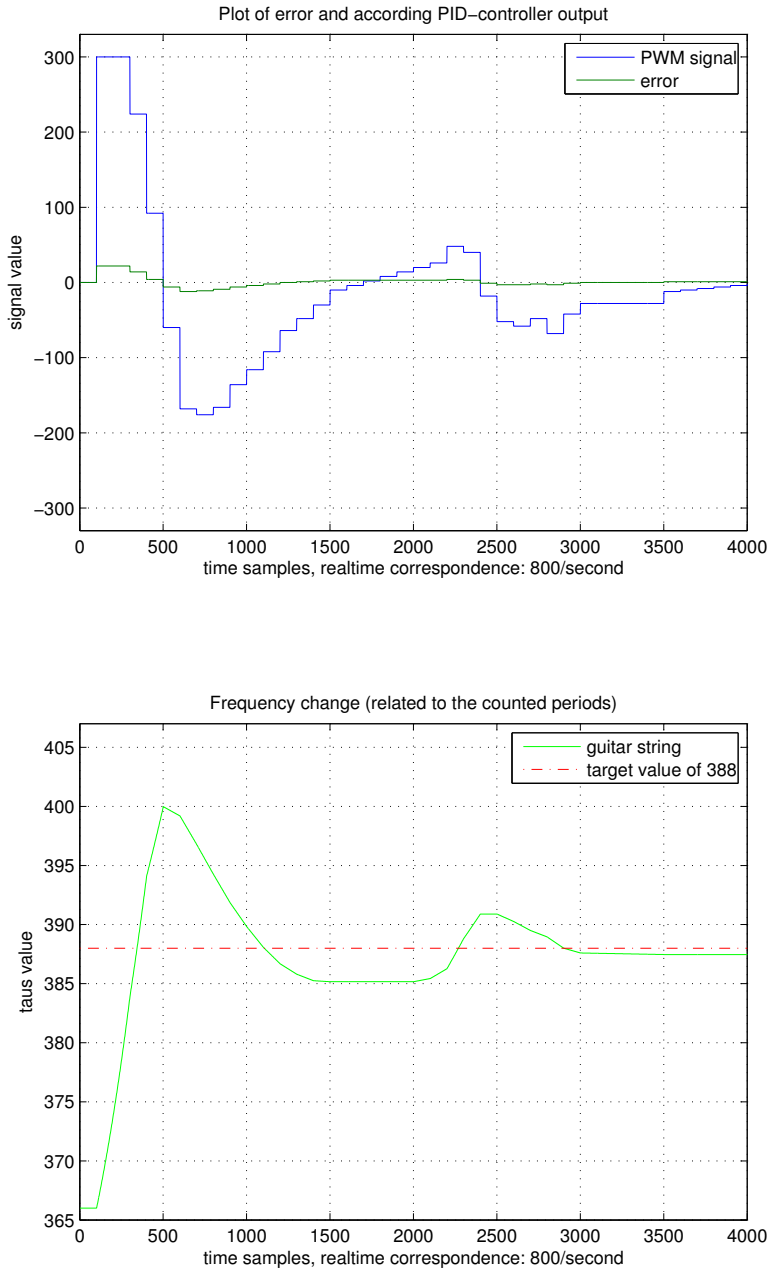

Figure 64: Simulation plots with P = 16, I = 2 and D = 0

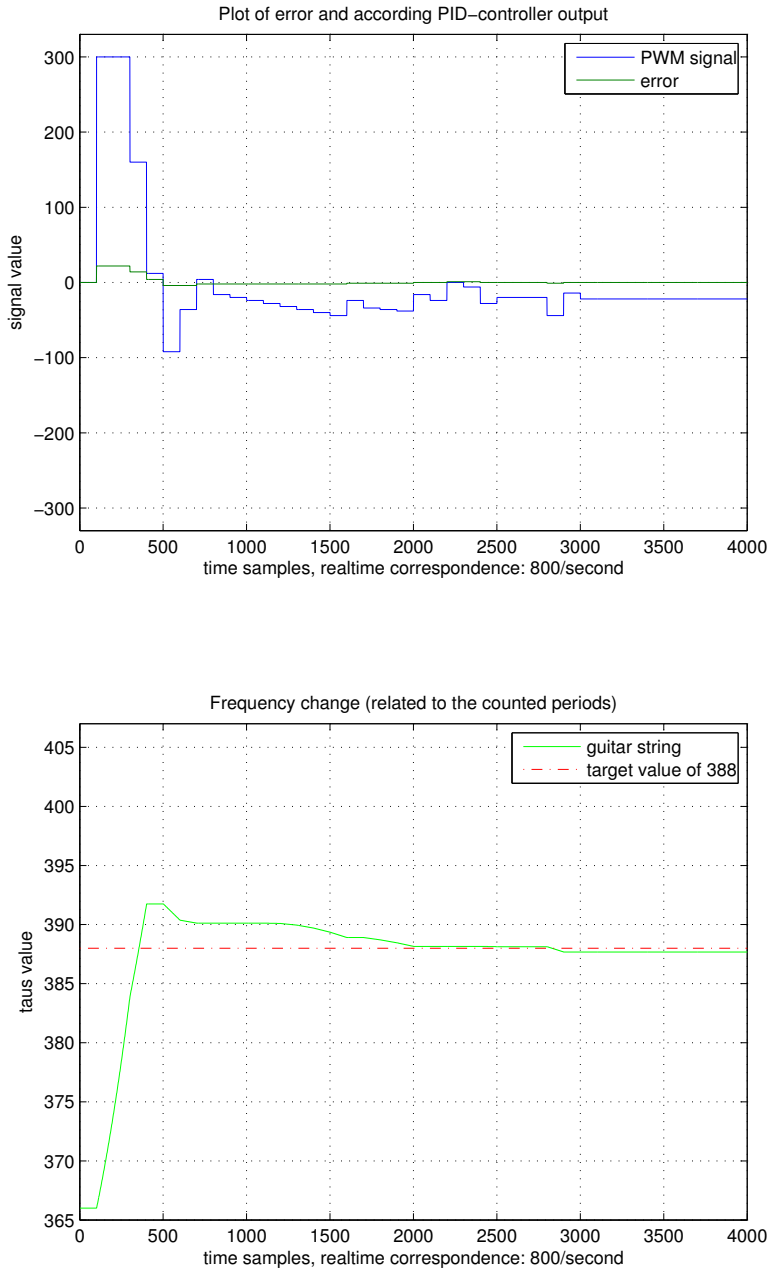

Figure 65: Simulation plots with P = 16, I = 2 and D = 16

After all this design procedure was used for all six controller types. It turned out that some controllers just need a proportional term for proper tuning behavior, such as the controller used for the high e-string, whose sense accuracy is limited anyway (detecting high frequencies).
Also another inconvenient characteristic of the guitar string appeared to disturb the tuning process: when a string is stroken, the immediate frequency is higher than it is while the string oscillation is fading out. Dependent on the guitar, this leads to a de-tuned sound if the musician is stroking the strings harder. To solve this problem, a constant error correction value (offset) had been added to the control output calculation (zero by default), which can be adjusted by menu, if desired.
In conclusion, the end-results of this software supported PID-controller simulations are shown in table 14.

Parameters	P	I_{up}	I_{down}	D
low E, A	4	-	1	3
D, G, H	5	-	1	-
high e	7	-	-	-

Table 14: PID-controller shifting parameters (modelled for the guitar *JACKSON® Soloist*)

As a consequence the higher e-string does not really need two separate controllers for up or down tuning, because of accuracy issues where more detailed controlling doesn't really make sense. In the end, this allows an implementation of only five different controllers.

3.4 Implementation

Discussing all implementation details would be too extensive, by this reason only a brief instruction about the control algorithm concept is explained.

To implement the whole control concept an array out of a PID-controller struct was built. This struct contains the individual shifting parameters of one PID-controller. The two *active* terms are used as boolean flag, because there is not always a need of an integral or derivative part in our control calculation.

```
typedef struct
{
  uint8_t P;
  uint8_t I;
  int32_t I_active;
  uint8_t D;
  int32_t D_active;
  int8_t  Correction;
} Pid;
```

Listing 8: The struct content, represeting one PID-controller

The so called controller-array contains five entries representing our PID controllers which are initialized to the according parameters at start-up. To actually choose the proper PID the target frequency value is used, which implicitly means, that the regarded string has to be in this frequency range, otherwise the chosen controller parameters would not fit to the string characteristics. The tune target value is dependent of the appropriate general-filter which has been either selected automatically or manually by menu configuration.
The case of up/down tuning is referred to the sign of the given error.

The tuning calculation is done by executing listing 9. First of all, the old error value has to be saved for the integral summation usage. Then the actual error value has to be determined. The relating PID-controller has to be searched only once, providing more efficiency. The output value called *control* is calculated with shift operators.
The integral term elimination is used to exclude the integral term from calculation when the target value was reached several times, because then integration in this range would be unnecessary. Also the windup effect is avoided by keeping the integral sum in a certain range. The saturation is motor dependent which is, as mentioned, ± 300. At this value it does not make sense for further increase (saturation of the motor speed).
Generally, the PWM signal calculation was done according to equation 22.

```
int16_t tuner(uint16_t target, uint16_t current)
{
  //update
  e_old = e;
  e = (int32_t) target - (int32_t) current;

  //find PID:
  if(!pid_found)
  {
    uint8_t pid = getPID(target, e);
    P_s = PID[pid].P;
    I_s = PID[pid].I;
    I_active = PID[pid].I_active;
    D_s = PID[pid].D;
    D_active = PID[pid].D_active;
    correction = PID[pid].Correction;
    pid_found = 1;
  }

  // string dependent error correction:
  e += correction;


  // Integral term elimination
  if(e == 0)
    count_e++;

  if(count_e > INTEGRAL_THRESHOLD)
  {
    esum = 0;
    I_active = 0;
  }

  //Integrator with Anti - Windup (300 Servo-Limit)
  if((control < WINDUP) && (control > -WINDUP))
    esum = esum + e;

  // Now calculate
  control = (e << P_s) + (I_active & (esum << I_s)) + (D_active
      & ((e - e_old) << D_s));

  // Saturation Limit(PWM +-300 -> WINDUP default =300)
  if(control > WINDUP)
    control = WINDUP;
  else if(control < -WINDUP)
    control = -WINDUP;

  //Servo-Control
  setPWM(control);
  return control;
}
```

Listing 9: Control value calculation and actuation

4 Conclusion

4.1 Results

As result of this bachelor thesis a full functional hand-held device for tuning an electrical guitar automatically could be presented.
Due to the low representation error of the introduced system-wide frequency unit, well designed filters and well done work on controlling the servo motor, quite good tuning results can be achieved by the "Motorized Guitar Tuner". The tuning results were confirmed by different people, including semi-professional musicians as well.
Decisive limits of the accuracy of the tuning process are given by the interaction of the different strings with each other and the guitar neck. The device tunes one string without having any information of the tension of the other strings. Changing the tuning of the whole guitar, often more than one tuning process per string is necessary. This effect can get much worse, when the guitar is equipped with a tremolo.
When a more precise tuning is required as the introduced unit is able to represent (compare with table 2 in section 2.2.2), this device is not applicable.
Based on the achieved speed of the tuning process, usually picking a string once is enough. Picking the string twice is sometimes necessary for higher strings, especially the high e string. A low amplitude of the signal requires a high gain setup of the preamplifier stage, which causes a significant high noise level. Sometimes when the string oscillation becomes very small, the device detects only the filtered noise and tries to tune the guitar according to this randomly generated frequency information.

Figure 66 shows the finished device when the back plane is opened. Nearly the whole space inside the case is taken by the components. Only due to precise measurements with a sliding caliper it was possible to fit in all components.

Figure 67 shows the finished populated and soldered main board. On the front view, the different connectors are highlighted.

Figure 68 shows the front view of the device with the different labeled components accessible by the user. The range of the external power supply is only limited by the voltage regulator which works with voltages from $7V$ up to $35V$ [16]. When plugging in the connector of an external power supply, the battery is internally disconnected. Hence no short-circuit or cross current can occur.
The tuning peg coupling is a selfmade graving project out of wood. The inside surface is padded by thin packaging material.

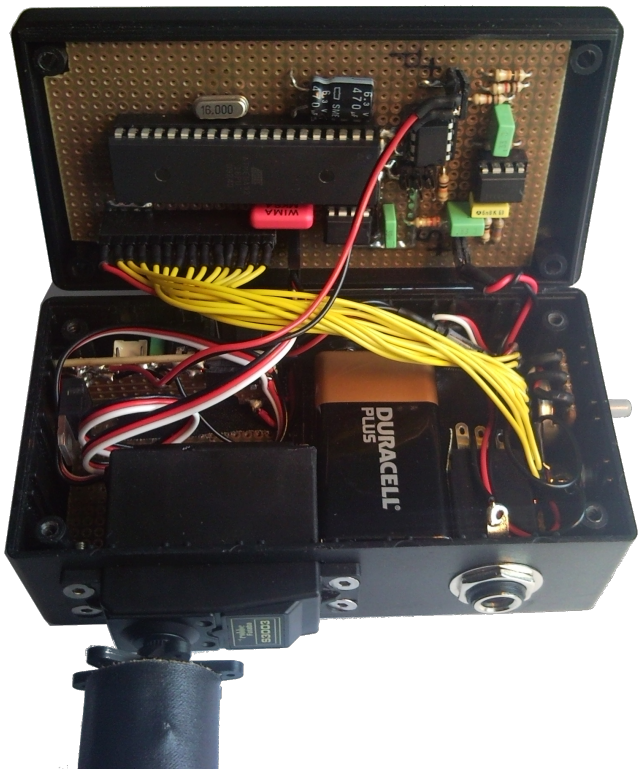

Figure 66: Inside view of the finished device

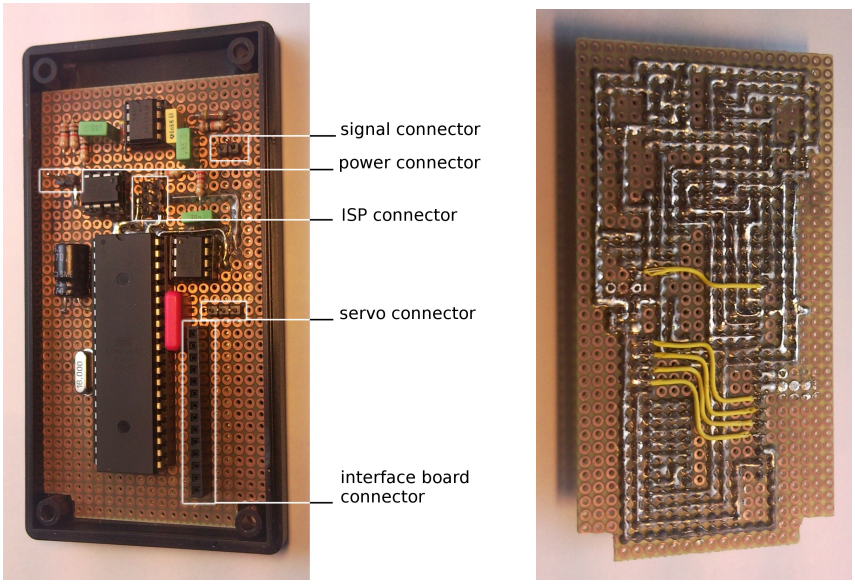

(a) Front view (b) Back view

Figure 67: Finished main board

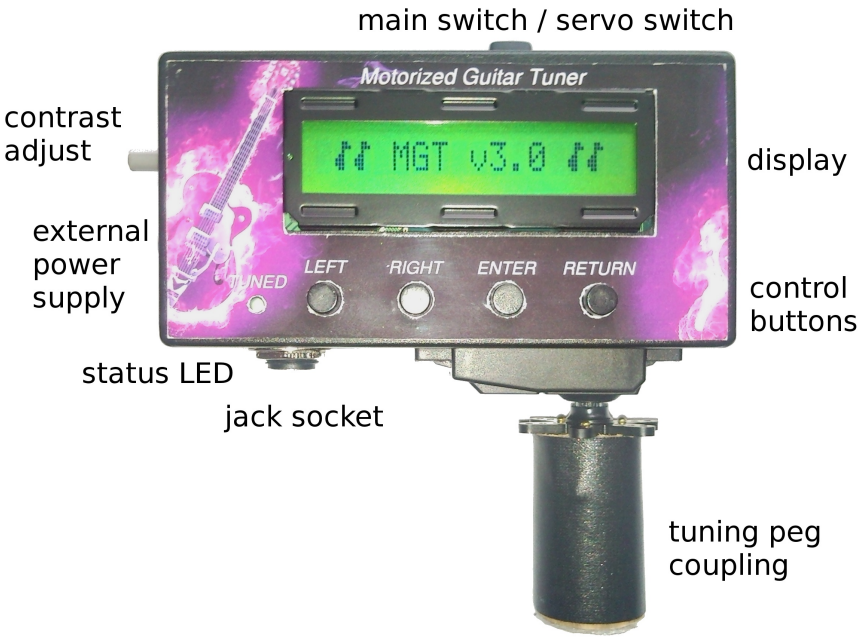

Figure 68: Front view of the device

4.2 User manual

The state diagram in figure 69 illustrates the menu structure. At the beginning the first entry of the main menu is shown (1 Auto Tune). The black arrows denote either LEFT or RIGHT, whereas the red ones mean RETURN or ENTER.
The Auto Tune menu contains the three different automatic tuning modes. The Single Tune menu, in contrary, contains the certain single tune options to activate. The Options menu provides some deeper menu structures which allow some PID-controller reconfiguration.
Generally, all menus are implemented as loops what gives more navigation comfort. For exiting an actual menu, the RETURN button is pressed. If RETURN is pressed at least several times, in the end the Start Tuning field will be reached, which allows entering the previously selected tuning mode. If *Tuning* is started the motorized guitar tuner will then be listening to the input signal accordingly. In this ready-mode the LEFT and RIGHT buttons can be used to drive the servo motor for positioning the tuning slot to fit the tuning pegs.
Finally, to start the actual tuning procedure, use the thumb to press the servo switch button and stroke the appropriate string.

For entering the main menu again, just push any of the four menu buttons.

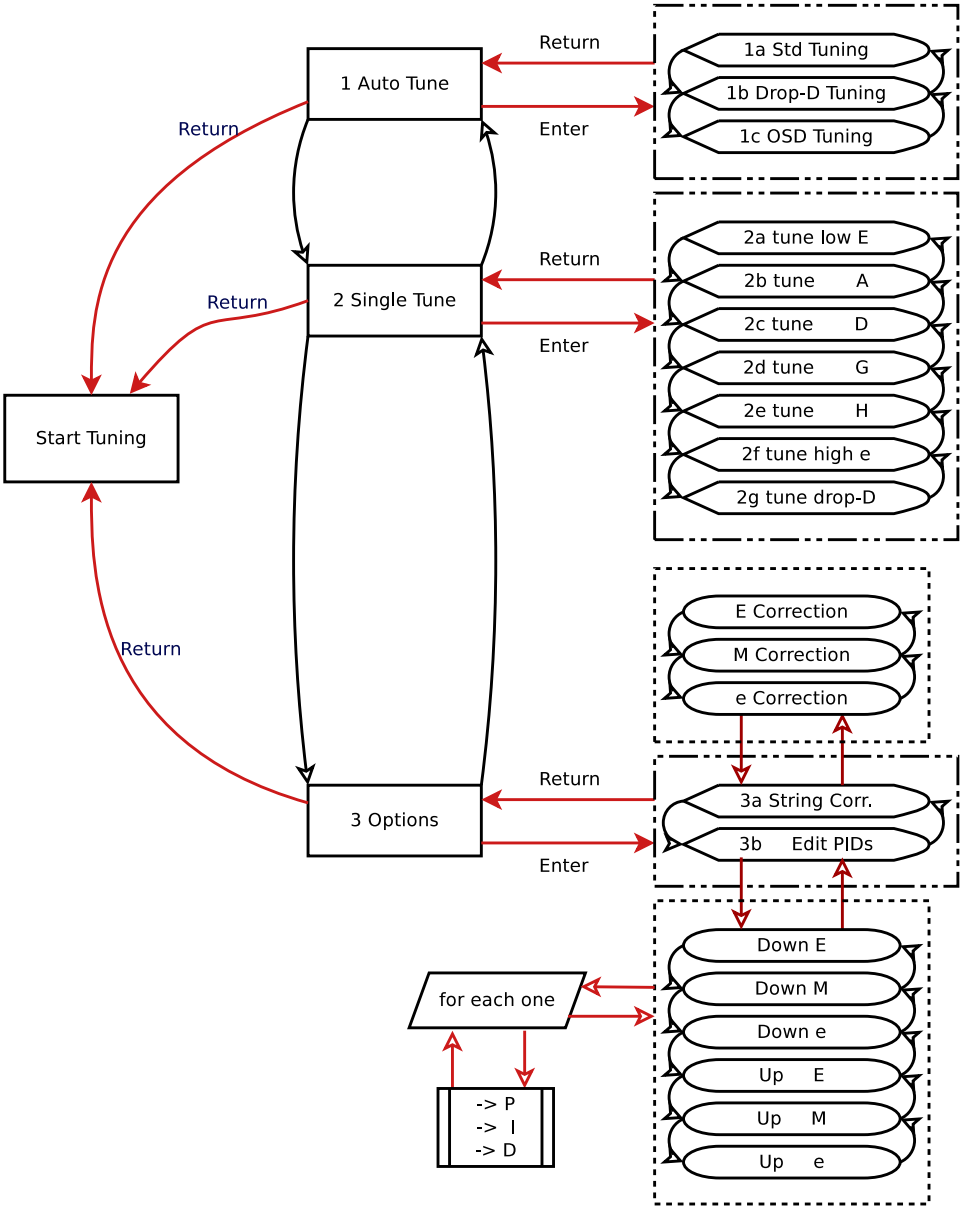

Figure 69: Menu entries

4.3 Connection diagrams

To complete the results, all connection schemes and the resulting board layouts are attached here. The connection scheme of the main circuit was already printed and discussed in chapter 2.1.4.

Figure 70, 71 and 72 show the connection diagrams of the designed boards. In figure 72 the elements `P0`, `BT1`, `SW1` and `P1` are only plotted to complete the power supply circuit. In reality, they are mounted floating or implicitly installed in components, like `SW1` in the external power jack. Hence these components are not shown on the board layout of the power circuit (figure 75).

Figure 73, 74 and 75 show the designed board layouts. The green lines represent backward tracks, the red lines front tracks and the blue lines floating wires. The magenta colored border of some components indicate that they are mounted on the backside of the board.

Figure 76, 75 and 78 show 3D simulations of the finished boards. This was very useful to keep the overview of the board during the designing and assembling processes.

The design of all connection diagrams, layouts and 3D simulations were aided by the open source suite "KiCAD" for Linux.

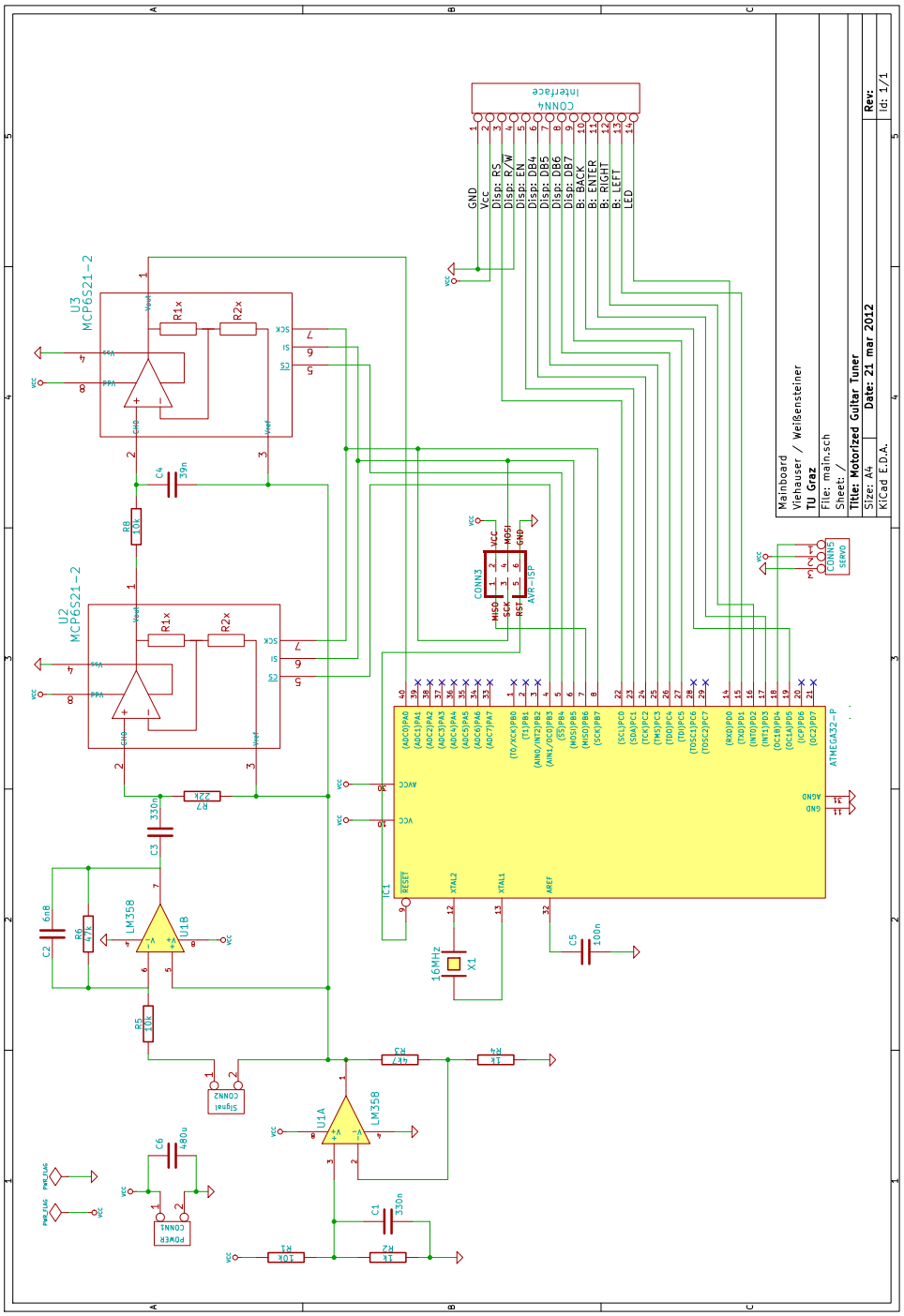

Figure 70: Connection scheme of the main electrical circuit

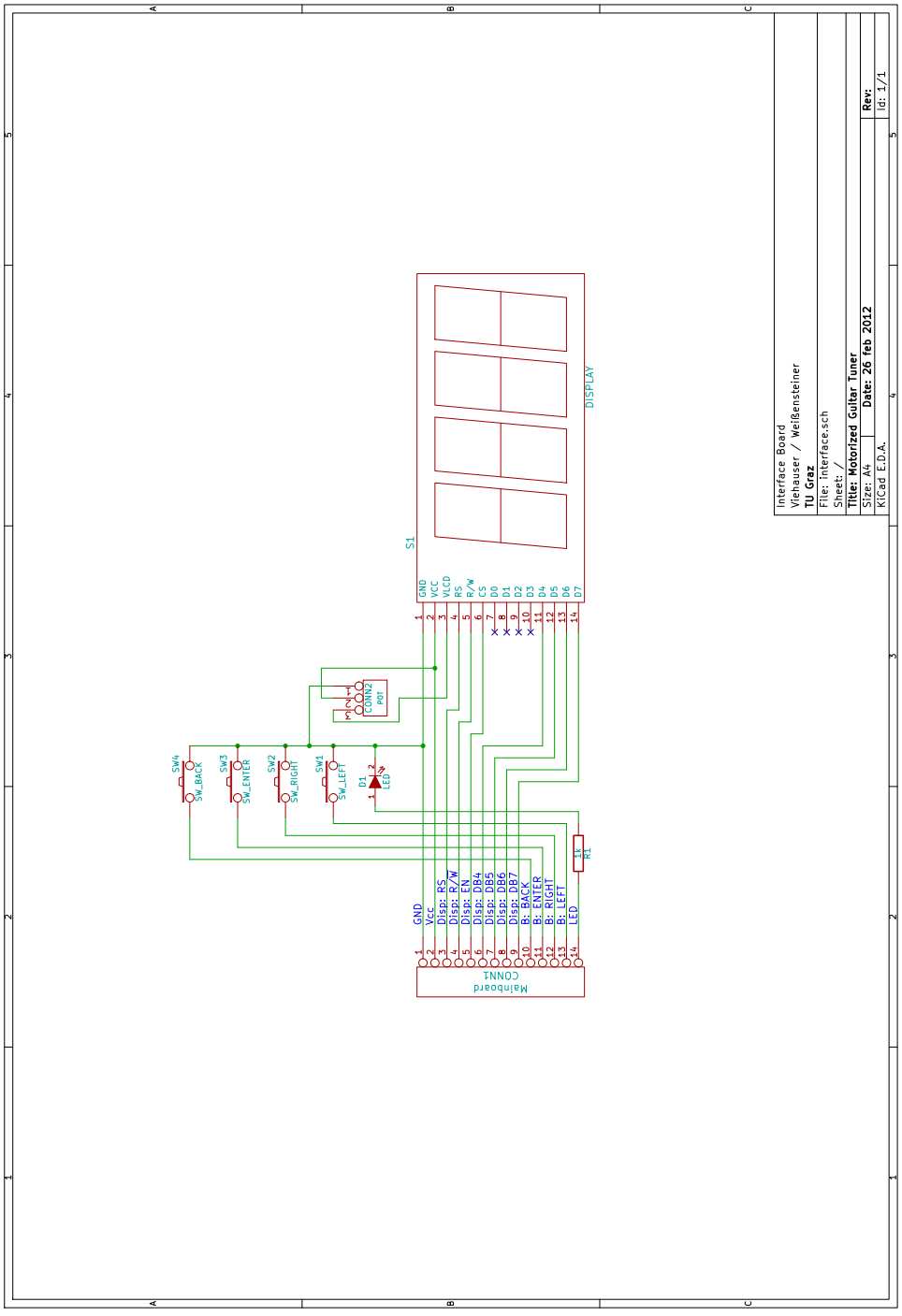

Figure 71: Connection scheme of the interface board

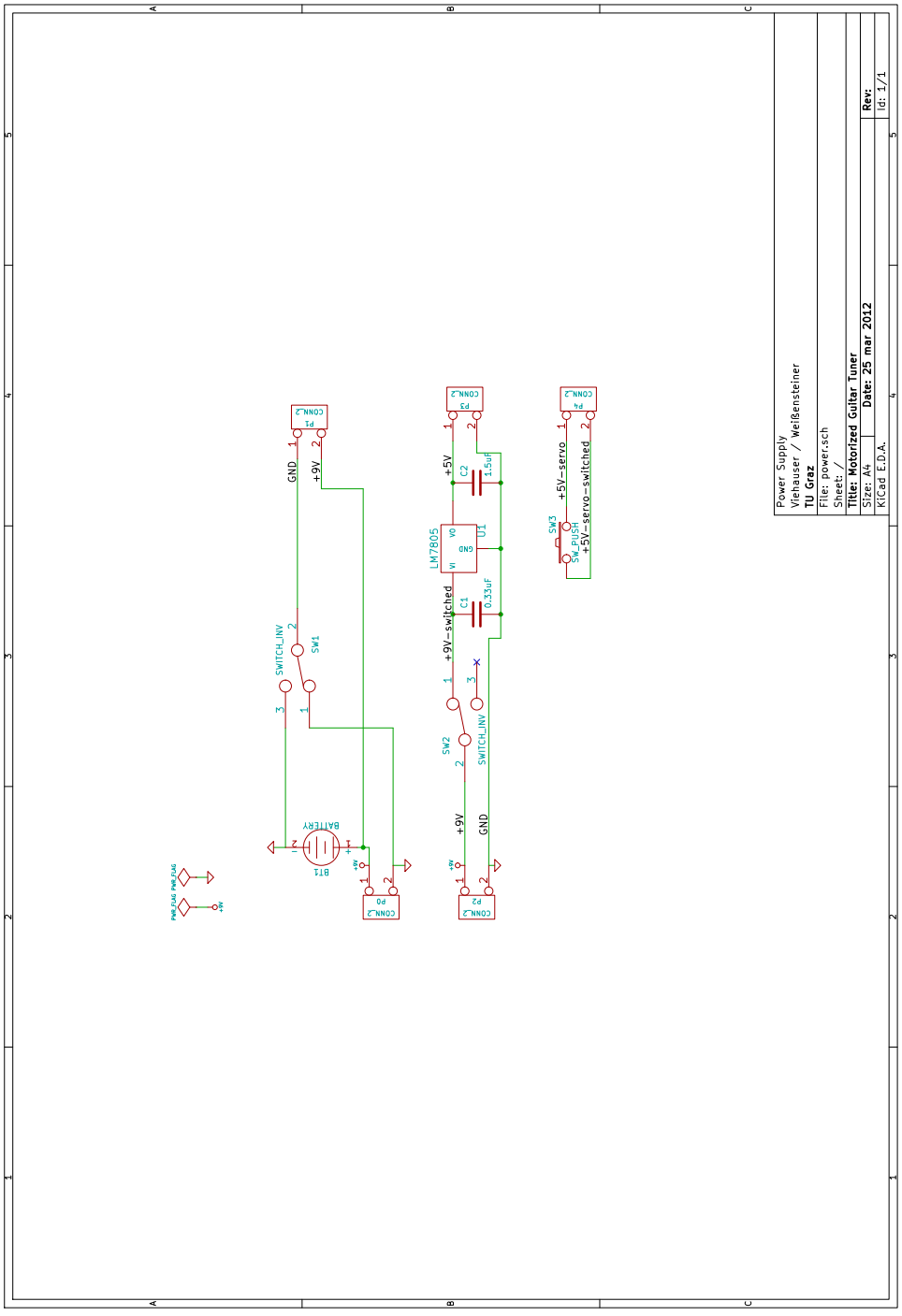

Figure 72: Connection scheme of the power supply

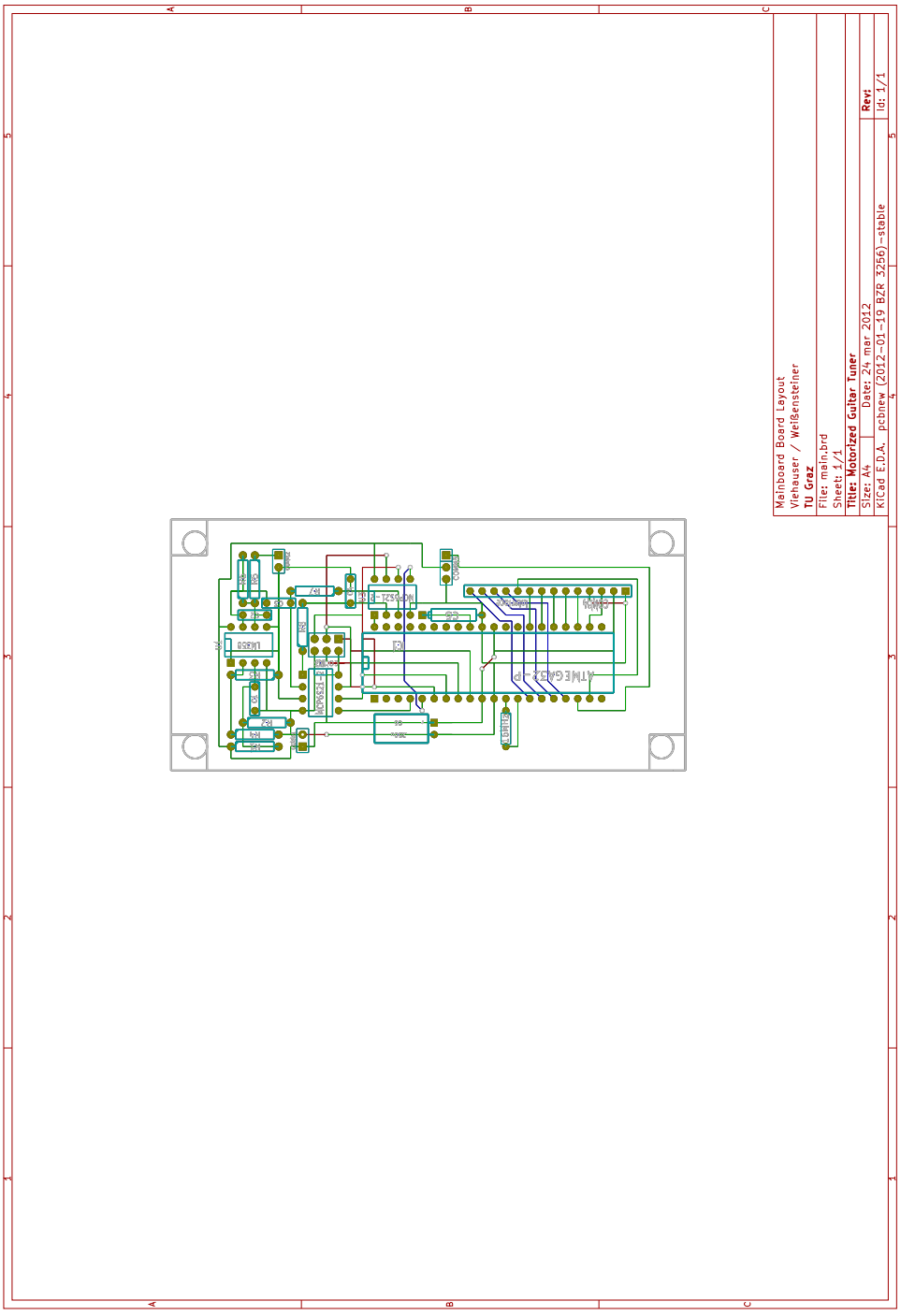

Figure 73: Board layout of the main circuit

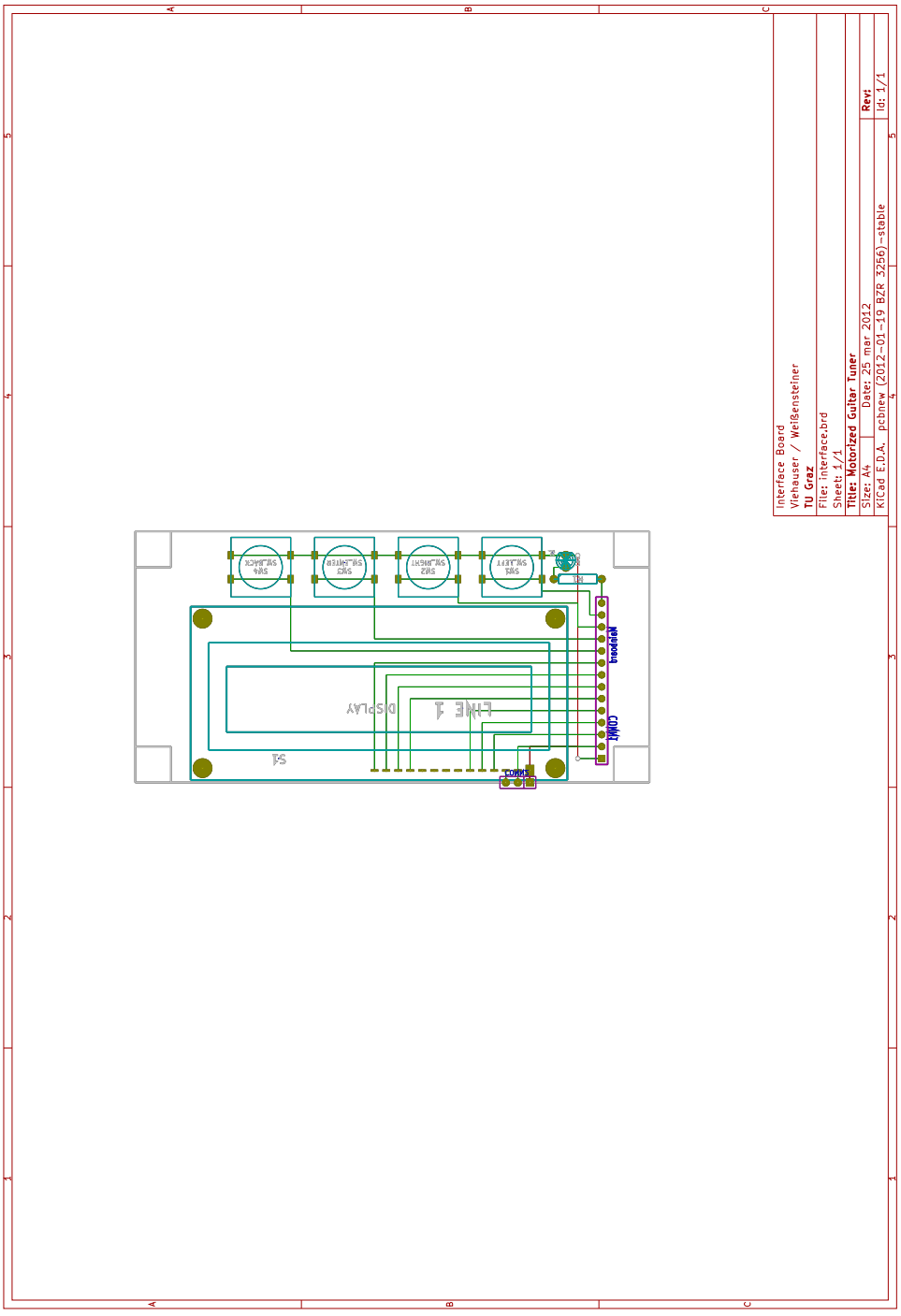

Figure 74: Layout of the interface board

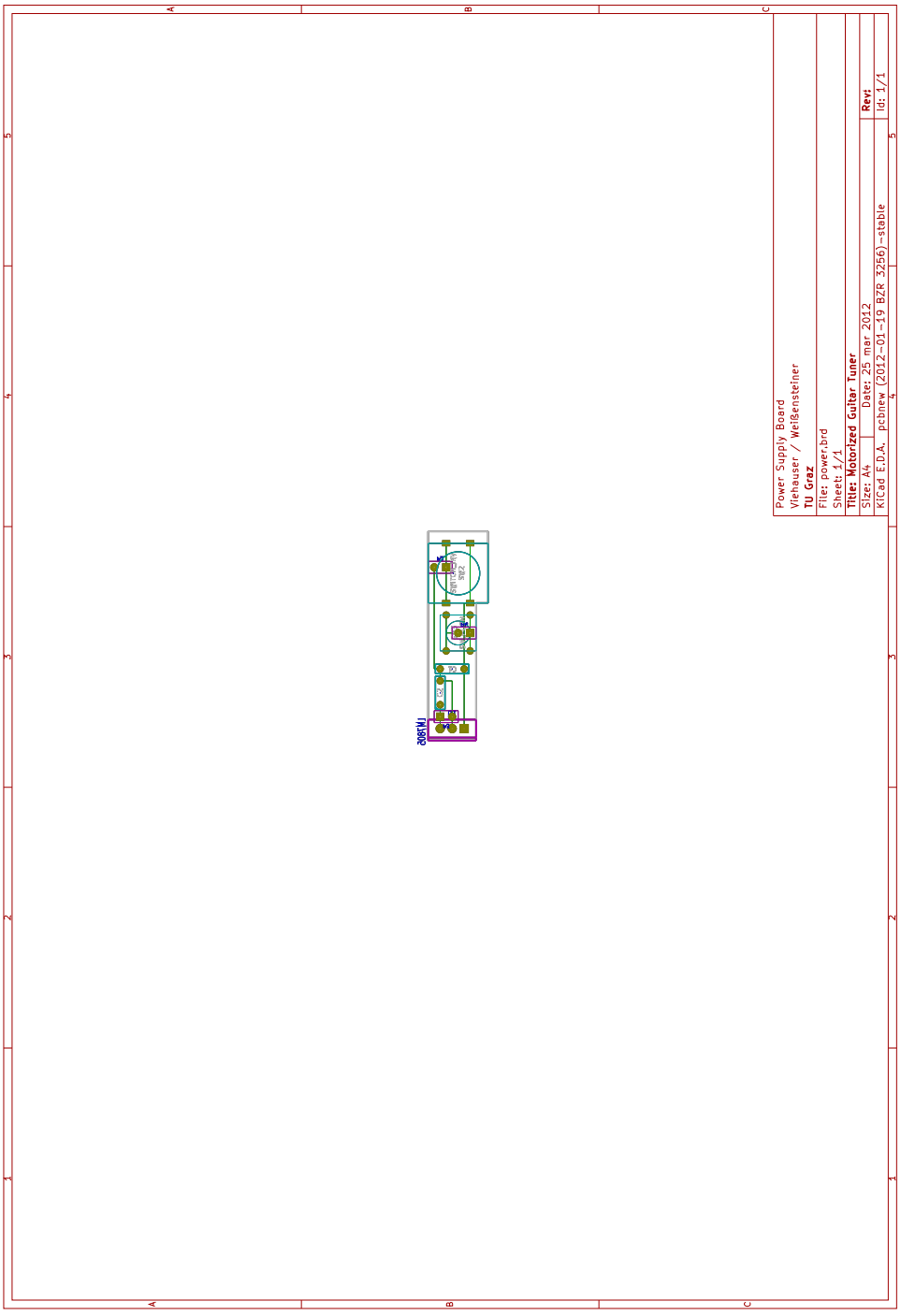

Figure 75: Board layout of the power supply circuit

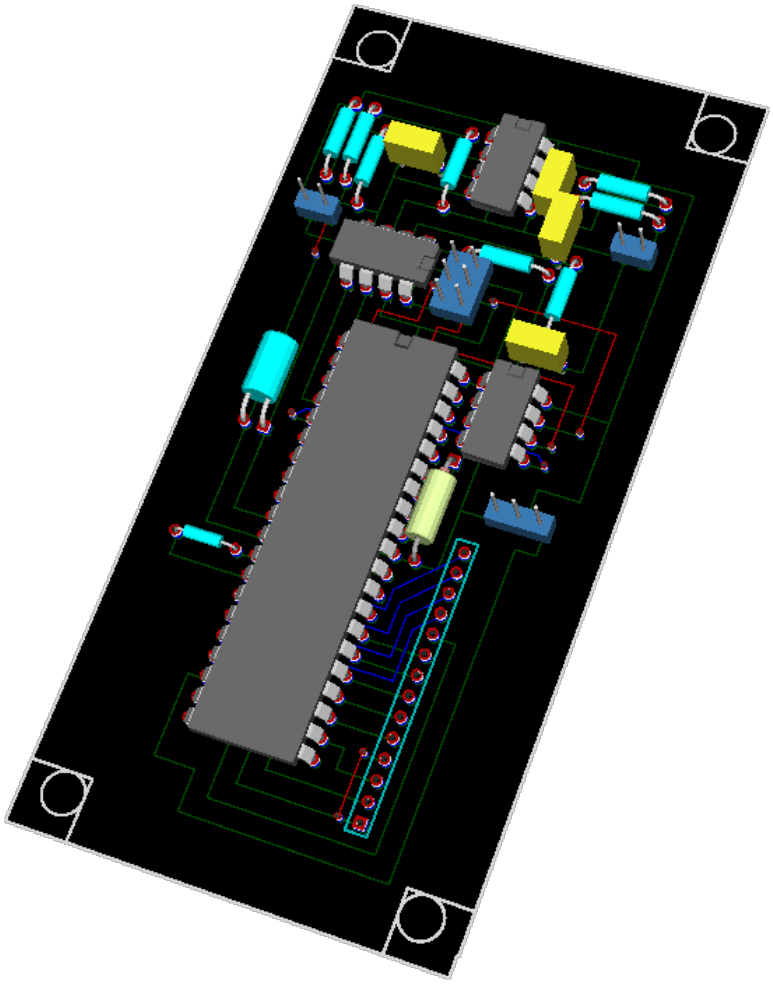

Figure 76: 3D simulation of the main board

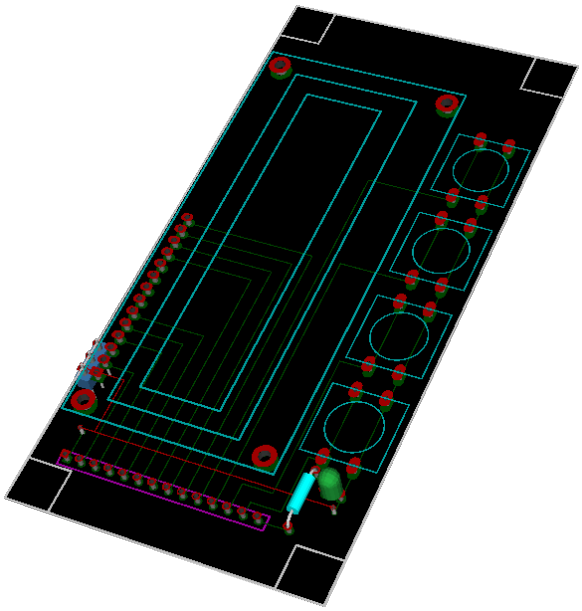

Figure 77: 3D simulation of the interface board

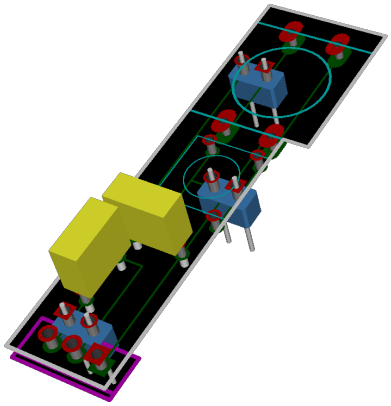

Figure 78: 3D simulation of the power supply board

4.4 List of parts

Category	Connection scheme	Symbol	Value / Name
Resistors	Main	R1	$10k$
	Main	R2	$1k$
	Main	R3	$4k7$
	Main	R4	$1k$
	Main	R5	$10k$
	Main	R6	$47k$
	Main	R7	$22k$
	Main	R8	$10k$
	Interface	R1	$1k$
Capacitors	Main	C1	$330n$
	Main	C2	$6n8$
	Main	C3	$330n$
	Main	C4	$39n$
	Main	C5	$100n$
	Main	C6	480μ
	Power	C1	$330n$
	Power	C2	1.5μ
Push buttons	Interface	SW1	LEFT
	Interface	SW2	RIGHT
	Interface	SW3	ENTER
	Interface	SW4	BACK
	Power	SW3	Servo Button
Switches	Power	SW2	Main Switch
Operational Amplifier	Main	U1A/B	LM358
	Main	U2	MCP6S21
	Main	U3	MCP6S21
Oscillation crystal	Main	X1	$16MHz$
LED	Interface	D1	green
LCD Display	Interface	S1	PC1601-A
Potentiometer	Interface	CONN2	$10k$
Voltage regulator	Power	U1	L7805CV
Battery + clip	Power	BT1	$9V$ block
Jack socket	Main	CONN2	$6.3mm$
Power socket	Power	P0 / SW1	$5mm$
Servo motor	Main	CONN5	Futaba S3003
μ-Controller	Main	IC1	Atmel Mega32-16PU
Hard case	-	-	$114x58x42mm$

Table 15: List of parts

4.5 Possible improvements

Even in course of this thesis by far overshot time limit, there is still space for improvements.
A possible extension would be an adapter for an acoustic microphone, to become able to tune acoustic guitars. Also the tuning of electrical guitars could then be made more comfortable, as it would become unnecessary to unplug the guitar from an attached amplifier.
But the additional noise added by the microphone adapter and possible distortion effects from a distortion module could drive the frequency detection part of the device onto its limits.
Another idea to upgrade the functionality of the device is to replace the 9V battery with a rechargeable battery, for instance with lithium polymer technology. The external power jack could be used to recharge the battery. We tried to implement this nice feature, but we couldn't find a rechargeable LiPo battery with the dimensions of a standard 9V block battery (or smaller).
Further, the PID-controller implementation could be enhanced, so for each string a proper controller is provided. This could result in even more stable tuning.
The actual accuracy limitation of detecting the high e-string frequency could also be improved by a higher sampling rate of the input signal, which would require other types of micro-controllers and an accordant restructuring and adaptation of the software.

5 References

Bibliography

[1] Atmel. *ATmega32 Datasheet*, 2011.

[2] Microchip. *MCP6S21 Datasheet*.

[3] Michael Simpson. Convert a futaba 3003 servo to continuous operation. http://www.kronosrobotics.com/an116/GAN116_3003.shtml, 2001-2007. KRSERVO1.

[4] Motorola. *LM358 Datasheet*, 1996.

[5] Wikipedia. Piano key frequencies. http://en.wikipedia.org/wiki/Piano_key_frequencies, 2012.

[6] Wikipedia. Control loop block diagram. http://upload.wikimedia.org/wikipedia/commons/2/24/Feedback_loop_with_descriptions.svg, 2008.

[7] A.; Bars R.; Keviczky L Hetthessy, J.; Barta. Basic course in control theory. *IEEE*, 2010.

[8] Atmel. Avr221. http://www.atmel.com/Images/doc2558.pdf, 2006.

[9] Atmel. Avr221 - figure 2-6. http://www.atmel.com/Images/doc2558.pdf, 2006.

[10] Wikipedia. Pid schematic block diagram. http://upload.wikimedia.org/wikipedia/commons/4/43/PID_en.svg, 2011.

[11] Inc. The Mathworks. *MATLAB Help Manual*, 1984 - 2010.

[12] www.indigitec.com. Electric guitar parts. http://indigitec.com/wp-content/uploads/2011/12/electric.png.

[13] Picture of guitar framus - billy lorento 10. http://t2.gstatic.com/images?q=tbn:ANd9GcSeyZJLWgf35JYgYM4_U32De7cHoXDutvcICKVRQQA98uaUytO9r2UIYoGUVA.

[14] Picture of guitar jackson - soloist sl2h (sam ash edition). http://www.gad.net/GAD/Guitar/S2H/_B0Z3776-CropAlt_800.jpg.

[15] Labor Elektroakustik Manfred Zollner, Hochschule Regensburg. Physik der elektrogitarre - saitenschwingungen. 2009.

[16] STMicroelectronics. *L7800 series Datasheet*, February 2003.

List of Figures